A Two-Step Perturbation Technique to Analyze
Nonuniform Single, Differential and Multiconductor Lines

Mykola Chernobryvko

Promotoren: prof. dr. ir. D. Vande Ginste, prof. dr. ir. D. De Zutter
Proefschrift ingediend tot het behalen van de graad van
Doctor in de Ingenieurswetenschappen: Elektrotechniek

Vakgroep Informatietechnologie
Voorzitter: prof. dr. ir. D. De Zutter
Faculteit Ingenieurswetenschappen en Architectuur
Academiejaar 2014 - 2015

UNIVERSITEIT
GENT

ISBN 978-90-8578-742-6
NUR 959
Wettelijk depot: D/2014/10.500/88

A Two-Step Perturbation Technique to Analyze Nonuniform Single, Differential and Multiconductor Lines

Mykola Chernobryvko

Dissertation submitted to obtain the academic degree of
Doctor of Electrical Engineering

Ghent University.

Supervisor:
prof. dr. ir. D. Vande Ginste
Electromagnetics group
Department of Information Technology
Faculty of Engineering and Architecture
Ghent University
St.-Pietersnieuwstraat 41
B-9000 Ghent, Belgium
http://emweb.intec.ugent.be

Supervisor:
prof. dr. ir. D. De Zutter
Electromagnetics Group
Department of Information Technology
Faculty of Engineering and Architecture
Ghent University
St.-Pietersnieuwstraat 41
B-9000 Ghent, Belgium
http://emweb.intec.ugent.be

Members of the examining board:

prof. dr. ir. L. Taerwe (chairman)	Ghent University, Belgium
prof. dr. ir. T. Dhaene (secretary)	Ghent University, Belgium
prof. dr. ir. D. Vande Ginste (supervisor)	Ghent University, Belgium
prof. dr. ir. D. De Zutter (supervisor)	Ghent University, Belgium
prof. dr. ir. J. Vanfleteren	Ghent University, Belgium
dr. ir. N. Stevens	KU Leuven, Belgium
dr. ir. P. Manfredi	Politecnico di Torino, Italy

Acknowledgments

First of all I would like to thank Prof. Daniël De Zutter for accepting me to do research in the Electromagnetics Group at Ghent University. I am very grateful for supervising me, for all your support, help and patience. I deeply appreciate the positive changes in my life because of my PhD, the knowledge I gained and the opportunity to understand the scientific world and the human relations at different levels of reality. This everything was made possible because of Daniël.

Very special thanks go to my supervisor Prof. Dries Vande Ginste for his patient guidance. I am thankful for my huge personal progress in science, academic English and interpersonal communication due to his permanent help and support. I admire his ability to clearly explain any complex problem in easy way with a very high enthusiasm. Also, I like his personal energy which can motivate and make you easily happy.

I'm also grateful to Prof. Hendrik Rogier for his help, cooperation and experience which I got during first two years of my research.

A special thanks go to Mrs. Isabelle Van Der Elstraeten for her support with administrative matters and always good mood during all these years.

I would like to thank the members of the examination board for participating to my PhD defence and for their valuable comments and remarks: Dr. Paolo Manfredy, Dr. Nobby Stevens, Prof. Jan Vanfleteren, Prof. Tom Dhaene, Prof. Dries Vande Ginste and Prof. Daniël De Zutter.

The life in INTEC wouldn't be so good for me without two smart and funny officemates called in Earth as Freek and Bart. Despite that their actions sometimes were too stable and predictable, Freek and Bart constantly showed me very good human values. They were fair, helpful and kind most of the time. I highly appreciate this. In their eyes I often saw the desire to optimize and improve this world, to fight for the best future of people on our planet. I am thankful also for showing me specialties of native Belgian people. Thank you for all funny and interesting moments which I had with both of you and for creation of "international days".

Yves, Dieter, Arnaut and Thomas are the old generation of PhD students for me, while Frederick, Luigi and Ignace are the old generation of doctors. Guys, I was very happy to interact with you during my PhD time. Gert-Jan, I was surprised to discover such a deep person inside you. I am sure that all your plans are very good and you will make them come true. Thanks for being so cool. Another a very deep and interesting for me person is Sam A. I didn't communicate much with him, but in his eyes I saw a very kind and awake person. Thanks for making our

Universe better with your presence. Luca De Camillis, thank you for all our very deep discussions which we had from the moment of your arrival till now.

I met here lots of nice and unusual people: Damiano, Pieter, Zdravko, Peter, Koen, Luc, Weigang, Patrick, Sofian, Marco, Sam L, Sam V, Sam V, Thijs, Karel, Bert, Annelies, Karlo, Vincent, Carla, Dieter DW, Kristof, Joris, Sara, Maria Lucia, Pieterjan, Wouter D, Wouter T., Olivier.

The women in our floor are very nice. Celina, Katya, Mima, Marina M., Marina S, Eline and Gemma, I am happy to know you. You charge men with your good energy and therefore they are so successful around you. Special thanks go to Celina for my first adaptation year, where I got a lot of support, help and opportunity to meet such nice people as Zlatka, Vincent, Danny, Peixia, Wenzhi, Haixia, Jiayu and Andres. And you still can surprise me. I am very thankful to Zlatka for all her good actions in my direction. Mima, thank you for our connection and for being always near.

The new generation of INTEC surprised me a lot. In so short time Arne, Irvin, Martijn, Niels and Steven became so close to me. I really appreciate that you are so open, smart and funny. I wish all of you to be good in your research and have success in your life. I hope Arne will be the richest among you. Thanks for the kind soul of Berg.

As long as I meet such people as Giorgos Karagounis, I'm sure that this world will develop in the correct direction. He has so wide and kind soul, a strong personality, bright energy, intelligence and a high level of empathy. In my opinion, such people as Giorgos must occupy the highest leading positions in our world. I wish you the best.

In my Dutch classes I met lot of nice people as well. The brightest among them are Antonella, Cristina, Vasilis, Goritsa, Kamila, Teodora, Tatiana, Lara, Helen, Sergey, Kevin, Luca, Eugenia and Viviana. Thanks for all nice moments experienced together with you.

I enjoyed my time together with Sasha, Natasha and Sveta. Thank you for the unusual world and happy moments with you.

I am happy to have such very close friends as Masha, Dasha, Marina and Katya. The energy of these women has always been a treasure for me. Thank you for the lots of fun, for deep conversations, for all your support and help. I wish to meet more often people like you. However, Dasha deserves to be repeated one more time since she loves me the most among you. Her son is also very brilliant. Days with you, Tim and Pieter are unforgettable. Marina and Erland need to be mentioned since I really like that couple for being so good and interesting. Masha, Sergey and Stepan, you know that I like all of you very much.

When I travelled to Ukraine, I always had a good time with Alina, Edge, Roma N, Roma Ts, Tanya, Sasha, Kostya, Nadya, Olya and Yulia in Kharkiv. Odessa-mother gave me positive emotions due to Dima, Ira, Pasha and Vlad. I associate Kiev

and Spain with Yulia. In my native city Lisychansk, there were always people as Victoria, Eva, Ira K, Zhenia K, Sonia, Ira, Olya, superwoman Larisa with her daughter Ksenia, Dmitriy and Natalya Danileychenko, Ludmila Nikolaieva with her big family, Leontij and Ludmila Chernobyrvko with their daughter Luda and my sister Natasha, who clearly showed their good attitude to me. Thank you for the good memories.

My infinite gratitude goes to my family. Thank you very much for giving me life and a chance to become such a strong person. My mother and father have not such an easy life. This year they experienced unfair War. However, they have a very strong son. He will fight as long as he has strength at the side of Truth. All people who are guilty in this unfair War need to be punished by the strictest version of law. Here, I want to mention the person who went through a concentration camp in Germany. Grandmother, I am proud to have DNA of a person, who had a difficult destiny but was able to stay positive. You will always be in my memory as super generous person who united our family.

The deepest gratitude I express to Nikolaiev Anton, Katya and Kira. They all are so awake, funny, kind and smart. I see you. I see you as one optimal structure intended to produce infinite flows of kindness in this world. I see you as exemplary friends. We have our own emotional language understandable only to us. I also know there is no need to express my love in words. Since I'm sure you can feel my love. You appreciate it so much that you keep windows closed in order to keep my love close to you.

This section of my acknowledgment I devote to people which I love. Marijn, Yura, Valia and Lena are really magical. They are unforgettable, since when I look at them I can see God or Devil. I see always something very bright. Marijn and Yura, such people as you must lead our world. Valia, just feel my love. My biggest thanks of course I express to Lena. You care about me, you make me happy and you wish me always to experience the best feelings. Thank you a lot for everything. It is necessary to mention that Lena is very beautiful, kind, smart, funny and wise.

In the last paragraph of this acknowledgment I would like to express my deepest respect to Ukrainian nation, to all people who would like to have honest life and to live in freedom. Our nation is going through the difficult times. However, as Yulia Tymosheko said in her famous speech after her release from prison, Ukrainian nation will never be conquered. I am proud to be Ukrainian. Heroes never die. They will be always with us. They will be our inspiration and our responsibility for every our step in the future.

Gent, oktober 2014
Mykola Chernobryvko

At each stage of human existence the adult man is off on his quest of his holy grail, the way of life he seeks by which to live. At his first level he is on a quest for automatic physiological satisfaction. At the second level he seeks a safe mode of living, and this is followed in turn, by a search for heroic status, for power and glory, by a search for ultimate peace; a search for material pleasure, a search for affectionate relations, a search for respect of self, and a search for peace in an incomprehensible world. And, when he finds he will not find that peace, he will be off on his ninth level quest. As he sets off on each quest, he believes he will find the answer to his existence. Yet, much to his surprise and much to his dismay, he finds at every stage that the solution to existence is not the solution he has come to find. Every stage he reaches leaves him disconcerted and perplexed. It is simply that as he solves one set of human problems he finds a new set in their place. The quest he finds is never ending.

CLARE W. GRAVES

Contents

Samenvatting

Onderhavig proefschrift behandelt de modellering van niet-uniforme transmissielijnen (NUTL) via een nieuwe twee-staps-perturbatietechniek. De NUTLs worden beschreven aan de hand van hun dwarsdoorsnede die variabel is langsheen de propagatierichting volgens dewelke de signalen lopen. Enerzijds spelen NUTLs een belangrijke rol in hedendaagse hogesnelheidselektronica. Microgolfingenieurs gebruiken NUTLs om impedantie-aanpassingsnetwerken te vervaardigen. In microgolftoepassingen zoals vermogenssplitsers en -combinatienetwerken, voedingsstructuren voor antennes en vermogensversterkers, worden NUTLs gebruikt als impedantie-omzetters, om zodoende een maximale vermogensoverdracht te verkrijgen. Daarenboven worden de directionele koppelaars die worden ingezet in microgolfcircuits vaak ontworpen en vervaardigd met behulp van niet-uniforme gekoppelde (micro)striplijnen. NUTLs worden tevens ingezet in de synthese van allerhande soorten filters, wat leidt tot een lage kost en een (relatief) eenvoudig ontwerp zonder daarbij de gewenste filterkarakteristiek te schaden. Het gebruik van NUTLs is ook nuttig gebleken tijdens het ontwerp van ultra-breedbandsystemen, meer bepaald om de ultra-breedbandpulsen de gewenste vorm te geven. Anderzijds is ook gebleken dat de niet-uniformiteiten niet altijd gewenst zijn tijdens het ontwerp, maar vaak onvermijdelijk. Transmissielijnen met niet-gewenste niet-uniformiteiten moeten echer ook nauwkeurig worden gemodelleerd, want de zogeheten huid-, nabijheids-, rand- en ruwheidseffecten die deze lijnen met zich meebrengen kunnen zeer schadelijk zijn voor wat betreft de signaalintegriteit. Jammer genoeg is het modelleren van NUTLs geen sinecure. Door de variabele dwarsdoorsnede kunnen de differentiaalvergelijkingen die de NUTLs beschrijven niet meer analytisch worden opgelost, tenzij in sommige speciale gevallen. Dit leidt ertoe dat methodes die toelaten om NUTLs op nauwkeurige en efficiënte wijze te modelleren erg belangrijk zijn voor het hedendaags ontwerp van elektronische producten.

Na een algemene inleiding over NUTLs in Hoofdstuk 1, wordt in Hoofdstuk 2 een nieuwe perturbatietechniek voor enkelvoudige transmissielijnen in het frequentiedomein beschreven. De dwarsdoorsnede van deze transmissielijnen mag arbitrair wijzigen langsheen de propagatierichting, wat toelaat deze techniek toe te passen op algemene niet-uniforme enkelvoudige lijnen met frequentie- en plaatsafhankelijke tranmissielijnparameters. Het formalisme wordt opgebouwd aan de hand van de welbekende per-eenheid-van-lengte (p.u.l., *per-unit-of-length*) RLGC-parameterbeschrijving van een uniforme transmissielijn in het quasi-TM regime. Deze uniforme lijn wordt hierbij beschouwd als het nominaal geval. Vervolgens worden de niet-uniformiteiten voorgesteld als perturbaties, relatief ten opzichte van de complexe capaciteits- en inductantiematrix van dit nominale geval. Dit laat dan meteen toe het effect van deze niet-uniformiteiten (of dus perturbaties)

te beoordelen. Uitgaande van de kennis van de nominale spanningen en stromen, verkregen door middel van de oplossing van de klassieke telegraafvergelijkingen, wordt een eerste-orde perturbatie verkregen, meer bepaald door een gelijkaardige set telegraafvergelijkingen op te lossen waarbij nu echter gedistribueerde spannings- en stroombronnen in rekening worden gebracht. Deze gedistribueerde bronnen hangen in ieder punt van de lijn af van de nominale spanningen, alsook van de veranderingen van de dwarsdoorsnede (of dus de p.u.l. parameters) t.o.v. het nominale, uniforme geval. Desalniettemin zijn de resultaten die verkregen worden na deze eerste-orde perturbatie niet zeer nauwkeurig. De nauwkeurigheid kan wel sterk worden opgedreven door de procedure nogmaals toe te passen, i.e. door een tweede perturbatie door te voeren, waarbij dan de spanningen en stromen van zowel het nominale geval als van de eerste-orde perturbatie worden in rekening gebracht. Dankzij de relatief eenvoudige vorm van de finale vergelijkingen is de nieuwe twee-staps-perturbatietechniek voor niet-uniforme enkelvoudige lijnen zeer efficiënt. Bij wijze van voorbeeld is de methode toegepast op een microstriplijn waarvan de breedte lineair toeneemt. Na vergelijking met een analytische oplossingsmethode blijkt dat de voorgestelde techniek zeer nauwkeurig is.

Vervolgens wordt de perturbatietechniek in Hoofdstuk 3 uitgebreid naar differentiële lijnenparen. De aandacht wordt hierbij niet enkel gevestigd op de theoretische beschrijving van de techniek, maar ook op de toepasbaarheid ervan en op zijn beperkingen. Hiervoor wordt gebruik gemaakt van een paar gekoppelde lijnen met arbitraire niet-uniformiteiten. Daarnaast wordt de techniek ook ingezet voor een belangrijke, maar zeer uitdagende, praktische toepassing. Met behulp van de nieuwe techniek wordt de differentiële signaaloverdracht geanalyseerd langsheen een lijnenpaar dat is ingebed in een substraat bestaande uit een geweven, composiete epoxy/glasvezelstructuur. Dergelijke substraten worden veel gebruikt. Het is echter waarschijnlijk dat één van de twee lijnen zich voornamelijk in het epoxyhars met lage diëlektrische constante bevindt, daar waar de tweede lijn gelocaliseerd is in de buurt van een glasvezel met hoge diëlektrische constante. Dit veroorzaakt een differentiële asymmetrie tussen de twee lijnen, wat op zijn beurt leidt tot (differentiële) transmissieverliezen langsheen het lijnenpaar. Daarenboven zal de onbalans ook zorgen voor modeconversie. Deze fenomenen zijn zeer schadelijk voor de goede werking van moderne elektronische systemen en ze beperken de maximale frequentie waarbij deze systemen kunnen werken. Met andere woorden, de mate waarin deze effecten optreden, bepaalt de maximale elektrische lengte van de differentiële interconnectiestructuren in nieuwe elektronische producten. Aangezien de nefaste effecten het best zichtbaar zijn bij zeer lange lijnen wordt in dit hoofdstuk een differentieel lijnenpaar met een totale lengte van 25 cm gemodelleerd in het frequentiebereik gaande van DC tot 50 GHz. Om de nauwkeurigheid verder op te drijven wordt deze (elektrisch zeer lange) lijn opgedeeld in een beperkt aantal kortere stukken, die elk apart worden gemodelleerd met de nieuwe techniek en nadien worden geconcateneerd. De resultaten tonen aan dat de effecten van het composiete, geweven materiaal heel precies kunnen worden voorspeld

door middel van de voorgestelde techniek. Daarenboven blijkt, na vergelijking met een klassieke referentiemethode, dat niet enkel de nauwkeurigheid zeer hoog is, maar dat de techniek ook zeer efficiënt is.

Nu de kracht van de voorgestelde methode voor enkelvoudige lijnen en voor differentiële lijnenparen is bewezen, wordt in Hoofdstuk 4 een uitbreiding van de techniek voorgesteld. In dit hoofdstuk wordt eerst de theoretische beschrijving gegeven van de algemene twee-staps-perturbatietechniek voor algemene niet-uniforme *multi*geleiderlijnen (NMTL). De dwarsdoorsnedes van deze NMTLs mogen hierbij op arbitraire wijzigen langsheen de propagatierichting. De niet-uniformiteiten worden opnieuw behandeld als perturbaties t.o.v. een nominale uniforme multigeleiderlijn. Gelijkaardig als wat werd beschreven in Hoofdstukken 2 en 3, wordt hier ook vertrokken van de telegraafvergelijkingen en worden twee opeenvolgende perturbatiestappen toegepast. Bij iedere stap worden de tweede-orde differentiaalvergelijkingen met gedistribueerde brontermen opgesteld. Deze vergelijkingen worden opgelost rekening houdende met de relevante randvoorwaarden, wat resulteert in de gezochte spanningen en stromen langsheen de multigeleiderinterconnectiestructuur. Om de nauwkeurigheid en efficiëntie van de techniek te illustreren, worden na deze theoretsiche beschrijving twee voorbeelden in detail uitgewerkt. Ten eerste wordt een NMTL met tien signaalgeleiders onderzocht in het frequentiedomein. De dwarsdoorsnede van deze NMTL varieert hierbij op willekeurige wijze. Studie van de transmissie van de signalen langsheen de NMTL en vergelijking met de oplossing verkregen via een klassieke referentiemethode, leert ons dat de nieuwe methode zeer nauwkeurig is. Daarenboven blijkt dat de CPU tijd die nodig is om de oplossing te verkrijgen met de nieuwe methode veel kleiner is dan de tijd die de referentiemethode vergt. Het tweede voorbeeld betreft een hogesnelheidsinterconnectiestructuur die zes niet-uniforme lijnen omvat. Om deze structuur te analyseren in het tijdsdomein worden de resultaten van de perturbatietechniek geïmporteerd in het professionele softwarepakket ADS van Agilent Technologies. Dit pakket laat tevens toe een volledige veldanalyse van het probleem door te voeren. Vergelijking van de resultaten in het tijdsdomein, verkregen via de perturbatietechniek enerzijds en de volledige veldoplossing anderzijds, toont opnieuw aan dat de nauwkeurigheid van de voorgestelde methode zeer hoog is. Het duurt echter zeer lang om de volledige veldoplossing te verkrijgen en qua CPU tijd is de perturbatietechniek dus opnieuw veel efficiënter.

In het laatste hoofdstuk van dit werk worden de algemene conclusies opgesomd. Daarenboven worden kort enkele suggesties voor verder onderzoek aangereikt, zoals het verder onderzoeken van de nauwkeurigheid van de voorgestelde methode, een alternatief paradigma om de perturbatiemethode op te stellen en een aantal andere toepassingsvoorbeelden. Samenvattend kan worden gesteld dat dit werk een duidelijke beschrijving en illustratie geeft van een nieuwe perturbatietechniek voor algemene niet-uniforme transmissielijnen. In tegenstelling tot bestaande methodes kan met deze techniek een zeer hoge nauwkeurigheid worden bereikt zonder dat daarbij de computationele efficiëntie in het gedrang gebracht wordt. De voorgestelde techniek is dan ook zeer belangrijk voor het ontwerp van innovatieve

elektronische producten.

Summary

The work presented in this doctoral thesis is devoted to the modeling of various nonuniform transmission lines (NUTLs) by means of a novel two-step perturbation technique. Such lines are characterized by cross-sections that vary along the longitudinal direction. On the one hand, NUTLs play an important role in modern high-speed electronic devices and systems. In microwave engineering, NUTLs have been widely used as impedance matching networks. Also, various microwave applications, such as power dividers, power combiners, antenna feed lines, power amplifiers, etc. employ NUTLs as impedance transformers for maximum power transfer. Moreover, many microwave circuits operate with directional couplers that are manufactured and designed using nonuniform coupled microstrip or striplines. Additionally, low-pass, bandpass or band-stop microwave filters can be manufactured by means of NUTLs. Such filters provide the necessary responses and are still low-cost and relatively simple to devise. Furthermore, the usage of NUTLs is very beneficial in UWB pulse shaping. On the other hand, engineering practice shows that nonuniformities are not always desired in transmission line structures, but sometimes, they are unavoidable. Transmission lines with (undesirable) nonuniformities must also be accurately modeled at the early stage of the design process, as skin, proximity, edge and roughness effects can lead to signal integrity problems at high frequencies. Unfortunately, the modeling of NUTLs is not straightforward. Due to the varying cross-section along the NUTL, the differential equations describing them cannot be solved analytically, except for some special cases. Therefore, methods allowing to accurately and efficiently model the behavior of NUTLs are of a great interest.

After a general introduction to the domain of NUTLs (Chapter 1), Chapter 2 presents a novel frequency domain perturbation technique with two perturbation steps for nonuniform single lines. The cross-sectional properties of such lines may vary in an arbitrary way, allowing to apply our technique to a large number of nonuniform single lines with frequency- and place-dependent line parameters. The formalism of the perturbation technique starts from the well-known per-unit-of-length (p.u.l.) resistance-inductance-conductance-capacitance (RLGC) parameter description of a uniform transmission line in the quasi-TM regime, which is considered to be the nominal structure. Next, the nonuniformities are represented as perturbations with respect to these nominal values of the complex inductance and capacitance matrices, allowing to see what the effect of perturbations might be. Starting from the knowledge of the nominal voltages and currents obtained by solving the classical Telegrapher's equations, a first-order perturbation is obtained. This first-order perturbation is found by solving the same set of Telegrapher's equations but now with distributed voltage and current

sources that depend on the nominal voltages and currents and on the deviation of the RLGC-values from their nominal value in each point along the transmission line. However, the obtained results are not sufficiently accurate after this first perturbation step. A substantial gain in accuracy is obtained by repeating the procedure, i.e. by introducing a second perturbation step, which takes voltages and currents of the nominal solution and of the first-order perturbation into account. Due to the relative simplicity of the final equations, the novel two-step perturbation technique for nonuniform single lines is very efficient. By way of example, the proposed method has been applied to a linearly tapered microstrip line. For this case, a high accuracy was achieved with respect to the reference analytical solution.

Next, in Chapter 3, the perturbation technique is extended to the differential line case. The main focus is on the theoretical description of the technique and on demonstrating its applicability and limitations by applying it to a pair of coupled lines with random nonuniformities. Furthermore, the perturbation approach is applied to a very important, but challenging, application example. Leveraging the novel perturbation technique, differential signaling analysis is performed using a pair of striplines embedded in a substrate that consists of an epoxy/fiberglass woven composite structure. In such a commonly used substrate, it is very likely that one trace of the differential pair is located mainly in the epoxy resin with low dielectric constant, while the other trace is located close to the glass fiber with a high dielectric constant. A differential skew between the lines is observed, as the two traces run through a different permittivity. This skew causes insertion loss suck-outs of the transmitted (differential) signal. Moreover, the imbalance leads to conversion from the differential mode to the common mode. All this may prohibit the use of these substrates at very high frequencies, or differently put, it poses a limit on the maximum (electrical) length of the lines. Since the fiber weave effect is best visible for very long lines, a line with a total length of 25 cm in the frequency range from DC to 50 GHz has been modeled. To improve the accuracy of the method at very high frequencies, this electrically very long line is subdivided into a limited number of shorter sections of about five to ten wavelengths. Next, these sections are modeled separately with the perturbation technique and concatenated to obtain the final solution. It is demonstrated that the fiber weave effects are precisely captured by the perturbation approach. Compared to a standard chain matrix approach, excellent accuracy and improved efficiency is obtained. In contrast to the chain matrix approach, the proposed perturbation technique can also handle continuously varying p.u.l. parameters.

Since the novel two-step perturbation technique has proven to be useful for single and differential lines, Chapter 4 is devoted to the extension of this method to the general nonuniform *multi*conductor transmission line (NMTL) case. As such, the perturbation approach can be applied to NMTLs for which the cross-sectional properties vary in an arbitrary way. Nonuniformities are treated again as perturbations with respect to the nominal uniform multiconductor line. Similarly as in Chapters 2 and 3, relying on the Telegrapher's equations and applying two consecu-

tive perturbations steps, at each step, second-order ordinary differential equations with distributed source terms are obtained. Solving these equations together with the appropriate boundary conditions provides the sought-for voltages and currents along the multiconductor interconnect structure. To illustrate the accuracy and efficiency of the general technique, two examples are worked out in detail. First, a nonuniform transmission line with ten signal conductors, for which the cross-sectional properties change randomly, is investigated in the frequency domain. Investigation of the relative error on the transmission coefficient with respect to the reference chain parameter matrix method demonstrates a very high accuracy of the perturbation method. Consideration of the CPU time needed for both perturbation and reference techniques reveals an improved efficiency of the proposed method. The second example is a high-speed packaging interconnect example composed of six nonuniform lines. To perform the analysis of the second structure in the time domain, the results of the perturbation approach are imported into Agilent's ADS framework and compared to the full-wave solution of ADS. The results of the perturbation technique represented in time domain are in a very good agreement with the reference full-wave solution. However, the CPU time needed for the transient analysis using the perturbation approach is significantly less than the CPU time needed for the full-wave modeling.

The final chapter describes the overall conclusions drawn from the research presented in this thesis. Additionally, suggestions concerning the accuracy of the method, an alternative way to develop a theoretical framework and other application examples to be considered during future work are outlined. In summary, this dissertation clearly describes and illustrates a novel perturbation technique intended to model general nonuniform transmission lines. In contrast to many traditional approaches, this technique allows to get a very high accuracy whilst still being very efficient in terms of computational costs. The proposed novel frequency domain modeling approach is of high importance for hardware engineers during the design of their innovative electronic products.

List of Abbreviations

ADS	Advanced Design System
CAD	Computer Aided Design
CPU	Central Processing Unit
DC	Direct Current
DQM	Differential Quadrature Method
FDTD	Finite-Difference Time-Domain
FEM	Finite Element Method
IEEE	Institute of Electrical and Electronics Engineers
LTML	Linearly Tapered Microstrip Line
MoM	Method of Moments
MTL	Multiconductor Transmission Line
NMTL	Nonuniform Multiconductor Transmission Lines
NUTL	Nonuniform Transmission Line
PCB	Printed Circuit Board
p.u.l.	per-unit-of-length
RAM	Random Access Memory
RV	Random Variable
UWB	Ultra-Wideband
VLSI	Very-Large-Scale Integration

List of Publications

Articles in International Journals

- M. Chernobryvko, D. Vande Ginste and D. De Zutter, "A two-step perturbation technique for nonuniform single and differential lines", *IEEE Transactions on Microwave Theory and Techniques*,vol. 61, no. 5, pp. 1758-1767, May 2013.
- M. Chernobryvko, D. Vande Ginste and D. De Zutter, "Nonuniform multiconductor transmission line analysis by a two-step perturbation technique", accepted for publication in *IEEE Transactions on Components Packaging and Manufacturing Technology*.

Articles in Conference Proceedings

- M. Chernobryvko, D. Vande Ginste and D. De Zutter, "A perturbation technique to analyze the influence of fiber weave effects on differential signaling", *IEEE 22nd Conference on Electrical Performance of Electronic Packaging and Systems (EPEPS)*, 27-30 Oct. 2013, , San Jose, CA, USA, pp. 15-18.
- A. Durier, H. Pues, D. Vande Ginste, M. Chernobryvko, C. Gazda and H. Rogier, "Novel modeling strategy for a BCI set-up applied in an automotive application: An industrial way to use EM simulation tools to help hardware and ASIC designers to improve their designs for immunity tests ", *8th Workshop on Electromagnetic Compatibility of Integrated Circuits (EMC Compo)*, 6-9 Nov. 2011, Dubrovnik, Croatia, pp. 41-46.

A Two-Step Perturbation Technique to Analyze Nonuniform Single, Differential and Multiconductor Lines

1 Introduction

Wired communication transfers information between a transmitter and a receiver using transmission lines and this domain has a quite long history. The first important creation in this field, i.e. the first electrical telegraph became possible due to the intensive study of the phenomenon of electricity. In 1753 Morrison Charles proposed to send information between two points transferring electrical charges through numerous isolated wires. His theoretical suggestions inspired many scientists to create a real electrical telegraph. Physicist Georges-Louis Le Sage made the first operating telegraph in 1774, giving life to a new age of wired communication.

Despite the fact that the 20^{th} century has shown widespread usage of wireless communication, wire communication and transmission lines as its main units, have never disappeared from modern devices and equipment. Modern technologies are characterized by the presence of transmission lines in the form of telephone wires, coaxial cables, optical fibers, twisted pairs for computer networks, microstrip and striplines for PCB interconnect, rectangular waveguides for high power signal transmission in radar applications, etc. The length of the transmission line can vary between hundreds of kilometers as for long distance telephone lines and less than a millimeter on chip.

In general the modeling of transmission lines is not an easy task since Maxwell's equations must be solved to completely understand all processes. However, the implementation of the full-wave solution usually requires high computing costs. Therefore, the characterization of transmission lines from a circuit point of view is more popular. Circuit theory describes signal propagation in terms of voltages and currents avoiding the necessity to solve Maxwell's equations in their full generality. For such analysis a transmission line is defined by a cross-section and perpendicular to it the signal propagation direction (also known as the longitudinal direction).

Details on this so-called quasi-TM method can be found in [1]. Applying the quasi-TM approach leads to the circuit representation of voltages and currents in terms of a set of partial differential equations better known as Telegrapher's equations. In these equations voltages and currents still depend on time or frequency but also on the coordinate in the longitudinal direction. In the Telegrapher's equations, the cross-sectional properties are represented by a per-unit-of-length (p.u.l.) capacitance, inductance, resistance and conductance matrix. The resistance matrix expresses the conductor losses while the conductance matrix expresses the substrate losses. The capacitance matrix describes charge coupling while the inductance matrix expresses magnetic flux coupling.

1.1 Nonuniform transmission lines (NUTLs) in microwave applications

Transmission line theory also deals with nonuniform transmission lines (NUTLs), i.e. lines with cross-sections that vary in the longitudinal direction. NUTLs are a very important part of modern high-speed electronic devices and systems. Several application examples of NULTs are shown in Fig. 1.1.

In microwave engineering, NUTLs have been extensively used as impedance-matching networks [2] since usage of lumped or mixed distributed/lumped elements for such purposes at high frequencies have limitations due to the effects of the discontinuities and the difficulties in realizing them. To overcome such problems in the microwave range, NUTLs are successfully used to match two impedances [3]. Also, various microwave applications such as power dividers, power combiners, antenna feed lines, power amplifiers, etc. employ NUTLs as impedance transformers for maximum power transfer. Many microwave circuits operate with directional couplers [4] manufactured and designed using nonuniform coupled microstrip or striplines.

Furthermore, various types of microwave filters as low-pass, bandpass or bandstop with coupled lines can be manufactured by means of NUTLs [5]. Such filters provide the necessary responses with low costs and relatively simple techniques. Additionally, ultra-wideband (UWB) pulse shaping [6] is important for spectral masking, pulse shape modulation and for enhancing radar resolution. Unfortunately, often temporally complex pulses are required to be created. Since such pulses cannot be obtained by means of simple filtering, the usage of NUTLs is very beneficial for UWB pulse shaping, avoiding expensive optical techniques.

Moreover, engineering practice demonstrates that nonuniformites are not always desired in transmission line structures, but that they cannot be avoided. For example, at high frequencies the proximity effect, characterized by nonuniform current distribution in a conductor with time varying current caused by the time varying current in nearby conductor, leads to increasing effective resistance. Also, skin effect causing current crowding, edge effects (nonrectangular cross-sections)

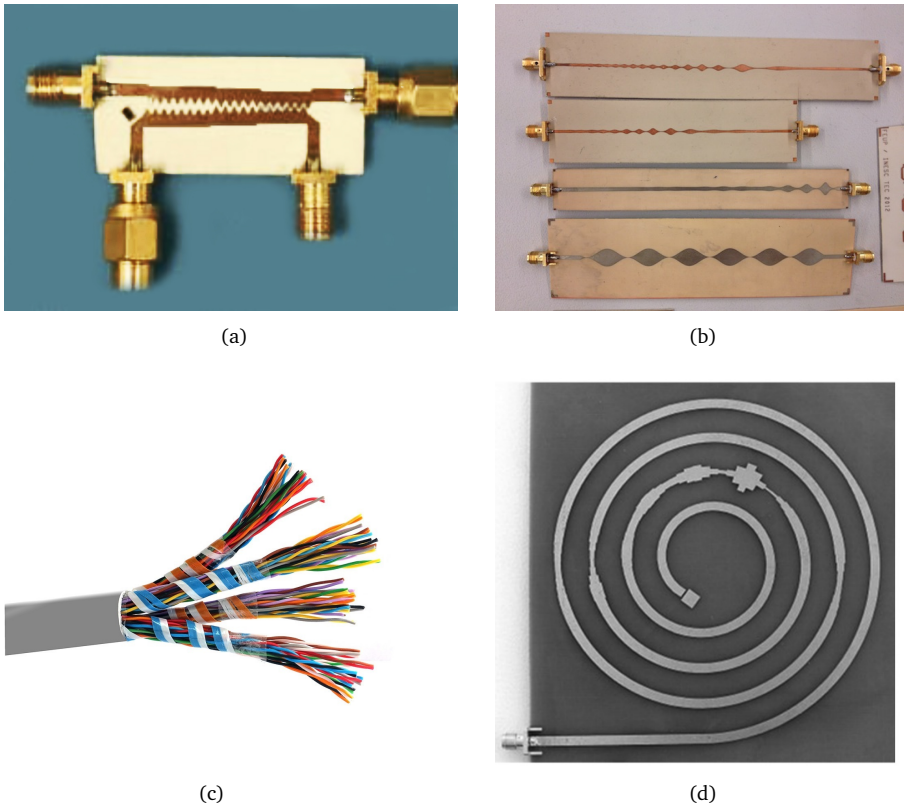

(a) (b)

(c) (d)

Figure 1.1: Applications of NUTLs. (a) A broadband directional coupler. (b) Microwave filters. (c) A twisted pair cable. (d) A UWB pulse shaper.

or roughness [7] could lead to signal integrity problems at high frequencies and therefore need to be accurately modeled at the early stages of the design process. Printed Circuit Boards (PCBs) are often manufactured using standard (low-cost) materials and substrates. The so-called "fiber weave" effect, described in [8] stems from the nonuniformity of the substrate and has potentially a huge influence on signal integrity.

1.2 Modeling of NUTLs

The differential equations describing the behavior of NUTLs with varying p.u.l. parameters cannot be solved with analytical techniques for most cases. Therefore, different methods to analyze NUTLs exist in both time and frequency domains.

The most straightforward solution is to approximate a NUTL as a cascade of dis-

crete uniform lines [9]. However, the number of separate sections must be quite large for an accurate modeling, leading to reduced efficiency of the method.

Frequency domain analysis of NUTLs for which p.u.l. parameters, voltages and currents along the transmission line are expanded in Fourier [10] or Tailor [11] series yields an exact solution, but only for the cases when the series converge.

Another popular technique to model NUTLs is based on the method of characteristics [12]. Using this recursive technique partial differential equations describing a transmission line are converted into ordinary differential equations along the characteristic lines. The method of characteristics using the extraction of the line-propagation delay provides a very accurate solution in the modeling of lossless NUTLs. However, when losses and frequency dependent p.u.l. parameters need to be taken into account, the method becomes inefficient as numerical techniques need to be applied in solving the differential equations.

NUTLs could be modeled as well by means of wavelet transform [13]. The method relies on a weak formulation of the transmission line equations obtained by expanding voltages and currents in terms of wavelet functions in space or in time. Transformation of differential equations to algebraic equations leads to the final solution. The accuracy of the method strongly depends on the number of components of the wavelet basis. Moreover, its complexity grows with the number of signal conductors.

The full-wave analysis of NUTLs using the method of moments (MoM) [14], the finite-difference time-domain method (FDTD) [15], the finite element method (FEM) [16] or the differential quadrature method (DQM) [17] yields very accurate results. Unfortunately, time costs required for such numerical techniques are considerably higher compared to quasi-TM approaches.

Therefore, in this dissertation, a novel two-step perturbation technique for the modeling of NUTLs in the frequency domain is described and investigated. In this perturbation method, nonuniformities are represented as perturbations with respect to a nominal configuration. Relying on the Telegrapher's equations, voltages and currents along the multiconductor interconnection are derived from second-order differential equations for the nominal configuration with source terms accounting for the perturbations.

1.3 Outline of this work

The remainder of this doctoral thesis is organized as follows. Chapter 2 describes the formalism of a two-step perturbation technique for transmission lines with a single signal conductor. The theory is validated by means of a linearly tapered microstrip line for which an analytical solution is known. Very good agreement between the theory and the analytical method confirms the validity of our approach. Some remarks are formulated as for the range of applicability of the perturbation method.

Chapter 3 extends the perturbation technique to the differential line case. The theory is applied to a pair of coupled lines with random variation of the p.u.l. parameters along the line and to differential lines embedded in a substrate composed of woven glass fibers. The ability to capture the fiber weave effects by the perturbation technique are shown for an electrically very long line. The methodology explaining how to deal with electrically long transmission lines is also considered. Comparison with a chain matrix approach demonstrates accuracy and efficiency for both cases. The necessity of employing a two-step perturbation to get sufficient accuracy for the transmission coefficients is highlighted.

The technique is extended to the general multiconductor case in Chapter 4. Frequency domain analysis for a ten conductor microstrip line with random uniformities shows the accuracy and efficiency compared to a chain-parameter method. Further, validation of the theory and comparison with the full-wave modeling of a high-speed packaging nonuniform interconnect is performed in the time domain.

In the last chapter, the main conclusions of the work are presented and new goals for future research are proposed.

References

[1] D. De Zutter, "Accurate broadband modeling of multiconductor line RLGC-parameters in the presence of good conductor and semiconducting substrates", *IEEE Electromagnetic Compatibility Magazine*, vol. 3, no. 2, pp. 74–84, 2014.

[2] A. Hamade, A. Kouki, and F. Ghannouchi, "Synthesis of impedance matching circuits using arbitrary nonuniform transmission lines", in *Microwave Symposium Digest*, 1997, pp. 1619 –1622.

[3] X. G. and K. Yashiro, "Impedance matching for complex loads through nonuniform transmission lines", *IEEE Trans. Microw. Theory Tech.*, vol. 50, no. 6, pp. 1520 –1525, Jul. 2002.

[4] H.-R. Ahn, "Complex impedance transformers consisting of only transmission-line sections", *IEEE Trans. Microw. Theory Tech.*, vol. 60, no. 7, pp. 2073 –2084, Jul. 2012.

[5] G. Xiao, K. Yashiro, N. Guan, and S. Ohkawa, "An effective method for designing nonuniformly coupled transmission-line filters", *IEEE Trans. Microw. Theory Tech.*, vol. 49, no. 6, pp. 1027 –1031, Jun. 2001.

[6] P. Rulikowski and J. Barrett, "Ultra-wideband pulse shaping using lossy and dispersive nonuniform transmission lines", *IEEE Trans. Microw. Theory Tech.*, vol. 59, no. 10, pp. 2431 –2440, Oct. 2011.

[7] B. Curran, I. Ndip, S. Guttowski, and H. Reichl, "A methodology for combined modeling of skin, proximity, edge, and surface roughness effects", *IEEE Trans. Microw. Theory Tech.*, vol. 58, no. 9, pp. 2448–2455, Sep. 2010.

[8] S. McMorrow and C. Heard, "The impact of PCB laminate weave on the electrical performance of differential signaling at multi-gigabit data", in *Proc. DesignCon*, 2005.

[9] C. R. Paul, *Analysis of Multiconductor Transmission Lines*. John Wiley & Sons, 1994.

[10] M. Khalaj-Amirhosseini, "Analysis of lossy inhomogeneous planar layers using Fourier series expansion", *IEEE Trans. Antennas Propag.*, vol. 55, no. 2, pp. 489–493, Feb. 2007.

[11] ——, "Analysis of coupled nonuniform transmission lines using Taylor's series expansion", *IEEE Trans. Electromagn. Compat.*, vol. 48, no. 3, pp. 594–600, Aug. 2006.

[12] N. Orhanovic, P. Wang, and V. K. Tripathi, "Time-domain simulation of uniform and nonuniform multiconductor lossy lines by the method of characteristics", *IEEE Trans. Comput.-Aided Design Integr. Circuits Syst.*, vol. 12, no. 6, pp. 900–904, Jun. 1993.

[13] S. Barmada and M. Raugi, "Transient numerical solutions of nonuniform MTL equations with nonlinear loads by wavelet expansion in time or space domain", *IEEE Trans. Circuits Syst. I*, vol. 47, no. 8, pp. 1178 –1190, Aug. 2000.

[14] M. Tong, G. Pan, and G. Lei, "Full-wave analysis of coupled lossy transmission lines using multiwavelet-based method of moments", *IEEE Trans. Microw. Theory Tech.*, vol. 53, no. 7, pp. 2362 –2370, Jul. 2005.

[15] K. Afrooz and A. Abdipour, "Efficient method for time-domain analysis of lossy nonuniform multiconductor transmission line driven by a modulated signal using FDTD technique", *IEEE Trans. Electromagn. Compat.*, vol. 54, no. 2, pp. 482 –494, Apr. 2012.

[16] H.-H. Chen, "Finite-element method coupled with method of lines for the analysis of planar or quasi-planar transmission lines", *IEEE Trans. Microw. Theory Tech.*, vol. 51, no. 3, pp. 848 –855, Mar. 2003.

[17] Q. Xu and P. Mazumder, "Accurate modeling of lossy nonuniform transmission lines by using differential quadrature methods", *IEEE Trans. Microw. Theory Tech.*, vol. 50, no. 10, pp. 2233–2246, Oct. 2002.

2

A Two-Step Perturbation Technique for Nonuniform Single Lines

Based on the publication:

Mykola Chernobryvko, Dries Vande Ginste and Daniël De Zutter, "A Two-Step Perturbation Technique for Nonuniform Single and Differential Lines", *IEEE Transactions on Microwave Theory and Techniques, MTT*, Vol. 61, no. 5, pp. 1758-1767, May 2013

★ ★ ★

A novel two-step perturbation technique to analyze nonuniform single transmission lines in the frequency domain is presented. Here, nonuniformities are considered as perturbations with respect to a nominal uniform line, allowing an interconnect designer to easily see what the effect of (unwanted) perturbations might be. Based on the Telegrapher's equations, the proposed approach yields second-order ordinary distributed differential equations with source terms. Solving these equations in conjunction with the pertinent boundary conditions leads to the sought-for currents and voltages along the lines. The accuracy of the perturbation technique is demonstrated for a linearly tapered microstrip line with respect to an analytical solution.

2.1 Introduction

Modeling of nonuniform transmission lines (NUTL), being part of modern high-speed electronic devices and systems, is often a challenging problem. NUTLs have been widely used in several microwave applications, such as filters [1], impedance transformers [2], directional couplers [3], and very large scale integration (VLSI) interconnections [4]. Also, they are applied for impedance matching [5] and ultra wideband pulse shaping [6]. Since skin, proximity, edge and roughness effects can lead to signal integrity problems at high frequencies [7], transmission lines with (undesirable) nonuniformities must be accurately modeled at the early stage of the design process. Due to the varying per-unit-length (p.u.l.) parameters along the NUTL, the differential equations describing them cannot be solved analytically, except for some special cases [8]–[10].

Therefore, plenty of research has been devoted to the numerical solution of nonuniform lines, both in the time and frequency domain. For instance, Precise Time-Step Integration [11] and Differential Quadrature Methods [12] are stable and demonstrate good accuracy, but they are very time consuming. One of the easiest ways to deal with a NUTL is to approximate it as a cascade of discrete uniform transmission lines [13], [14]. Unfortunately, in modern applications, the number of discrete sections of the line must be quite large to accurately account for all nonuniformities and increasing the number of sections reduces the efficiency of the method. Another technique, based on the method of characteristics [15], allows to convert the hyperbolic partial differential equations of the NUTLs into a set of ordinary differential equations. However, to account for frequency-dependent p.u.l. parameters of the lines, convolutions need to be computed [16], again increasing the calculation time. Methods proposed in [17] and [18] use Tailor and Fourier expansions to describe the properties of nonuniform lines, but can only be applied as long as the series converge. Other contributions are based on waveform relaxation, see e.g. [19], congruence transforms, see e.g. [20], or wavelet expansion, see e.g. [21]. In [22] an improved averaging technique for single lines with subwavelength nonuniformities is presented. Finally, [23] presents an equivalent source technique for single lines solving the pertinent integral equation in an iterative way and presenting examples using two iterations.

In this chapter, we propose a novel frequency domain perturbation technique with two perturbation steps for nonuniform single lines. For such lines, the cross-sectional properties can change in an arbitrary way, allowing to apply our technique to a large number of nonuniform single lines with frequency- and place-dependent line parameters. To construct the presented technique, we start from the well-known RLGC-matrix description of a *uniform* transmission line in the quasi-TM regime [24], which is considered to be the nominal structure. Next, the nonuniformities are treated as perturbations with respect to (w.r.t.) these nominal values of the complex inductance and capacitance matrices. Starting from the knowledge of the nominal voltages and currents obtained by solving the classical Telegrapher's equations, a first-order perturbation is obtained. This first-order

perturbation is found by solving the same set of Telegrapher's equations but now with distributed voltage and current sources depending on the nominal voltages and currents and on the deviation of the RLGC-values from their nominal value in each point along the transmission line. However, it turns out that the obtained result is not sufficiently accurate. A substantial gain in accuracy is obtained by repeating the procedure, i.e. by introducing a second perturbation step, which now takes voltages and currents of the nominal solution and of the first-order perturbation into account. Due to the relative simplicity of the final equations, the novel *two-step* perturbation technique for nonuniform single lines is very efficient. The accuracy is demonstrated by applying it to a linearly tapered microstrip line.

The chapter is organized as follows. In a first step, we construct the perturbation technique for a single line (Section 2.2). At the end of Section 2.2.2, some remarks are formulated as to the range of applicability of the proposed method. The theory is validated and illustrated in Section 2.3. The example comprises the application of the proposed technique to a linearly tapered microstrip line. Finally, conclusions are summarized in Section 2.4.

2.2 Perturbation solution for a single signal conductor

We will first outline the theory for a single signal conductor as this keeps the notational burden to a minimum while all salient features of the approach emerge, except of course for mode coupling, which will be discussed in the next chapter. Working within the framework of the quasi-TM approach and in the frequency domain (with the $e^{j\omega t}$ dependence suppressed), we only have to consider a single voltage V and a single current I while the p.u.l. inductance L and capacitance C are scalar quantities. Note that for ease of notation, L and C are considered to be complex, i.e. the p.u.l. resistance R and conductance G are understood to be part of L and C ($L = L_{lossless} + \frac{R}{j\omega}$ and $C = C_{lossless} + \frac{G}{j\omega}$). Our starting point are the well-known Telegrapher's equations:

$$\frac{dV(z)}{dz} = -j\omega L(z) I(z), \tag{2.1}$$

$$\frac{dI(z)}{dz} = -j\omega C(z) V(z), \tag{2.2}$$

with z the signal propagation direction and where we have explicitly made clear that C and L depend on z. To perform a perturbation analysis, we introduce the following expansions

$$\begin{aligned} V(z) &= \tilde{V}(z) + \Delta V_1(z) + \Delta V_2(z) + \ldots, \\ I(z) &= \tilde{I}(z) + \Delta I_1(z) + \Delta I_2(z) + \ldots, \\ C(z) &= \tilde{C} + \Delta C(z), \\ L(z) &= \tilde{L} + \Delta L(z). \end{aligned} \tag{2.3}$$

In (2.3), the leading terms of the series expansions for voltage and current, i.e. $\tilde{V}(z)$ and $\tilde{I}(z)$, will be labeled as the *unperturbed* values. The remaining terms are perturbations of order one, two, etc. $\tilde{C}$ and $\tilde{L}$ are the unperturbed values of the p.u.l. capacitance and inductance. $\Delta C(z)$ and $\Delta L(z)$ are the variations of the capacitance and inductance along the line which remain when subtracting the constant values $\tilde{C}$ and $\tilde{L}$ from $C(z)$ and $L(z)$ respectively. At this point $\tilde{C}$ and $\tilde{L}$ are not necessarily the mean values of C and L over the line. We only suppose that $\Delta C(z)$ and $\Delta L(z)$ are small enough with respect to $\tilde{C}$ and $\tilde{L}$. Note that $C(z)$ and $L(z)$ in (2.3) are not expanded in a series but are only written as the sum of a constant part and a place-dependent part. Substituting (2.3) into (2.1) and (2.2) and collecting terms of the same order, yields

$$\frac{d\tilde{V}(z)}{dz} = -j\omega\tilde{L}\tilde{I}(z), \tag{2.4}$$

$$\frac{d\tilde{I}(z)}{dz} = -j\omega\tilde{C}\tilde{V}(z), \tag{2.5}$$

$$\frac{d\Delta V_1(z)}{dz} = -j\omega\tilde{L}\Delta I_1(z) - j\omega\Delta L(z)\tilde{I}(z), \tag{2.6}$$

$$\frac{d\Delta I_1(z)}{dz} = -j\omega\tilde{C}\Delta V_1(z) - j\omega\Delta C(z)\tilde{V}(z), \tag{2.7}$$

$$\frac{d\Delta V_2(z)}{dz} = -j\omega\tilde{L}\Delta I_2(z) - j\omega\Delta L(z)\Delta I_1(z), \tag{2.8}$$

$$\frac{d\Delta I_2(z)}{dz} = -j\omega\tilde{C}\Delta V_2(z) - j\omega\Delta C(z)\Delta V_1(z). \tag{2.9}$$

Higher-order perturbations will not be considered, but could be obtained in a similar way. From this point on, for ease of notation, the argument z will be omitted.

2.2.1 Unperturbed solution for a single line

Solving (2.4) and (2.5) readily gives

$$\tilde{V} = Ae^{-jk_0z} + Be^{+jk_0z}, \tag{2.10}$$

$$\tilde{I} = \frac{1}{Z_0}(Ae^{-jk_0z} - Be^{+jk_0z}), \tag{2.11}$$

with the unperturbed characteristic impedance $Z_0 = \sqrt{\tilde{L}/\tilde{C}}$ and the unperturbed wave number $k_0 = \omega\sqrt{\tilde{L}\tilde{C}}$. Now we introduce the boundary conditions. Consider a signal conductor of length l terminated in a load Z_L and excited by a Thévenin source V_g with internal impedance Z_g. The load will be placed at $z = l$ and the source at $z = 0$. This will make calculations more tractable. With these boundary

conditions, we have that

$$A = \frac{V_g}{1+\frac{Z_g}{Z_0}} \frac{1}{1-K_L K_g e^{-2jk_0 l}}, \tag{2.12}$$

$$B = K_L A e^{-2jk_0 l}, \tag{2.13}$$

with the reflection coefficients K_L and K_g at the load and at the generator, resp., as usual given by:

$$\begin{aligned} K_L &= \frac{Z_L - Z_0}{Z_L + Z_0}, \\ K_g &= \frac{Z_g - Z_0}{Z_g + Z_0}. \end{aligned} \tag{2.14}$$

2.2.2 Perturbation solution of the single line

From (2.6) and (2.7), the first-order perturbation ΔV_1 satisfies

$$\frac{d^2 \Delta V_1}{dz^2} + k_0^2 \Delta V_1 = -k_0^2 \tau_C \tilde{V} - jk_0 \frac{d}{dz}(\tau_L Z_0 \tilde{I}), \tag{2.15}$$

with $\tau_C = \frac{\Delta C}{\tilde{C}}$ and $\tau_L = \frac{\Delta L}{\tilde{L}}$. Similarly, (2.8) and (2.9) yield

$$\frac{d^2 \Delta V_2}{dz^2} + k_0^2 \Delta V_2 = -k_0^2 \tau_C \Delta V_1 - jk_0 \frac{d}{dz}(\tau_L Z_0 \Delta I_1). \tag{2.16}$$

We can now solve the above differential equations (2.15) and (2.16) by applying the general theory for second-order differential equations with an arbitrary source term, see e.g. [1] or the Appendix A of [23]. For this we need two independent solutions, $y_1(z)$ and $y_2(z)$ of the homogeneous differential equation. Representing the source term as $g(z)$, the particular solution $y_p(z)$ to the differential equation becomes

$$y_p(z) = -y_1(z) \int^z \frac{y_2(z')g(z')}{\mathcal{W}} dz' + y_2(z) \int^z \frac{y_1(z')g(z')}{\mathcal{W}} dz', \tag{2.17}$$

with $\mathcal{W}$ the Wronskian defined as

$$\mathcal{W} = y_1(z) \frac{dy_2(z)}{dz} - y_2(z) \frac{dy_1(z)}{dz}. \tag{2.18}$$

In our case, one easily sees that

$$\begin{aligned} y_1(z) &= e^{-jk_0 z}, \\ y_2(z) &= e^{+jk_0 z}, \\ \mathcal{W} &= 2jk_0. \end{aligned} \tag{2.19}$$

Some straightforward calculations show that the solutions of (2.15) and (2.16) take the following form:

$$\Delta V_i = C_i e^{-jk_0 z} + D_i e^{+jk_0 z} + \Delta V_{ip}, \tag{2.20}$$

$$Z_0 \Delta I_i = C_i e^{-jk_0 z} - D_i e^{+jk_0 z} + Z_0 \Delta I_{ip}. \tag{2.21}$$

with $i = 1, 2$. The particular solutions ΔV_{ip} and ΔI_{ip} can be cast in the following form

$$\Delta V_{ip}(z) = -\frac{jk_0}{2}\left[F_i(z)e^{-jk_0 z} + G_i(z)e^{+jk_0 z}\right], \tag{2.22}$$

$$Z_0 \Delta I_{ip}(z) = -\frac{jk_0}{2}\left[F_i(z)e^{-jk_0 z} - G_i(z)e^{+jk_0 z}\right]. \tag{2.23}$$

Specifically note that $F_i(z=0) = 0$ and $G_i(z=0) = 0$. The values of F_1 and G_1 at the first perturbation step are found to be

$$F_1(z) = \gamma A + \beta B, \quad G_1(z) = -(\alpha A + \gamma B), \tag{2.24}$$

where A and B are given in (2.12) and (2.13) respectively and with

$$\alpha(z) = \int_0^z [\tau_C(z') - \tau_L(z')] e^{-2jk_0 z'} dz', \tag{2.25}$$

$$\beta(z) = \int_0^z [\tau_C(z') - \tau_L(z')] e^{+2jk_0 z'} dz', \tag{2.26}$$

$$\gamma(z) = \int_0^z [\tau_C(z') + \tau_L(z')] dz'. \tag{2.27}$$

At the second perturbation step the values $F_2(z)$ and $G_2(z)$ are the following

$$\begin{aligned} F_2(z) &= \gamma C_1 + \beta D_1 - \frac{jk_0}{2}(\delta_1 A + \delta_2 B) \\ &\quad + \frac{jk_0}{2}(\delta_3 A + \delta_4 B), \\ G_2(z) &= -\alpha C_1 - \gamma D_1 + \frac{jk_0}{2}(\delta_5 A + \delta_6 B) \\ &\quad - \frac{jk_0}{2}(\delta_7 A + \delta_1 B), \end{aligned} \tag{2.28}$$

with

$$\delta_1(z) = \int_0^z [\tau_C(z') + \tau_L(z')]\gamma(z')dz', \tag{2.29}$$

$$\delta_2(z) = \int_0^z [\tau_C(z') + \tau_L(z')]\beta(z')dz', \tag{2.30}$$

$$\delta_3(z) = \int_0^z [\tau_C(z') - \tau_L(z')]\alpha(z')e^{+2jk_0z'}dz', \tag{2.31}$$

$$\delta_4(z) = \int_0^z [\tau_C(z') - \tau_L(z')]\gamma(z')e^{+2jk_0z'}dz', \tag{2.32}$$

$$\delta_5(z) = \int_0^z [\tau_C(z') - \tau_L(z')]\gamma(z')e^{-2jk_0z'}dz', \tag{2.33}$$

$$\delta_6(z) = \int_0^z [\tau_C(z') - \tau_L(z')]\beta(z')e^{-2jk_0z'}dz', \tag{2.34}$$

$$\delta_7(z) = \int_0^z [\tau_C(z') + \tau_L(z')]\alpha(z')dz'. \tag{2.35}$$

The unknown coefficients C_i and D_i are found by enforcing the following boundary conditions:

$$\Delta V_i(z=0) = -Z_g \Delta I_i(z=0), \tag{2.36}$$

$$\Delta V_i(z=l) = Z_L \Delta I_i(z=l). \tag{2.37}$$

Note that the source V_g itself drops out in the perturbed boundary conditions. Indeed, as already $\tilde{V}(z=0) = -Z_g\tilde{I}(z=0) + V_g$ and as this boundary condition must also remain satisfied by the total voltage and current, it follows that ΔV_i and ΔI_i must satisfy (2.36) and (2.37). As $F_i(z=0) = G_i(z=0) = 0$, the first boundary condition immediately yields

$$C_i = K_g D_i. \tag{2.38}$$

The second boundary condition then leads to

$$D_i = \frac{[Z_L \Delta I_{ip}(z=l) - \Delta V_{ip}(z=l)]e^{-jk_0l}}{(1+\frac{Z_L}{Z_0})(1-K_LK_ge^{-2jk_0l})}. \tag{2.39}$$

At this point the following remark is important. The final expressions for ΔV_{ip} and ΔI_{ip} depend on (2.25), (2.26) and (2.27). It is now possible to simplify these expressions by explicitly choosing $\gamma(z=l)$ to be zero. This can be achieved by choosing $\tilde{C}$ and $\tilde{L}$ to be the mean values over the line of $C(z)$ and $L(z)$, respectively. This is the option that was also taken in [23]. However, we have chosen to derive our expressions for the more general case aiming at applications that might be of

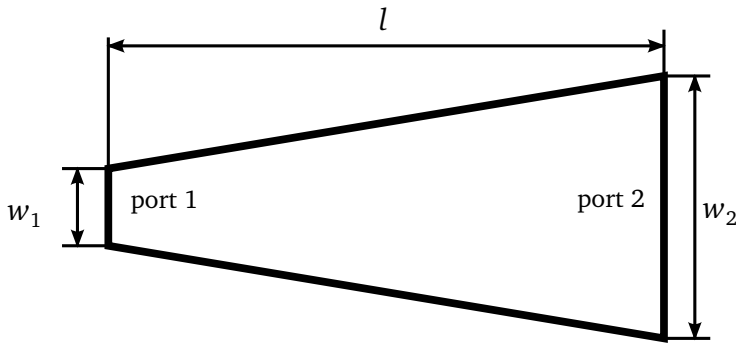

Figure 2.1: Top view of a linearly tapered microstrip line.

particular interest to high-speed designers. In high-speed design, a nominal L_{nom} and C_{nom} will typically have been selected according to the wanted impedance level and the used substrate technology. From this point of view, it might be preferable to take these nominal design values as the unperturbed ones, i.e. $\tilde{L} = L_{nom}$ and $\tilde{C} = C_{nom}$, to next evaluate the effect of variations of these nominal values due to the manufacturing process. In such a case $\gamma(z = l)$ will not be zero.

As will become clear from the numerical results, adding a second-order perturbation greatly improves the accuracy. For an intuitive understanding of the reason for this, we refer the reader to Section 3.3.1. Note that, in the single line analysis of [23], the first iteration corresponds to what is above called the unperturbed case, but only provided $\gamma(z = l)$ is selected to be zero. The second iteration in [23] then corresponds to what we call the first perturbation step.
It was not possible to derive hard mathematical conditions under which this second-order perturbation (or higher-order ones) will always increase accuracy. Nevertheless, from an engineering point of view, and as confirmed by the examples given below, it is obvious that when the variation of $L(z)$ and $C(z)$ remains reasonable, a very good accuracy is obtained. It is interesting to mention that (2.12) and (2.39) indicate that high K_L and/or K_g values should be avoided because the unperturbed solution will then exhibit a high voltage standing wave pattern. With typical applications in high-speed design in mind, such highly non-matched lines will rarely occur.

2.3 Linearly tapered microstrip line

The aforementioned technique for a single TL is validated by means of comparison with the approach described in [9]. The analytical model for lossy linearly tapered microstrip lines (LTML) of [9] thereby acts as an exact reference solution. This model results from a quasi-TEM approximation which is a special case of the more general quasi-TM approximation in [24]. The top view of the investigated struc-

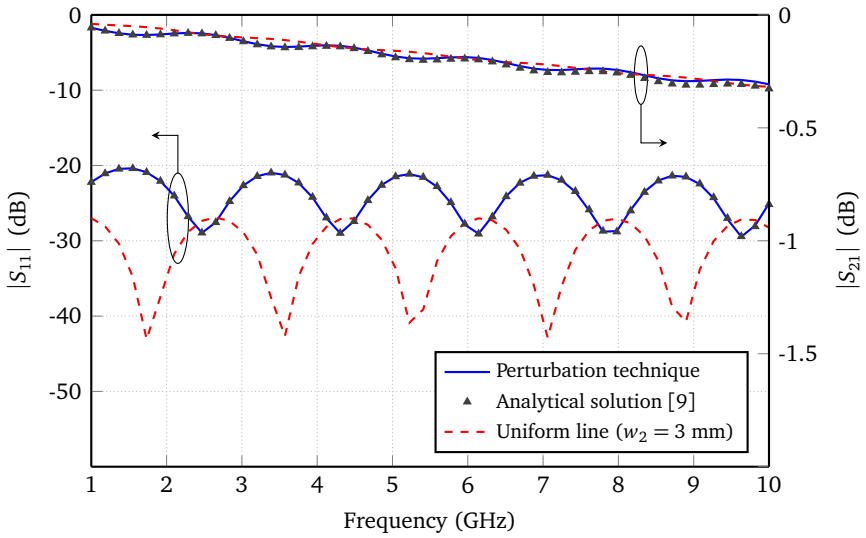

Figure 2.2: Magnitude of S_{11} and S_{21} as a function of frequency for the tapered line of Fig. 2.1 with $w_1 = 3$ mm, $w_2 = 4$ mm and $l = 50$ mm, using the novel perturbation technique with two perturbation steps and the analytical reference solution [9]. To indicate the influence of the tapering, the S-parameters of a uniform line with $w_1 = w_2 = 3$ mm are also shown.

ture is shown in Fig. 2.1. It concerns a tapered microstrip line of length $l = 50$ mm, residing on a RO4350B substrate with a thickness $h = 1.524$ mm, a relative permittivity $\varepsilon_r = 3.66$ and a loss tangent $\tan\delta = 0.003$. The metal thickness and conductivity of the taper are $t = 35$ μm and $\sigma = 5.8{\cdot}10^7$ S/m, respectively. The line width w_1 at port 1 is kept constant at 3 mm, while the width w_2 is a parameter in our study. Approximate models for the varying complex p.u.l. capacitance $C(z)$ and p.u.l. inductance $L(z)$ along the line are calculated with the technique described in [9], which leads to an analytical solution, based on Airy functions.

First, we compute the S-parameters for this tapered line, w.r.t. 50 Ω reference impedances at both ports, using the analytical solution and the novel perturbation technique with the two perturbation steps. The obtained absolute value of the S-parameters are depicted in Fig. 2.2 for the case that $w_2 = 4$ mm. From this figure, the high accuracy of the novel technique is appreciated. In addition, the S-parameters of the uniform, non-perturbed line, i.e. when $w_2 = 3$ mm, are also shown, clearly illustrating the influence of the tapering. Obviously, the novel approach is intended for NUTLs for which the nonuniformities can be considered as perturbations w.r.t. a nominal case, i.e. for cases in which ΔL and ΔC are not too large. Therefore, second, to clearly demonstrate and to quantify the accuracy of our technique as well as illustrating its limitations, a parameter study is performed. We define the relative error on S_{11} and S_{21} (taking both magnitude and phase into

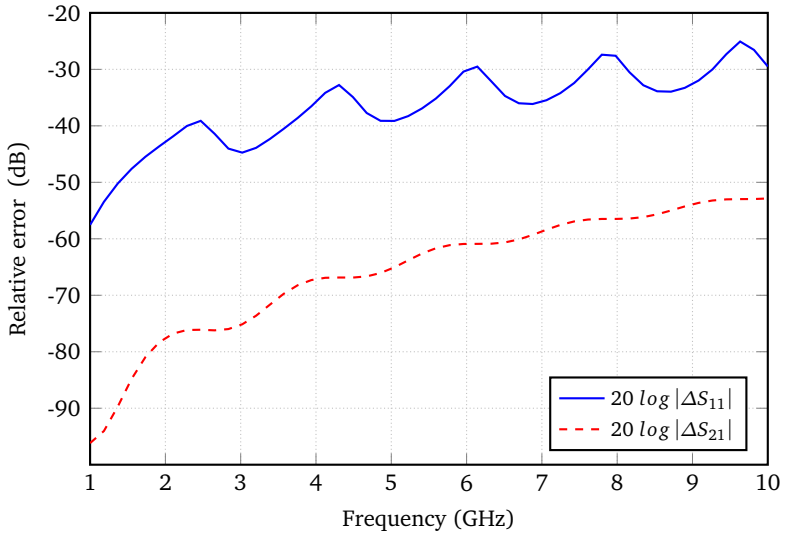

Figure 2.3: Relative errors on S_{11} and S_{21} for the case of Fig. 2.1.

account) as follows:

$$\Delta S_{11} = \left| \frac{S_{11}^{(a)} - S_{11}^{(p)}}{S_{11}^{(a)}} \right|, \tag{2.40}$$

$$\Delta S_{21} = \left| \frac{S_{21}^{(a)} - S_{21}^{(p)}}{S_{21}^{(a)}} \right|, \tag{2.41}$$

where $S_{11}^{(a)}$ and $S_{21}^{(a)}$ are the analytical results and $S_{11}^{(p)}$ and $S_{21}^{(p)}$ are obtained by means of our perturbation technique with the two perturbation steps. In Fig. 2.3, these relative errors are shown in dB over the entire frequecy range for the case when $w_2 = 4$ mm, demonstrating again the accuracy of the proposed technique. Obviously, low values of $S_{11}^{(a)}$ in the denominator of (2.40) can lead to higher relative errors. Also, the relative error on S_{21} increases for increasing frequencies and therefore, we now analyze the relative error on S_{21} at 10 GHz in our parameter study. Table 2.1 shows how changing the width w_2 influences the maximum variations of capacitance and inductance, expressed in percent w.r.t. the nominal values, and it shows the relative error ΔS_{21} at 10 GHz. As can be seen from Table 2.1, if ΔL and ΔC increase, ΔS_{21}, obviously, grows too. However, even for a ΔL and ΔC up to 30% w.r.t. the nominal values, for this example, the relative error remains limited to about 0.5%.

Third, of course, the electrical length of the line also plays an important role, as phase errors can accumulate. For the taper of Fig. 2.1, which is already rather long, i.e. 50 mm at 10 GHz, the perturbation technique gives a relative error equal to

Table 2.1: Influence of varying the width w_2 ($w_1 = 3$ mm, $l = 50$ mm)

w_2 (mm)	Maximum $\Delta L(z)$ (%)	Maximum $\Delta C(z)$ (%)	ΔS_{21} @ 10 GHz (%)
1	65.7	43.9	3.35
1.5	40.8	32.4	1.18
2	23.4	21.4	0.37
2.5	10.3	10.6	0.07
3	0	0	0
3.5	8.4	10.5	0.06
4	15.4	21.1	0.23
4.5	21.3	31.8	0.51
5	26.4	42.2	0.90

0.23% when $w_2 = 4$ mm (see Table 2.1). The relative error increases to 0.98% for an even longer taper with length $l = 100$ mm. For a shorter taper with $l = 25$ mm, the relative error becomes very small, i.e. 0.05%.

2.4 Conclusion

In this chapter, a novel perturbation technique has been presented to analyze nonuniform single transmission lines in the frequency domain. Nonuniformities were represented as perturbations w.r.t. a nominal configuration as such allowing to easily see the effect of (unwanted) perturbation during interconnect design. Starting from the Telegrapher's equations and applying two consecutive perturbations, leads to second order differential equations, describing the sought-for currents and voltages along the interconnect structure.

By way of example, the proposed method has been applied to a linearly tapered microstrip line. For such a case a high accuracy was achieved with respect to the reference analytical solution. The relative error on transmission coefficient at the highest frequency of 10 GHz remains limited to 0.5% if the deviation of the capacitance and inductance do not exceed 30% with respect to the nominal values.

References

[1] L. A. Hayden and V. K. Tripathi, "Nonuniformly coupled microstrip transversal filters for analog signal-processing", *IEEE Trans. Microw. Theory Tech.*, vol. 39, no. 1, pp. 47–53, Jan. 1991.

[2] R. N. Ghose, "Exponential transmission lines as resonators and transformers", *IEEE Trans. Microw. Theory Tech.*, vol. 5, no. 3, pp. 213–217, Jul. 1957.

[3] P. Salem, C. Wu, and M. Yagoub, "Non-uniform tapered ultra wideband directional coupler design and modern ultra wideband balun integration", in *Asia Pacific Microw. Conf., Yokohama, Japan*, Dec. 2006, pp. 891–894.

[4] T. Dhaene, L. Martens, and D. De Zutter, "Transient simulation of arbitrary nonuniform interconnection structures characterized by scattering parameters", *IEEE Circuits Syst. Mag.*, vol. 39, no. 11, pp. 928–937, Nov. 1992.

[5] Y.-W. Hsu and E. F. Kuester, "Direct synthesis of passband impedance matching with nonuniform transmission lines", *IEEE Trans. Microw. Theory Tech.*, vol. 58, no. 4, pp. 1012–1021, Apr. 2010.

[6] P. Rulikowski and J. Barrett, "Application of nonuniform transmission lines to ultra wideband pulse shaping", *IEEE Microw. Wireless Compon. Lett.*, vol. 19, no. 12, pp. 795 –797, Dec. 2009.

[7] B. Curran, I. Ndip, S. Guttowski, and H. Reichl, "A methodology for combined modeling of skin, proximity, edge, and surface roughness effects", *IEEE Trans. Microw. Theory Tech.*, vol. 58, no. 9, pp. 2448–2455, Sep. 2010.

[8] L. Vegni, F. Urbani, and A. Toscano, "Exponentially tapered non uniform transmission lines", *IEEE Trans. Magn.*, vol. 33, no. 2, pp. 1492–1495, Mar. 1997.

[9] C. Edwards, M. Edwards, S. Cheng, and C. C. Stitwell R. K. Davis, "A simplified analytic CAD model for linearly tapered microstrip lines including losses", *IEEE Trans. Microw. Theory Tech.*, vol. 52, no. 3, pp. 823–830, Mar. 2004.

[10] J. Nitsch and F. Gronwald, "Analytical solutions in nonuniform multiconductor transmission line theory", *IEEE Trans. Electromagn. Compat.*, vol. 41, no. 4, pp. 469 –479, Nov. 1999.

[11] M. Tang and J. F. Mao, "A precise time-step integration method for transient analysis of lossy nonuniform transmission lines", *IEEE Trans. Electromagn. Compat.*, vol. 50, no. 1, pp. 166–174, Feb. 2008.

[12] Q. Xu and P. Mazumder, "Accurate modeling of lossy nonuniform transmission lines by using differential quadrature methods", *IEEE Trans. Microw. Theory Tech.*, vol. 50, no. 10, pp. 2233–2246, Oct. 2002.

[13] C. R. Paul, *Analysis of Multiconductor Transmission Lines*. John Wiley & Sons, 1994.

[14] J. F. Mao and Z. F. Li, "Analysis of the time response of nonuniform multiconductor transmission lines with a method of equivalent cascaded network chain", *IEEE Trans. Microw. Theory Tech.*, vol. 40, no. 5, pp. 948–954, May 1992.

[15] N. Orhanovic, P. Wang, and V. K. Tripathi, "Time-domain simulation of uniform and nonuniform multiconductor lossy lines by the method of characteristics", *IEEE Trans. Comput.-Aided Design Integr. Circuits Syst.*, vol. 12, no. 6, pp. 900–904, Jun. 1993.

[16] J. F. Mao and Z. F. Li, "Analysis of the time response of multiconductor transmission lines with frequency-dependent losses by the method of convolution-characteristics", *IEEE Trans. Microw. Theory Tech.*, vol. 40, no. 4, pp. 637–644, Apr. 1992.

[17] M. Khalaj-Amirhosseini, "Analysis of coupled nonuniform transmission lines using Taylor's series expansion", *IEEE Trans. Electromagn. Compat.*, vol. 48, no. 3, pp. 594–600, Aug. 2006.

[18] ——, "Analysis of lossy inhomogeneous planar layers using Fourier series expansion", *IEEE Trans. Antennas Propag.*, vol. 55, no. 2, pp. 489–493, Feb. 2007.

[19] F. Y. Chang, "Waveform relaxation analysis of nonuniform lost transmission lines characterized with frequency dependent parameters", *IEEE Trans. Circuits Syst.*, vol. 38, no. 12, pp. 1484–1500, Dec. 1991.

[20] E. Gad and M. Nakhla, "Efficient simulation of nonuniform transmission lines using integrated congruence transform", *IEEE Trans. VLSI Syst.*, vol. 12, no. 12, pp. 1307 –1320, Dec. 2004.

[21] S. Barmada and M. Raugi, "Transient numerical solutions of nonuniform MTL equations with nonlinear loads by wavelet expansion in time or space domain", *IEEE Trans. Circuits Syst. I*, vol. 47, no. 8, pp. 1178 –1190, Aug. 2000.

[22] S. Javadzadeh, Z. Mardy, K. Mehrany, F. Farzaneh, and M. Fardmanesh, "Fast and efficient analysis of transmission lines with arbitrary nonuniformities of sub-wavelength scale", *IEEE Trans. Microw. Theory Tech.*, vol. 60, no. 8, pp. 2378–2384, Aug. 2012.

[23] M. Khalaj-Amirhosseini, "Analysis of nonuniform transmission lines using the equivalent sources", *Progress In Electromagnetics Research*, vol. 71, pp. 95–107, 2007.

[24] T. Demeester and D. De Zutter, "Quasi-TM transmission line parameters of coupled lossy lines based on the Dirichlet to Neumann boundary operator", *IEEE Trans. Microw. Theory Tech.*, vol. 56, no. 7, pp. 1649–1660, Jul. 2008.

3

A Two-Step Perturbation Technique to Analyse Nonuniform Differential Transmission Lines

Based on the publications:

Mykola Chernobryvko, Dries Vande Ginste and Daniël De Zutter, "A Two-Step Perturbation Technique for Nonuniform Single and Differential Lines", *IEEE Transactions on Microwave Theory and Techniques, MTT*, Vol.61, no.5, pp. 1758-1767, May 2013

Mykola Chernobryvko, Dries Vande Ginste and Daniël De Zutter, "A Perturbation Technique to Analyze The Influence of Fiber Weave Effects on Differential Signaling", *IEEE 22nd Conference on Electrical Performance of Electronic Packaging and Systems (EPEPS)*, San Jose, CA, USA, 27-30 Oct. 2013, pp. 15-18

★ ★ ★

A novel two-step perturbation technique to analyze nonuniform differential transmission lines in the frequency domain is presented. Its accuracy and efficiency is demonstrated for a pair coupled lines with random nonuniformities. We also study differential signaling via a pair of striplines in a substrate that is comprised of an epoxy/fiberglass woven composite structure. The transmission characteristics, which are deteriorated due to the presence of the fiber weave, are analyzed via an efficient modeling technique for nonuniform transmission lines. This technique is based on the solution of the pertinent differential equations using a perturbation approach. For a challenging application example, it is shown that the unavoidable phase errors can be controlled by subdividing electrically long lines into smaller pieces, as such increasing accuracy whilst maintaining efficiency. Moreover, the necessity of adopting a two-step perturbation in order to get a good accuracy is also illustrated.

3.1 Introduction

Nonuniform differential transmission lines are found in various applications, such as filters, impedance transformers, etc. The modeling of these interconnects has, however, always been a challenging problem. Due to the varying p.u.l. parameters along the line, the differential equations describing them cannot be solved analytically, except for some very special cases.

In this chapter, we extend the perturbation technique of the previous chapter to the differential line case. We focus on on the theoretical description of the technique and on demonstrating its applicability and limitations by applying it to a pair of coupled lines with random nonuniformities. Moreover, the perturbation approach is also applied to a very important, but challenging, application example. Leveraging the novel perturbation technique, we analyze differential signaling using a pair of striplines embedded in a substrate that is comprised of an epoxy/fiberglass woven composite structure [1], [2]. In such a commonly used substrate, it is very likely that one trace of the differential pair is located mainly in the epoxy resin with low dielectric constant, while the other trace is located close to the glass fiber with a high dielectric constant. As the two traces "see" a different permittivity, a differential skew between the lines is observed. This skew results in insertion loss suck-outs of the transmitted (differential) signal. Additionally, the imbalance leads to conversion from the differential mode to the common mode [3]. All this may prohibit the use of these substrates at very high frequencies, or differently put, it poses a limit on the maximum (electrical) length of the lines.

The organization of this chapter is as follows. Section 3.2 describes the formalism of the perturbation technique for differential lines. The theory is validated and illustrated in Section 3.3. The examples comprise the application of the proposed technique to a pair of nonuniform coupled lines with random nonuniformities (Sec-

tion 3.3.1) and to differential lines embedded in a substrate composed of woven glass fibers(Section 3.3.2). Conlusions are presented in Section 3.4.

3.2 Perturbation solution for a differential line pair

We analyse nonuniform differential lines within the framework of the quasi-TM approach and in the frequency domain (with the $e^{j\omega t}$ dependency suppressed). Consider voltage and current column vectors $\mathcal{V} = [V_1\, V_2]^T$ and $\mathcal{I} = [I_1\, I_2]^T$, holding the two voltages and two currents along the lines. To simplify the notations we work with 2×2 complex p.u.l. inductance $\mathcal{L}$ and capacitance $\mathcal{C}$ matrices, i.e. the p.u.l. resistance $\mathcal{R}$ and conductance $\mathcal{G}$ are understood to be part of $\mathcal{L}$ and $\mathcal{C}$ ($\mathcal{L} = \mathcal{L}_{lossless} + \frac{\mathcal{R}}{j\omega}$ and $\mathcal{C} = \mathcal{C}_{lossless} + \frac{\mathcal{G}}{j\omega}$). Our starting point is the well-known Telegrapher's equations:

$$\frac{d\mathcal{V}(z)}{dz} = -j\omega\mathcal{L}(z)\mathcal{I}(z), \tag{3.1}$$

$$\frac{d\mathcal{I}(z)}{dz} = -j\omega\mathcal{C}(z)\mathcal{V}(z), \tag{3.2}$$

with z being the signal propagation direction. To perform a perturbation technique, the following expansions are introduced:

$$\begin{aligned}
\mathcal{V}(z) &= \tilde{\mathcal{V}}(z) + \Delta\mathcal{V}_1(z) + \Delta\mathcal{V}_2(z) + ...,\\
\mathcal{I}(z) &= \tilde{\mathcal{I}}(z) + \Delta\mathcal{I}_1(z) + \Delta\mathcal{I}_2(z) + ...,\\
\mathcal{C}(z) &= \tilde{\mathcal{C}} + \Delta\mathcal{C}(z),\\
\mathcal{L}(z) &= \tilde{\mathcal{L}} + \Delta\mathcal{L}(z).
\end{aligned} \tag{3.3}$$

The leading terms of the series expansions (3.3), i.e. the voltage $\tilde{\mathcal{V}}(z)$ and current $\tilde{\mathcal{I}}(z)$, are labeled as the *unperturbed* values. The remaining terms are perturbations of order one, two, etc. $\mathcal{C}(z)$ and $\mathcal{L}(z)$ in (3.3) are simply written as the sum of a constant part and a place-dependent part. Here, $\tilde{\mathcal{C}}$ and $\tilde{\mathcal{L}}$ are the unperturbed values. $\Delta\mathcal{C}(z)$ and $\Delta\mathcal{L}(z)$ are the variations of the capacitance and inductance along the line which remain after subtracting the constant martrices $\tilde{\mathcal{C}}$ and $\tilde{\mathcal{L}}$ from $\mathcal{C}(z)$ and $\mathcal{L}(z)$ respectively. Remark that $\tilde{\mathcal{C}}$ and $\tilde{\mathcal{L}}$ are not necessarily the mean values of $\mathcal{C}$ and $\mathcal{L}$ over the line. We only suppose that $\Delta\mathcal{C}(z)$ and $\Delta\mathcal{L}(z)$ are small enough with respect to $\tilde{\mathcal{C}}$ and $\tilde{\mathcal{L}}$. The unperturbed matrices can be written as:

$$\tilde{\mathcal{C}} = \begin{pmatrix} C_a & -C_b \\ -C_b & C_a \end{pmatrix} \qquad \tilde{\mathcal{L}} = \begin{pmatrix} L_a & L_b \\ L_b & L_a \end{pmatrix}. \tag{3.4}$$

Substituting (3.3) into (3.1) and (3.2) and collecting terms of the same order for the unperturbed quantities we have:

$$\frac{d\tilde{\mathcal{V}}}{dz} = -j\omega\tilde{\mathcal{L}}\tilde{\mathcal{I}}, \tag{3.5}$$

$$\frac{d\tilde{\mathcal{I}}}{dz} = -j\omega\tilde{\mathcal{C}}\tilde{\mathcal{V}}, \tag{3.6}$$

while the perturbations of order one and two satisfy

$$\frac{d\Delta\mathcal{V}_1}{dz} = -j\omega\tilde{\mathcal{L}}\Delta\mathcal{I}_1 - j\omega\Delta\mathcal{L}\tilde{\mathcal{I}}, \tag{3.7}$$

$$\frac{d\Delta\mathcal{I}_1}{dz} = -j\omega\tilde{\mathcal{C}}\Delta\mathcal{V}_1 - j\omega\Delta\mathcal{C}\tilde{\mathcal{V}}, \tag{3.8}$$

$$\frac{d\Delta\mathcal{V}_2}{dz} = -j\omega\tilde{\mathcal{L}}\Delta\mathcal{I}_2 - j\omega\Delta\mathcal{L}\Delta\mathcal{I}_1, \tag{3.9}$$

$$\frac{d\Delta\mathcal{I}_2}{dz} = -j\omega\tilde{\mathcal{C}}\Delta\mathcal{V}_2 - j\omega\Delta\mathcal{C}\Delta\mathcal{V}_1. \tag{3.10}$$

3.2.1 Excitation and termination of the differential line pair

In order to remain sufficiently general, consider the generalised Thevenin equivalent of the excitation of the line pair at $z = 0$ as shown in Fig. 3.1. V_a and I_a are the voltage and current at line 1 and V_b and I_b are the corresponding quantities at line 2. Sources and impedances are arbitrary. Rather lengthy calculations show that the following relationships between the voltages and the currents hold:

$$\begin{aligned}
\frac{V_a - V_b}{2} &= \frac{Z_3}{2(Z_1+Z_2+Z_3)}\Big[(Z_2-Z_1)\frac{I_a+I_b}{2} \\
&- (Z_2+Z_1)\frac{I_a-I_b}{2} \\
&+ V_{1s} - V_{2s} - \frac{Z_1+Z_2}{Z_3}V_{3s}\Big], \\
\frac{V_a + V_b}{2} &= \frac{1}{2(Z_1+Z_2+Z_3)}\Big[Z_3(Z_2-Z_1)\frac{I_a-I_b}{2} \\
&- (4Z_1Z_2 + Z_2Z_3 + Z_1Z_3)\frac{I_a+I_b}{2} \\
&+ (2Z_2+Z_3)V_{1s} + (2Z_1+Z_3)V_{2s} \\
&+ (Z_2-Z_1)V_{3s}\Big].
\end{aligned} \tag{3.11}$$

To allow further calculations to deal with mode coupling, we have expressed the relationships between voltages and currents at the source in terms of even and odd contributions. At $z = l$ the differential line pair is terminated in the circuit shown

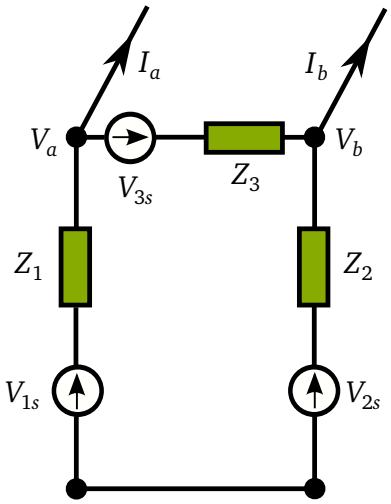

Figure 3.1: Excitation of the differential line pair.

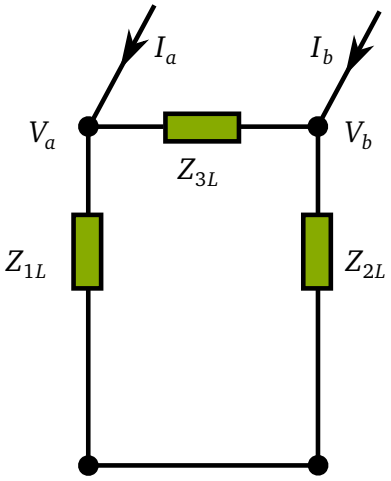

Figure 3.2: Termination of the differential line pair.

in Fig. 3.2. We have retained the same notation for the voltages and the currents but remark that the direction in which the currents flow has been reversed. The

relationships between the voltages and the currents readily follow from (3.11):

$$\begin{aligned}
\frac{V_a - V_b}{2} &= \frac{-Z_{3L}}{2(Z_{1L}+Z_{2L}+Z_{3L})}[(Z_{2L}-Z_{1L})\frac{I_a+I_b}{2} \\
&- (Z_{2L}+Z_{1L})\frac{I_a-I_b}{2}], \\
\frac{V_a + V_b}{2} &= \frac{-1}{2(Z_{1L}+Z_{2L}+Z_{3L})}[Z_{3L}(Z_{2L}-Z_{1L})\frac{I_a-I_b}{2} \\
&- (4Z_{1L}Z_{2L}+Z_{2L}Z_{3L}+Z_{1L}Z_{3L})\frac{I_a+I_b}{2}]. \qquad (3.12)
\end{aligned}$$

To simplify further calculations, even and odd voltages and currents are introduced:

$$\begin{aligned}
V_e(z) &= \frac{V_a+V_b}{2}, & V_o(z) &= \frac{V_a-V_b}{2}, \\
I_e(z) &= \frac{I_a+I_b}{2}, & I_o(z) &= \frac{I_a-I_b}{2}. \qquad (3.13)
\end{aligned}$$

With this notation, (3.11) and (3.12) can be recast as:

$$\begin{aligned}
V_e(z=0) &= -Z_{ee}I_e(z=0) - Z_{eo}I_o(z=0) + V_{se}, \\
V_o(z=0) &= -Z_{oe}I_e(z=0) - Z_{oo}I_o(z=0) + V_{so}, \\
V_e(z=l) &= Z_{eeL}I_e(z=l) + Z_{eoL}I_o(z=l), \\
V_o(z=l) &= Z_{oeL}I_e(z=l) + Z_{ooL}I_o(z=l), \qquad (3.14)
\end{aligned}$$

with

$$\begin{aligned}
Z_{oe} = Z_{eo} &= \frac{Z_3}{2(Z_1+Z_2+Z_3)}(Z_1-Z_2), \\
Z_{oo} &= \frac{Z_3}{2(Z_1+Z_2+Z_3)}(Z_2+Z_1), \\
V_{so} &= \frac{Z_3}{2(Z_1+Z_2+Z_3)}[V_{1s}-V_{2s}-\frac{Z_1+Z_2}{Z_3}V_{3s}], \\
Z_{ee} &= \frac{1}{2(Z_1+Z_2+Z_3)}(4Z_1Z_2+Z_2Z_3+Z_1Z_3), \\
V_{se} &= \frac{1}{2(Z_1+Z_2+Z_3)}[(2Z_2+Z_3)V_{1s} \\
&\quad +(2Z_1+Z_3)V_{2s}+(Z_2-Z_1)V_{3s}]. \qquad (3.15)
\end{aligned}$$

The corresponding values at the load side are readily obtained by replacing Z_1, Z_2 and Z_3 by Z_{1L}, Z_{2L} and Z_{3L} resp. For further use, (3.14) is finally rewritten in matrix form as

$$\mathcal{V}(z=0) + \mathcal{Z}_s\mathcal{I}(z=0) = \mathcal{V}_s, \qquad (3.16)$$

with

$$\mathcal{Z}_s = \begin{pmatrix} Z_{ee} & Z_{eo} \\ Z_{oe} & Z_{oo} \end{pmatrix}, \qquad \mathcal{V}_s = \begin{pmatrix} V_{se} \\ V_{so} \end{pmatrix}. \tag{3.17}$$

At the load side, the corresponding expression is

$$\mathcal{V}(z = l) = \mathcal{Z}_L \mathcal{I}(z = l). \tag{3.18}$$

Remark that both $\mathcal{Z}_s$ and $\mathcal{Z}_L$ are symmetric and also $\mathcal{Z}_s = \mathcal{Z}_L$.

3.2.2 Solution for the unperturbed signal

Completely analogues to the reasoning followed in Chapter 2, the unperturbed wave equation for $\tilde{\mathcal{V}}$ becomes:

$$\frac{d^2\tilde{\mathcal{V}}}{dz^2} + \omega^2(\tilde{\mathcal{L}}\tilde{\mathcal{C}})\tilde{\mathcal{V}} = 0. \tag{3.19}$$

To solve (3.19), $\tilde{\mathcal{V}}$ is expanded in the eigenvectors V_1 and V_2 of $(\tilde{\mathcal{L}}\tilde{\mathcal{C}})$:

$$\tilde{\mathcal{V}} = \alpha_1 V_1 + \alpha_1 V_2, \tag{3.20}$$

with

$$(\tilde{\mathcal{L}}\tilde{\mathcal{C}})V_1 = \lambda_1 V_1, \tag{3.21}$$
$$(\tilde{\mathcal{L}}\tilde{\mathcal{C}})V_2 = \lambda_2 V_2, \tag{3.22}$$

where λ_1 and λ_2 are the eigenvalue of the eigenvectors V_1 and V_2 respectively. Substituting (3.20) into (3.19) shows that

$$\sum_{i=1}^{2} \frac{d^2\alpha_i}{dz^2} V_i + \omega^2 \sum_{i=1}^{2} \lambda_i \alpha_i V_i = 0, \tag{3.23}$$

At this point it should be noted that the voltage eigenvectors are in general not orthogonal as the product of $\tilde{\mathcal{L}}\tilde{\mathcal{C}}$ of two symmetric matrices is in general not symmetric. However, following (3.1) and (3.2), the currents satisfy

$$\frac{d^2\mathcal{I}}{dz^2} + \omega^2(\tilde{\mathcal{C}}\tilde{\mathcal{L}})\mathcal{I} = 0. \tag{3.24}$$

Let us denote the current eigenvectors as I_i. These are the eigenvectors of $\tilde{\mathcal{C}}\tilde{\mathcal{L}}$. One can now proof the following (see Appendix A): the eigenvalues λ_i of voltages and currents are identical and the eigenvectors of voltages and currents, i.e. V_i and I_i are orthognal (provided all eigenvalues are distinct). In the sequel we will suppose that the two sets of orthogonal eigenvectors have been chosen such that

they are orthonormal i.e. $(V_i)^T I_j = \delta_{ij}$ with δ_{ij} the Kronecker delta. Multiplying (3.23) with $(I_j)^T$ thus shows that

$$\frac{d^2\alpha_1}{dz^2} + \omega^2\lambda_1\alpha_1 = 0, \tag{3.25}$$

$$\frac{d^2\alpha_2}{dz^2} + \omega^2\lambda_2\alpha_2 = 0, \tag{3.26}$$

i.e., the first and the second unperturbed eigenvector amplitude satisfy a wave equation with wave number $k_1 = \omega\sqrt{\lambda_1}$ and $k_2 = \omega\sqrt{\lambda_2}$ respectively. Hence, the corresponding mode velocities are $v_1 = \frac{1}{\sqrt{\lambda_1}}$ and $v_2 = \frac{1}{\sqrt{\lambda_2}}$.
To start the analysis we need the two eigenvectors V_1 and V_2. One readily proves that

$$V_1 = \frac{1}{2}\begin{pmatrix}1\\1\end{pmatrix} \qquad V_2 = \frac{1}{2}\begin{pmatrix}1\\-1\end{pmatrix}. \tag{3.27}$$

The corresponding eigenvalues are

$$\begin{aligned}\lambda_1 &= (L_a + L_b)(C_a - C_b),\\ \lambda_2 &= (L_a - L_b)(C_a + C_b).\end{aligned} \tag{3.28}$$

The unperturbed voltage amplitudes are the solutions to (3.25) and (3.26), i.e.

$$\begin{aligned}\alpha_1 &= A_1 e^{-jk_1 z} + B_1 e^{+jk_1 z},\\ \alpha_2 &= A_2 e^{-jk_2 z} + B_2 e^{+jk_2 z},\end{aligned} \tag{3.29}$$

with $k_i = \omega\sqrt{\lambda_i}$. Hence, the unperturbed voltage become:

$$\tilde{\mathcal{V}} = (A_1 e^{-jk_1 z} + B_1 e^{+jk_1 z})V_1 + (A_2 e^{-jk_2 z} + B_2 e^{+jk_2 z})V_2. \tag{3.30}$$

We also need the corresponding currents. From (3.1) we see that:

$$\tilde{\mathcal{I}} = -\frac{1}{j\omega}\mathcal{L}^{-1}\frac{d\tilde{\mathcal{V}}}{dz}. \tag{3.31}$$

As the voltage vector is the superposition of a common (even) mode contribution and a differential (odd) mode contribution, we need to evaluate (3.31) for $\mathcal{V} = V_1$ and for $\mathcal{V} = V_2$. Remark that:

$$\begin{aligned}\mathcal{L}^{-1}V_1 &= \frac{1}{L_a + L_b}V_1,\\ \mathcal{L}^{-1}V_2 &= \frac{1}{L_a - L_b}V_2.\end{aligned} \tag{3.32}$$

This finally results in the current:

$$\begin{aligned}\tilde{\mathcal{I}} &= (A_1 e^{-jk_1 z} - B_1 e^{+jk_1 z})V_1/Z_e\\ &+ (A_2 e^{-jk_2 z} - B_2 e^{+jk_2 z})V_2/Z_o,\end{aligned} \tag{3.33}$$

with the even and odd mode impedances given by

$$Z_e = \sqrt{\frac{L_a + L_b}{C_a - C_b}},$$
$$Z_o = \sqrt{\frac{L_a - L_b}{C_a + C_b}}. \tag{3.34}$$

Remark that the common mode and differential mode impedances are given by $Z_c = Z_e/2$ and $Z_d = 2Z_o$. For later use we rewrite the current as:

$$\tilde{\mathcal{I}} = \gamma_1 V_1/Z_e + \gamma_2 V_2/Z_o \tag{3.35}$$

In order to determine A_1, B_1, A_2 and B_2, boundary conditions (3.16) and (3.18) must be enforced. With the above notations, (3.30) and (3.33) at $z = 0$ can be written as:

$$\tilde{\mathcal{V}}(z=0) = \begin{pmatrix} V_e(z=0) \\ V_o(z=0) \end{pmatrix} = \mathcal{T}_V \mathcal{X},$$
$$\tilde{\mathcal{I}}(z=0) = \begin{pmatrix} I_e(z=0) \\ I_o(z=0) \end{pmatrix} = \mathcal{Y}_m \mathcal{T}_I \mathcal{X}, \tag{3.36}$$

where the column matrix $\mathcal{X} = (A_1 B_1 A_2 B_2)^T$ holds the as yet unknown coefficients introduced in (3.29) and with

$$\mathcal{T}_V = \begin{pmatrix} 1 & 1 & 0 & 0 \\ 0 & 0 & 1 & 1 \end{pmatrix},$$
$$\mathcal{T}_I = \begin{pmatrix} 1 & -1 & 0 & 0 \\ 0 & 0 & 1 & -1 \end{pmatrix},$$
$$\mathcal{Y}_m = \begin{pmatrix} \frac{1}{Z_e} & 0 \\ 0 & \frac{1}{Z_0} \end{pmatrix}. \tag{3.37}$$

Finally, (3.36) and (3.16) lead to

$$\mathcal{T}_V \mathcal{X} + \mathcal{Z}_s \mathcal{Y}_m \mathcal{T}_I \mathcal{X} = \mathcal{V}_s. \tag{3.38}$$

Turning to the load side at $z = l$, (3.30) and (3.33) at $z = l$ become:

$$\tilde{\mathcal{V}}(z=l) = \begin{pmatrix} V_e(z=l) \\ V_o(z=l) \end{pmatrix} = \mathcal{P}\mathcal{U}_V \mathcal{X},$$
$$\tilde{\mathcal{I}}(z=l) = \begin{pmatrix} I_e(z=l) \\ I_o(z=l) \end{pmatrix} = \mathcal{Y}_m \mathcal{P}\mathcal{U}_I \mathcal{X}, \tag{3.39}$$

with

$$\mathcal{U}_V = \begin{pmatrix} 1 & e^{+2jk_1 l} & 0 & 0 \\ 0 & 0 & 1 & e^{+2jk_2 l} \end{pmatrix},$$
$$\mathcal{U}_I = \begin{pmatrix} 1 & -e^{+2jk_1 l} & 0 & 0 \\ 0 & 0 & 1 & -e^{+2jk_2 l} \end{pmatrix},$$
$$\mathcal{P} = \begin{pmatrix} e^{-jk_1 l} & 0 \\ 0 & e^{-jk_2 l} \end{pmatrix}. \tag{3.40}$$

Now, (3.40) and (3.18) lead to

$$\mathcal{P}\mathcal{U}_V \mathcal{X} = \mathcal{Z}_L \mathcal{Y}_m \mathcal{P}\mathcal{U}_I \mathcal{X}. \tag{3.41}$$

Combining (3.38) and (3.41) yields the final set of equations that has to be solved:

$$\begin{pmatrix} \mathcal{T}_V + \mathcal{Z}_s \mathcal{Y}_m \mathcal{T}_I \\ \mathcal{P}\mathcal{U}_V - \mathcal{Z}_L \mathcal{Y}_m \mathcal{P}\mathcal{U}_I \end{pmatrix} \mathcal{X} = \begin{pmatrix} \mathcal{V}_s \\ 0 \end{pmatrix}. \tag{3.42}$$

If the impedance termination at source and load side remains symmetric, i.e. $Z_1 = Z_2$ and $Z_{1L} = Z_{2L}$, matrices $\mathcal{Z}_s$ and $\mathcal{Z}_L$ become diagonal and this will of course remain so for their product with $\mathcal{Y}_m$. As $\mathcal{P}$ in (3.42) is also diagonal, it commutes with $\mathcal{Z}_L \mathcal{Y}_m$ and hence, in that particular case, $\mathcal{P}$ could be left out altogether.

3.2.3 First order perturbation solution

Let us now turn to the wave equation satisfied by the first-order perturbed voltage $\Delta\mathcal{V}_1$ obtained using (3.7) and (3.8):

$$\frac{d^2 \Delta\mathcal{V}_1}{dz^2} + \omega^2(\tilde{\mathcal{L}}\tilde{\mathcal{C}})\Delta\mathcal{V}_1 = -\omega^2(\tilde{\mathcal{L}}\Delta\mathcal{C})\tilde{\mathcal{V}} - j\omega\frac{d(\Delta\mathcal{L}\tilde{\mathcal{I}})}{dz}. \tag{3.43}$$

The perturbations $\Delta\mathcal{C}$ and $\Delta\mathcal{L}$ are represented as

$$\Delta\mathcal{C} = \begin{pmatrix} \Delta C_{a1} & -\Delta C_b \\ -\Delta C_b & \Delta C_{a2} \end{pmatrix}, \tag{3.44}$$

$$\Delta\mathcal{L} = \begin{pmatrix} \Delta L_{a1} & \Delta L_b \\ \Delta L_b & \Delta L_{a2} \end{pmatrix}. \tag{3.45}$$

We can only assert that the above matrices are symmetric but the entries of the matrices can either be positive or negative. We do know that $\tilde{\mathcal{C}} + \Delta\mathcal{C}$ and $\tilde{\mathcal{L}} + \Delta\mathcal{L}$ must have all the properties of a proper capacitance matrix in each point along the propagation direction.

To solve (3.43) we again expand the sought for $\Delta\mathcal{V}_1$ in the eigenvectors V_1 and V_2 used in the unperturbed case:

$$\Delta\mathcal{V}_1 = \beta_1 V_1 + \beta_2 V_2. \tag{3.46}$$

Substituting (3.20) and (3.46) into (3.43) and using the orthonormality of the voltage and current eigenvectors, leads to

$$\frac{d^2\beta_i}{dz^2} + \omega^2\lambda_i\beta_i = -\omega^2 \sum_{j=1}^{2} \alpha_j I_i^T(\tilde{\mathcal{L}}\Delta\mathcal{C})V_j - j\omega \sum_{j=1}^{2} I_i^T \frac{d(\gamma_j \Delta\mathcal{L} V_j/Z_j)}{dz}. \tag{3.47}$$

with $Z_i = Z_e$ for $i = 1$ and $Z_i = Z_o$ for $i = 2$. The superscript "T" stands for the transpose and we have assumed that the eigenvectors are distinct (which will be the case in our technological applications). We conclude that the amplitudes of the eigenvector expansion of the first-order perturbation satisfy the same wave equations as the corresponding amplitudes for the unperturbed case. However, these wave equations are no longer sourceless but have a place-dependent source. This source is a function of *all* unperturbed modes. In view of the differential signal propagation we are interested in, we will not pursue the general case here but readily turn to our target system.
Let us rewrite (3.44) and (3.45) as:

$$\begin{aligned}
\Delta\mathcal{C} &= \begin{pmatrix} \frac{\Delta C_{a1}+\Delta C_{a2}}{2} & -\Delta C_b \\ -\Delta C_b & \frac{\Delta C_{a1}+\Delta C_{a2}}{2} \end{pmatrix} \\
&+ \begin{pmatrix} \frac{\Delta C_{a1}-\Delta C_{a2}}{2} & 0 \\ 0 & -\frac{\Delta C_{a1}-\Delta C_{a2}}{2} \end{pmatrix} \\
&= \mathcal{C}_1 + \mathcal{C}_2.
\end{aligned} \tag{3.48}$$

and

$$\begin{aligned}
\Delta\mathcal{L} &= \begin{pmatrix} \frac{\Delta L_{a1}+\Delta L_{a2}}{2} & \Delta L_b \\ \Delta L_b & \frac{\Delta L_{a1}+\Delta L_{a2}}{2} \end{pmatrix} \\
&+ \begin{pmatrix} \frac{\Delta L_{a1}-\Delta L_{a2}}{2} & 0 \\ 0 & -\frac{\Delta L_{a1}-\Delta L_{a2}}{2} \end{pmatrix} \\
&= \mathcal{L}_1 + \mathcal{L}_2.
\end{aligned} \tag{3.49}$$

In the right-hand side of (3.47) we need $(\tilde{\mathcal{L}}\Delta\mathcal{C})V_j$ and $\Delta\mathcal{L}V_j$ for $j = 1, 2$. We immediately remark that

$$\begin{aligned}
(\tilde{\mathcal{L}}\mathcal{C}_1)V_1 &= \mu_1 V_1, & \mathcal{L}_1 V_1 &= \theta_1 V_1, \\
(\tilde{\mathcal{L}}\mathcal{C}_1)V_2 &= \mu_2 V_2, & \mathcal{L}_2 V_2 &= \theta_2 V_1, \\
(\tilde{\mathcal{L}}\mathcal{C}_2)V_1 &= \kappa_1 V_2, & \mathcal{L}_2 V_1 &= \theta_2 V_2, \\
(\tilde{\mathcal{L}}\mathcal{C}_2)V_2 &= \kappa_2 V_1, & \mathcal{L}_1 V_2 &= \theta_3 V_2,
\end{aligned} \tag{3.50}$$

with

$$\begin{aligned}
\mu_1 &= (L_a + L_b)(\frac{\Delta C_{a1} + \Delta C_{a2}}{2} - \Delta C_b),\\
\mu_2 &= (L_a - L_b)(\frac{\Delta C_{a1} + \Delta C_{a2}}{2} + \Delta C_b),\\
\kappa_1 &= (L_a - L_b)(\frac{\Delta C_{a1} - \Delta C_{a2}}{2}),\\
\kappa_2 &= (L_a + L_b)(\frac{\Delta C_{a1} - \Delta C_{a2}}{2}),\\
\theta_1 &= \frac{\Delta L_{a1} + \Delta L_{a2}}{2} + \Delta L_b,\\
\theta_2 &= \frac{\Delta L_{a1} - \Delta L_{a2}}{2},\\
\theta_3 &= \frac{\Delta L_{a1} + \Delta L_{a2}}{2} - \Delta L_b.
\end{aligned} \tag{3.51}$$

From the above, we see that $\mathcal{C}_2$ and $\mathcal{L}_2$ are responsable for the coupling between the common and the differential mode.
The perturbed common mode, i.e. (3.47) for $i = 1$, satisfies

$$\begin{aligned}
\frac{d^2\beta_1}{dz^2} + \omega^2\lambda_1\beta_1 =\\
-\omega^2[\alpha_1 V_1^T(\tilde{\mathcal{L}}\mathcal{C}_1 + \tilde{\mathcal{L}}\mathcal{C}_2)V_1 + \alpha_2 V_1^T(\tilde{\mathcal{L}}\mathcal{C}_1 + \tilde{\mathcal{L}}\mathcal{C}_2)V_2]\\
-j\omega\left[\frac{1}{Z_e}\frac{d(\gamma_1 V_1^T(\mathcal{L}_1 + \mathcal{L}_2)V_1}{dz} + \frac{1}{Z_o}\frac{d(\gamma_2 V_1^T(\mathcal{L}_1 + \mathcal{L}_2)V_2}{dz}\right].
\end{aligned} \tag{3.52}$$

The perturbed differential mode, i.e. (3.47) for $i = 2$, satisfies

$$\begin{aligned}
\frac{d^2\beta_2}{dz^2} + \omega^2\lambda_2\beta_2 =\\
-\omega^2[\alpha_1 V_2^T(\tilde{\mathcal{L}}\mathcal{C}_1 + \tilde{\mathcal{L}}\mathcal{C}_2)V_1 + \alpha_2 V_2^T(\tilde{\mathcal{L}}\mathcal{C}_1 + \tilde{\mathcal{L}}\mathcal{C}_2)V_2]\\
-j\omega\left[\frac{1}{Z_e}\frac{d(\gamma_1 V_2^T(\mathcal{L}_1 + \mathcal{L}_2)V_1}{dz} + \frac{1}{Z_o}\frac{d(\gamma_2 V_2^T(\mathcal{L}_1 + \mathcal{L}_2)V_2}{dz}\right]
\end{aligned} \tag{3.53}$$

.

Taking into account (3.50), the above expressions become

$$\begin{aligned}
\frac{d^2\beta_1}{dz^2} + \omega^2\lambda_1\beta_1 &= -\omega^2[\alpha_1\mu_1 + \alpha_2\kappa_2] - j\omega\left[\frac{1}{Z_e}\frac{d(\gamma_1\theta_1)}{dz} + \frac{1}{Z_o}\frac{d(\gamma_2\theta_2)}{dz}\right],\\
\frac{d^2\beta_2}{dz^2} + \omega^2\lambda_2\beta_2 &= -\omega^2[\alpha_1\kappa_1 + \alpha_2\mu_2] - j\omega\left[\frac{1}{Z_e}\frac{d(\gamma_1\theta_2)}{dz} + \frac{1}{Z_o}\frac{d(\gamma_2\theta_3)}{dz}\right].
\end{aligned} \tag{3.54}$$

The amplitudes of the modal voltages satisfy (3.54). These equations can be solved using the same technique as in Section 2.2.2 for a single line. The final result is

$$\begin{aligned}\beta_1 &= P_1 e^{-jk_1 z} + Q_1 e^{+jk_1 z} + a_1(z)e^{-jk_1 z} + b_1(z)e^{+jk_1 z},\\ \beta_2 &= P_2 e^{-jk_2 z} + Q_2 e^{+jk_2 z} + a_2(z)e^{-jk_2 z} + b_2(z)e^{+jk_2 z},\end{aligned} \tag{3.55}$$

with

$$\begin{aligned}a_1(z) &= -\frac{j\omega}{2}\int_0^z e^{+jk_1 z'} s_{1a}(z')dz',\\ b_1(z) &= \frac{j\omega}{2}\int_0^z e^{-jk_1 z'} s_{1b}(z')dz',\\ a_2(z) &= -\frac{j\omega}{2}\int_0^z e^{+jk_2 z'} s_{2a}(z')dz',\\ b_2(z) &= \frac{j\omega}{2}\int_0^z e^{-jk_2 z'} s_{2b}(z')dz',\\ s_{1a}(z) &= \frac{\omega}{k_1}[\alpha_1\mu_1 + \alpha_2\kappa_2] + \frac{1}{Z_e}\gamma_1\theta_1 + \frac{1}{Z_o}\gamma_2\theta_2,\\ s_{1b}(z) &= \frac{\omega}{k_1}[\alpha_1\mu_1 + \alpha_2\kappa_2] - \frac{1}{Z_e}\gamma_1\theta_1 - \frac{1}{Z_o}\gamma_2\theta_2,\\ s_{2a}(z) &= \frac{\omega}{k_2}[\alpha_1\kappa_1 + \alpha_2\mu_2] + \frac{1}{Z_e}\gamma_1\theta_2 + \frac{1}{Z_o}\gamma_2\theta_3,\\ s_{2b}(z) &= \frac{\omega}{k_2}[\alpha_1\kappa_1 + \alpha_2\mu_2] - \frac{1}{Z_e}\gamma_1\theta_2 - \frac{1}{Z_o}\gamma_2\theta_3.\end{aligned} \tag{3.56}$$

The contributions in the as yet undetermined coefficients P_i and Q_i are general solutions of the homogeneous differential equation, while the terms in a_i and b_i form the particular solution. Using the above and (3.1), which remains valid for the voltage and current perturbation, the following final results are found for the first perturbation step:

$$\begin{aligned}\Delta\mathcal{V}_1 &= [P_1 e^{-jk_1 z} + Q_1 e^{+jk_1 z}]V_1 + [a_1(z)e^{-jk_1 z} + b_1(z)e^{+jk_1 z}]V_1\\ &+ [P_2 e^{-jk_2 z} + Q_2 e^{+jk_2 z}]V_2 + [a_2(z)e^{-jk_2 z} + b_2(z)e^{+jk_2 z}]V_2,\\ \Delta\mathcal{I}_1 &= [P_1 e^{-jk_1 z} - Q_1 e^{+jk_1 z}]V_1/Z_e + [a_1(z)e^{-jk_1 z} - b_1(z)e^{+jk_1 z}]V_1/Z_e\\ &+ [P_2 e^{-jk_2 z} - Q_2 e^{+jk_2 z}]V_2/Z_o + [a_2(z)e^{-jk_2 z} - b_2(z)e^{+jk_2 z}]V_2/Z_o.\end{aligned} \tag{3.57}$$

For later use $\Delta\mathcal{I}_1$ is rewritten as:

$$\Delta\mathcal{I}_1 = \xi_1 V_1/Z_e + \xi_2 V_2/Z_o. \tag{3.58}$$

We now have to again enforce the appropriate boundary conditions, i.e.

$$\Delta\mathcal{V}_1(z=0) + \mathcal{Z}_s\Delta\mathcal{I}_1(z=0) = 0, \tag{3.59}$$

$$\Delta\mathcal{V}_1(z=l) = \mathcal{Z}_L\Delta\mathcal{I}_1(z=l). \tag{3.60}$$

At $z = 0$ we simply have that $a_1(z = 0) = a_2(z = 0) = b_1(z = 0) = b_2(z = 0) = 0$. At $z = l$ these coefficients become:

$$\begin{aligned}
a_1(z = l) &= q_{ee,1}A_1 + q_{eo,1}A_2 + q_{ee,2}B_1 + q_{eo,2}B_2,\\
a_2(z = l) &= q_{oe,1}A_1 + q_{oo,1}A_2 + q_{oe,2}B_1 + q_{oo,2}B_2,\\
b_1(z = l) &= p_{ee,1}A_1 + p_{eo,1}A_2 + p_{ee,2}B_1 + p_{eo,2}B_2,\\
b_2(z = l) &= p_{oe,1}A_1 + p_{oo,1}A_2 + p_{oe,2}B_1 + p_{oo,2}B_2,
\end{aligned} \tag{3.61}$$

with

$$\begin{aligned}
q_{ee,1} &= (\eta_1\mu_1 + \eta_3\theta_1, 0),\\
q_{eo,1} &= (\eta_1\kappa_2 + \eta_4\theta_2, k_1 - k_2),\\
q_{ee,2} &= (\eta_1\mu_1 - \eta_3\theta_1, 2k_1),\\
q_{eo,2} &= (\eta_1\kappa_2 - \eta_4\theta_2, k_1 + k_2),\\
q_{oe,1} &= (\eta_2\kappa_1 + \eta_3\theta_2, -k_1 + k_2),\\
q_{oo,1} &= (\eta_2\mu_2 + \eta_4\theta_3, 0),\\
q_{oe,2} &= (\eta_2\kappa_1 - \eta_3\theta_2, k_1 + k_2),\\
q_{oo,2} &= (\eta_2\mu_2 - \eta_4\theta_3, 2k_2),\\
p_{ee,1} &= (-\eta_1\mu_1 + \eta_3\theta_1, -2k_1),\\
p_{eo,1} &= (-\eta_1\kappa_2 + \eta_4\theta_2, -k_1 - k_2),\\
p_{ee,2} &= (-\eta_1\mu_1 - \eta_3\theta_1, 0),\\
p_{eo,2} &= (-\eta_1\kappa_2 - \eta_4\theta_2, -k_1 + k_2),\\
p_{oe,1} &= (-\eta_2\kappa_1 + \eta_3\theta_2, -k_1 - k_2),\\
p_{oo,1} &= (-\eta_2\mu_2 + \eta_4\theta_3, -2k_2),\\
p_{oe,2} &= (-\eta_2\kappa_1 - \eta_3\theta_2, k_1 - k_2),\\
p_{oo,2} &= (-\eta_2\mu_2 - \eta_4\theta_3, 0),
\end{aligned} \tag{3.62}$$

and with $\eta_1 = \frac{\omega^2}{2jk_1}$, $\eta_2 = \frac{\omega^2}{2jk_2}$, $\eta_3 = -\frac{j\omega}{2Z_e}$ and $\eta_4 = -\frac{j\omega}{2Z_o}$. Above, we have introduced the following notation:

$$(f, \tau) = \int_0^l e^{+j\tau z'} f(z')dz'. \tag{3.63}$$

A closer look at the relevant integrands in (3.62) reveals that the following quantities play a role:

$$\begin{aligned}
\eta_1 \int_0^l \mu_1(z')dz' \quad &+ \quad \eta_3 \int_0^l \theta_1(z')dz',\\
\eta_2 \int_0^l \mu_2(z')dz' \quad &+ \quad \eta_4 \int_0^l \theta_3(z')dz'.
\end{aligned} \tag{3.64}$$

Defining the capacitance matrix in (3.4) still leaves freedom in the actual choice of C_a, C_b, L_a and L_b. For the following choices the integrals in (3.64) become zero:

$$\begin{aligned}
\frac{1}{l}\int_0^l |C_{12}(z')|dz' &= C_b, \\
\frac{1}{l}\int_0^l [C_{11}(z') + C_{22}(z')]dz' &= 2C_a, \\
\frac{1}{l}\int_0^l |L_{12}(z')|dz' &= L_b, \\
\frac{1}{l}\int_0^l [L_{11}(z') + L_{22}(z')]dz' &= 2L_a.
\end{aligned} \tag{3.65}$$

However, remark that it might not always be indicated to make the above choice for C_a, C_b, L_a and L_b and to leave sufficient freedom in the choice of these “nominal" values.
It is easily seen that at $z = 0$ we get exactly the same equations as in the unperturbed case with A_i and B_i replaced by P_i and Q_i and with $\mathcal{V}_s = 0$ (see (3.59)). Hence,

$$\mathcal{T}_V \Delta\mathcal{X}_1 + \mathcal{Z}_s\mathcal{Y}_m\mathcal{T}_I\Delta\mathcal{X}_1 = 0, \tag{3.66}$$

with the column matrix $\Delta\mathcal{X}_1 = (P_1Q_1P_2Q_2)^T$. For $z = l$, enforcing boundary condition (3.60) also leads to equations similar to those found in the unperturbed case (see (3.41)) but the unperturbed signal contributes in the form of a source term:

$$\mathcal{P}(\mathcal{U}_V\Delta\mathcal{X}_1 + \Delta\mathcal{U}_V\mathcal{X}) = \mathcal{Z}_L\mathcal{Y}_m\mathcal{P}(\mathcal{U}_I\Delta\mathcal{X}_1 + \Delta\mathcal{U}_I\mathcal{X}), \tag{3.67}$$

with

$$\begin{aligned}
\Delta\mathcal{U}_V &= \begin{pmatrix} q_{ee,1}+t_1p_{ee,1} & q_{ee,2}+t_1p_{ee,2} & q_{eo,1}+t_1p_{eo,1} & q_{eo,2}+t_1p_{eo,2} \\ q_{oe,1}+t_2p_{oe,1} & q_{oe,2}+t_2p_{oe,2} & q_{oo,1}+t_2p_{oo,1} & q_{oo,2}+t_2p_{oo,2} \end{pmatrix}, \\
\Delta\mathcal{U}_I &= \begin{pmatrix} q_{ee,1}-t_1p_{ee,1} & q_{ee,2}-t_1p_{ee,2} & q_{eo,1}-t_1p_{eo,1} & q_{eo,2}-t_1p_{eo,2} \\ q_{oe,1}-t_2p_{oe,1} & q_{oe,2}-t_2p_{oe,2} & q_{oo,1}-t_2p_{oo,1} & q_{oo,2}-t_2p_{oo,2} \end{pmatrix},
\end{aligned} \tag{3.68}$$

and $t_1 = e^{2jk_1l}$, $t_2 = e^{2jk_2l}$. Combination of (3.66) and (3.67) yields the final set of equations for P_i and Q_i:

$$\begin{pmatrix} \mathcal{T}_V + \mathcal{Z}_s\mathcal{Y}_m\mathcal{T}_I \\ \mathcal{P}\mathcal{U}_V - \mathcal{Z}_L\mathcal{Y}_m\mathcal{P}\mathcal{U}_I \end{pmatrix}\Delta\mathcal{X}_1 = \begin{pmatrix} 0 \\ -\mathcal{P}\Delta\mathcal{U}_V + \mathcal{Z}_L\mathcal{Y}_m\mathcal{P}\Delta\mathcal{U}_I \end{pmatrix}\mathcal{X}. \tag{3.69}$$

Remark that the right-hand sides of (3.42) and (3.69) are identical. Hence, the same set of equations has to be solved twice. In the unperturbed case the only sources are the voltages sources $\mathcal{V}_s$. For the first perturbation step, these voltages become zero but the effect of the varying capacitance and inductance is now represented as equivalent sources at the load side both depending on that varying capacitance and inductance (through a number of weighted averages over the length of the line) and on the unperturbed solution.

3.2.4 Second order perturbation solution

The wave equation satisfied by the second-order perturbed voltage $\Delta\mathcal{V}_2$ is obtained using (3.9) and (3.10):

$$\frac{d^2\Delta\mathcal{V}_2}{dz^2} + \omega^2(\tilde{\mathcal{L}}\tilde{\mathcal{C}})\Delta\mathcal{V}_2 = -\omega^2(\tilde{\mathcal{L}}\Delta\mathcal{C})\Delta\mathcal{V}_1 - j\omega\frac{d(\Delta\mathcal{L}\Delta\mathcal{I}_1)}{dz}. \tag{3.70}$$

To find the solution of (3.70), the sought for $\Delta\mathcal{V}_2$ is again expanded in the eigenvectors V_1 and V_2 used in the unperturbed case:

$$\Delta\mathcal{V}_2 = \psi_1 V_1 + \psi_2 V_2. \tag{3.71}$$

Analogous to the first perturbation step, we substitute (3.20) and (3.71) into (3.70) and using the orthonormality of the voltage and current eigenvectors, we get

$$\frac{d^2\psi_i}{dz^2} + \omega^2\lambda_i\psi_i = -\omega^2\sum_{j=1}^{2}\beta_j I_i^T(\tilde{\mathcal{L}}\Delta\mathcal{C})V_j - j\omega\sum_{j=1}^{2}I_i^T\frac{d(\xi_j\Delta\mathcal{L}V_j/Z_j)}{dz}, \tag{3.72}$$

with $Z_i = Z_e$ for $i = 1$ and $Z_i = Z_o$ for $i = 2$.
Following the same procedure as for the first perturbation step, we see that the perturbed common mode, i.e. (3.72) for $i = 1$, satisfies

$$\frac{d^2\psi_1}{dz^2} + \omega^2\lambda_1\psi_1 = -\omega^2[\beta_1\mu_1 + \beta_2\kappa_2] - j\omega\left[\frac{1}{Z_e}\frac{d(\xi_1\theta_1)}{dz} + \frac{1}{Z_o}\frac{d(\xi_2\theta_2)}{dz}\right]. \tag{3.73}$$

The perturbed differential mode, i.e. (3.72) for $i = 2$, satisfies

$$\frac{d^2\psi_2}{dz^2} + \omega^2\lambda_2\psi_2 = -\omega^2[\beta_1\kappa_1 + \beta_2\mu_2] - j\omega\left[\frac{1}{Z_e}\frac{d(\xi_1\theta_2)}{dz} + \frac{1}{Z_o}\frac{d(\xi_2\theta_3)}{dz}\right]. \tag{3.74}$$

As can be seen, the wave equations (3.73) and (3.74) satisfied by the eigenvector amplitudes for the second perturbation step are similar to the wave equations (3.54) satisfied by the first-order eigenvector amplitudes. Remark, that the right part of (3.73) and (3.74) contain the eigenvector amplitudes from the first perturbation step instead of unperturbed ones used in (3.54). The equations (3.73) and

(3.74) can be solved using the same technique as for the first perturbation step, leading to

$$\begin{aligned}\psi_1 &= M_1 e^{-jk_1 z} + N_1 e^{+jk_1 z} + c_1(z)e^{-jk_1 z} + d_1(z)e^{+jk_1 z},\\ \psi_2 &= M_2 e^{-jk_2 z} + N_2 e^{+jk_2 z} + c_2(z)e^{-jk_2 z} + d_2(z)e^{+jk_2 z},\end{aligned} \tag{3.75}$$

with

$$\begin{aligned}c_1(z) &= -\frac{j\omega}{2}\int_0^z e^{+jk_1 z'} s_{1c}(z')dz',\\ d_1(z) &= \frac{j\omega}{2}\int_0^z e^{-jk_1 z'} s_{1d}(z')dz',\\ c_2(z) &= -\frac{j\omega}{2}\int_0^z e^{+jk_2 z'} s_{2c}(z')dz',\\ d_2(z) &= \frac{j\omega}{2}\int_0^z e^{-jk_2 z'} s_{2d}(z')dz',\\ s_{1c}(z) &= \frac{\omega}{k_1}[\beta_1\mu_1 + \beta_2\kappa_2] + \frac{1}{Z_e}\xi_1\theta_1 + \frac{1}{Z_o}\xi_2\theta_2,\\ s_{1d}(z) &= \frac{\omega}{k_1}[\beta_1\mu_1 + \beta_2\kappa_2] - \frac{1}{Z_e}\xi_1\theta_1 - \frac{1}{Z_o}\xi_2\theta_2,\\ s_{2c}(z) &= \frac{\omega}{k_2}[\beta_1\kappa_1 + \beta_2\mu_2] + \frac{1}{Z_e}\xi_1\theta_2 + \frac{1}{Z_o}\xi_2\theta_3,\\ s_{2d}(z) &= \frac{\omega}{k_2}[\beta_1\kappa_1 + \beta_2\mu_2] - \frac{1}{Z_e}\xi_1\theta_2 - \frac{1}{Z_o}\xi_2\theta_3.\end{aligned} \tag{3.76}$$

The contributions in the as yet undetermined coefficients M_i and N_i are general solutions of the homogeneous differential equation, while the terms in c_i and d_i form the particular solution. Using the above and (3.1), the following final results are found for the second perturbation step:

$$\begin{aligned}\Delta\mathcal{V}_2 &= [M_1 e^{-jk_1 z} + N_1 e^{+jk_1 z}]V_1 + [c_1(z)e^{-jk_1 z} + d_1(z)e^{+jk_1 z}]V_1\\ &+ [M_2 e^{-jk_2 z} + N_2 e^{+jk_2 z}]V_2 + [c_2(z)e^{-jk_2 z} + d_2(z)e^{+jk_2 z}]V_2,\\ \Delta\mathcal{I}_2 &= [M_1 e^{-jk_1 z} - N_1 e^{+jk_1 z}]V_1/Z_e + [c_1(z)e^{-jk_1 z} - d_1(z)e^{+jk_1 z}]V_1/Z_e\\ &+ [M_2 e^{-jk_2 z} - N_2 e^{+jk_2 z}]V_2/Z_o + [c_2(z)e^{-jk_2 z} - d_2(z)e^{+jk_2 z}]V_2/Z_o.\end{aligned} \tag{3.77}$$

At this point, the appropriate boundary conditions, have to be again enforced, i.e.

$$\Delta\mathcal{V}_2(z=0) + \mathcal{Z}_s\Delta\mathcal{I}_2(z=0) = 0, \tag{3.78}$$

$$\Delta\mathcal{V}_2(z=l) = \mathcal{Z}_L\Delta\mathcal{I}_2(z=l). \tag{3.79}$$

At $z = 0$ we simply have that $c_1(z = 0) = c_2(z = 0) = d_1(z = 0) = d_2(z = 0) = 0$. At $z = l$ these coefficients become:

$$\begin{aligned}
c_1(z=l) &= q_{ee,1}P_1 + q_{eo,1}P_2 + q_{ee,2}Q_1 + q_{eo,2}Q_2 + \tilde{q}_{ee,1} + \tilde{q}_{eo,1} + \tilde{q}_{ee,2} + \tilde{q}_{eo,2},\\
c_2(z=l) &= q_{oe,1}P_1 + q_{oo,1}P_2 + q_{oe,2}Q_1 + q_{oo,2}Q_2, + \tilde{q}_{oe,1} + \tilde{q}_{oo,1} + \tilde{q}_{oe,2} + \tilde{q}_{oo,2},\\
d_1(z=l) &= p_{ee,1}P_1 + p_{eo,1}P_2 + p_{ee,2}Q_1 + p_{eo,2}Q_2, + \tilde{p}_{ee,1} + \tilde{p}_{eo,1} + \tilde{p}_{ee,2} + \tilde{p}_{eo,2}\\
d_2(z=l) &= p_{oe,1}P_1 + p_{oo,1}P_2 + p_{oe,2}Q_1 + p_{oo,2}Q_2, + \tilde{p}_{oe,1} + \tilde{p}_{oo,1} + \tilde{p}_{oe,2} + \tilde{p}_{oo,2}.
\end{aligned} \tag{3.80}$$

with

$$\begin{aligned}
\tilde{q}_{ee,1} &= (a_1[\eta_1\mu_1 + \eta_3\theta_1], 0),\\
\tilde{q}_{eo,1} &= (a_2[\eta_1\kappa_2 + \eta_4\theta_2], k_1 - k_2),\\
\tilde{q}_{ee,2} &= (b_1[\eta_1\mu_1 - \eta_3\theta_1], 2k_1),\\
\tilde{q}_{eo,2} &= (b_2[\eta_1\kappa_2 - \eta_4\theta_2], k_1 + k_2),\\
\tilde{q}_{oe,1} &= (a_1[\eta_2\kappa_1 + \eta_3\theta_2], -k_1 + k_2),\\
\tilde{q}_{oo,1} &= (a_2[\eta_2\mu_2 + \eta_4\theta_3], 0),\\
\tilde{q}_{oe,2} &= (b_1[\eta_2\kappa_1 - \eta_3\theta_2], k_1 + k_2),\\
\tilde{q}_{oo,2} &= (b_2[\eta_2\mu_2 - \eta_4\theta_3], 2k_2),\\
\tilde{p}_{ee,1} &= (a_1[-\eta_1\mu_1 + \eta_3\theta_1], -2k_1),\\
\tilde{p}_{eo,1} &= (a_2[-\eta_1\kappa_2 + \eta_4\theta_2], -k_1 - k_2),\\
\tilde{p}_{ee,2} &= (b_1[-\eta_1\mu_1 - \eta_3\theta_1], 0),\\
\tilde{p}_{eo,2} &= (b_2[-\eta_1\kappa_2 - \eta_4\theta_2], -k_1 + k_2),\\
\tilde{p}_{oe,1} &= (a_1[-\eta_2\kappa_1 + \eta_3\theta_2], -k_1 - k_2),\\
\tilde{p}_{oo,1} &= (a_2[-\eta_2\mu_2 + \eta_4\theta_3], -2k_2),\\
\tilde{p}_{oe,2} &= (b_1[-\eta_2\kappa_1 - \eta_3\theta_2], k_1 - k_2),\\
\tilde{p}_{oo,2} &= (b_2[-\eta_2\mu_2 - \eta_4\theta_3], 0),
\end{aligned} \tag{3.81}$$

It is easily seen that at $z = 0$ we get exactly the same equations as in the unperturbed case with P_i and Q_i replaced by M_i and N_i. Hence,

$$\mathcal{T}_V \Delta\mathcal{X}_2 + \mathcal{Z}_s\mathcal{Y}_m\mathcal{T}_I\Delta\mathcal{X}_2 = 0, \tag{3.82}$$

with the column matrix $\Delta\mathcal{X}_2 = (M_1N_1M_2N_2)^T$. For $z = l$ enforcing boundary condition (3.79) gives us the following equations:

$$\mathcal{P}(\mathcal{U}_V\Delta\mathcal{X}_2 + \Delta\mathcal{U}_V\Delta\mathcal{X}_1 + \Delta\tilde{\mathcal{U}}_V) = \mathcal{Z}_L\mathcal{Y}_m\mathcal{P}(\mathcal{U}_I\Delta\mathcal{X}_2 + \Delta\mathcal{U}_I\Delta\mathcal{X}_1 + \Delta\tilde{\mathcal{U}}_I), \tag{3.83}$$

with

$$\Delta\tilde{\mathcal{U}}_V = \begin{pmatrix} \tilde{q}_{ee,1} + t_1\tilde{p}_{ee,1} & \tilde{q}_{ee,2} + t_1\tilde{p}_{ee,2} & \tilde{q}_{eo,1} + t_1\tilde{p}_{eo,1} & \tilde{q}_{eo,2} + t_1\tilde{p}_{eo,2} \\ \tilde{q}_{oe,1} + t_2\tilde{p}_{oe,1} & \tilde{q}_{oe,2} + t_2\tilde{p}_{oe,2} & \tilde{q}_{oo,1} + t_2\tilde{p}_{oo,1} & \tilde{q}_{oo,2} + t_2\tilde{p}_{oo,2} \end{pmatrix},$$
$$\Delta\tilde{\mathcal{U}}_I = \begin{pmatrix} \tilde{q}_{ee,1} - t_1\tilde{p}_{ee,1} & \tilde{q}_{ee,2} - t_1\tilde{p}_{ee,2} & \tilde{q}_{eo,1} - t_1\tilde{p}_{eo,1} & \tilde{q}_{eo,2} - t_1\tilde{p}_{eo,2} \\ \tilde{q}_{oe,1} - t_2\tilde{p}_{oe,1} & \tilde{q}_{oe,2} - t_2\tilde{p}_{oe,2} & \tilde{q}_{oo,1} - t_2\tilde{p}_{oo,1} & \tilde{q}_{oo,2} - t_2\tilde{p}_{oo,2} \end{pmatrix}. \tag{3.84}$$

The final set of equations for M_i and N_i are obtained from combination of (3.82) and (3.83):

$$\begin{aligned} \begin{pmatrix} \mathcal{T}_V + \mathcal{Z}_s\mathcal{Y}_m\mathcal{T}_I \\ \mathcal{P}\mathcal{U}_V - \mathcal{Z}_L\mathcal{Y}_m\mathcal{P}\mathcal{U}_I \end{pmatrix}\Delta\mathcal{X}_2 &= \begin{pmatrix} 0 \\ -\mathcal{P}\Delta\mathcal{U}_V + \mathcal{Z}_L\mathcal{Y}_m\mathcal{P}\Delta\mathcal{U}_I \end{pmatrix}\Delta\mathcal{X}_1 \\ &+ \begin{pmatrix} 0 \\ -\mathcal{P}\Delta\tilde{\mathcal{U}}_V + \mathcal{Z}_L\mathcal{Y}_m\mathcal{P}\Delta\tilde{\mathcal{U}}_I \end{pmatrix}. \end{aligned} \tag{3.85}$$

The effect of the varying capacitance and inductance is now again represented as equivalent sources at the load side both depending on that varying capacitance and inductance and on the solution from the previous perturbation step.

3.3 Numerical results

3.3.1 Pair of coupled lines with random nonuniformities

For this example, we focus on a pair of coupled lines. The nominal cross-section of this pair is the one also used in [3] and it is shown in Fig. 3.3. The track width is $w = 1.8$ mm, the spacing between the lines is $s = 700$ μm. The microstrip lines and the ground plane have a thickness $t = 35$ μm and a conductivity $\sigma = 5.8{\cdot}10^7$ S/m. The parameters of the substrate are the same as for the LTML described in Chapter 2 and the lines are given a length $l = 50$ mm. For this uniform transmission line, which is considered to be the nominal structure, the nominal frequency dependent $\tilde{\mathcal{L}}$- and $\tilde{\mathcal{C}}$-matrices are calculated with the technique of [4], [5]. This technique is a 2-D electromagnetic numerical method that assumes a quasi-TM behavior of the fields and that in essence solves the pertinent complex capacitance and complex inductance problem. By introducing a differential surface admittance operator, these two problems are cast as boundary integral equations, which can be solved efficiently and accurately. For further details on the usage of this method we refer the reader to [6] and the references therein.

Now, random nonuniformities are introduced by dividing the 50 mm lines into 100 equal sections, and for each section the p.u.l. parameters are varied by multiplying

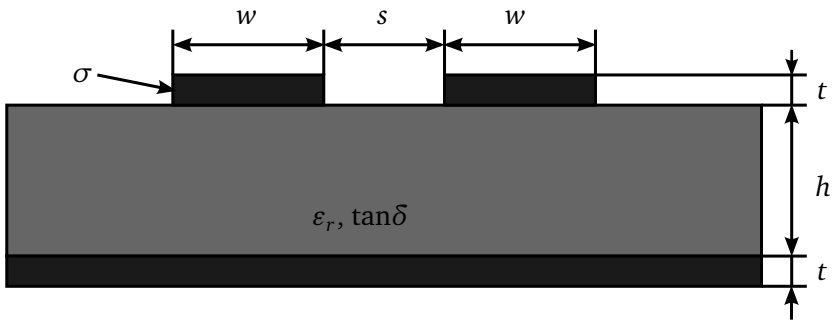

Figure 3.3: Nominal cross-section of the two coupled microstrip lines with w = 1.8 mm, $s = 700$ μm, $h = 1.524$ mm, $t = 35$ μm, $\sigma = 5.8{\cdot}10^7$ S/m, $\varepsilon_r = 3.66$ and $\tan\delta = 0.003$.

each matrix element L_{11}, L_{22}, $L_{12} = L_{21}$, C_{11}, C_{22} and $C_{12} = C_{21}$ of $\tilde{\mathcal{L}}$ and $\tilde{\mathcal{C}}$ with a random variable (RV) that is uniformly distributed within the interval [1 - ξ, 1 + ξ]. The six RVs so used are independent of each other. The number ξ determines the maximum deviation from the nominal case and it is a parameter of our study.

As a reference solution we use the chain parameter matrix approach described in [7]. Based on Telegrapher's equations for each individual section, the voltages and currents at the output of this section are related to the voltages and currents at its input by means of a 4×4 chain parameter matrix. The overall chain parameter matrix of the entire interconnect structure is then obtained as a product of the 100 chain parameter matrices of the individual sections. From this overall chain parameter matrix, the 4×4 S-parameter matrix can be easily derived.

We present the results of the novel perturbation technique and the reference solution by means of mixed-mode S-parameters, characterizing the nonuniform pair of coupled lines in terms of the response to common and differential mode signals [8] w.r.t. 50 Ω references impedances, i.e. $Z_1 = Z_2 = Z_{1L} = Z_{2L} = 50$ Ω and Z_3 and Z_{3L} are open circuits (see Figs. 3.1 and 3.2). Since transmission of a differential signal is the most interesting for practical applications, Figs. 3.4 and 3.5 show the magnitude of the differential-to-common mode conversions S_{cd11} and S_{cd21}, the differential reflection coefficient S_{dd11} and the differential transmission coefficient S_{dd21}, when the maximum variations are $\xi = 20\%$ w.r.t. the nominal values of the $\tilde{\mathcal{L}}$- and $\tilde{\mathcal{C}}$- matrices' elements. We can see from Figs. 3.4 and 3.5 that, these mixed-mode S-parameters are captured with a very high accuracy by our novel method. In Fig. 3.5, the magnitude of the reflection coefficient S_{dd11} and the transmission coefficient S_{dd21} of the differential line with the nominal $\tilde{\mathcal{L}}$ and $\tilde{\mathcal{C}}$ along the line are also shown to demonstrate the influence of the random perturbations. Obviously, there is no mode conversion for the uniform, symmetric line of Fig. 3.3, and hence, this is not shown in Figs. 3.4.

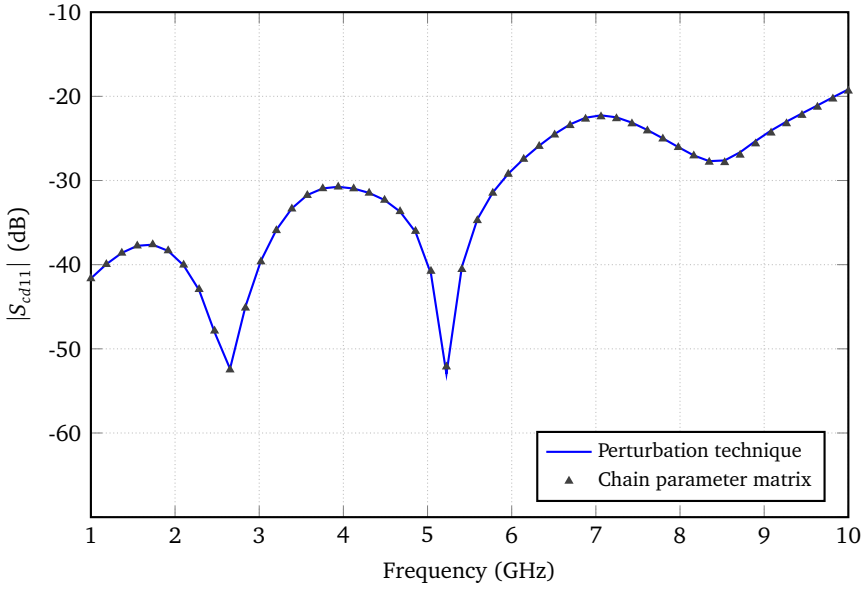

(a)

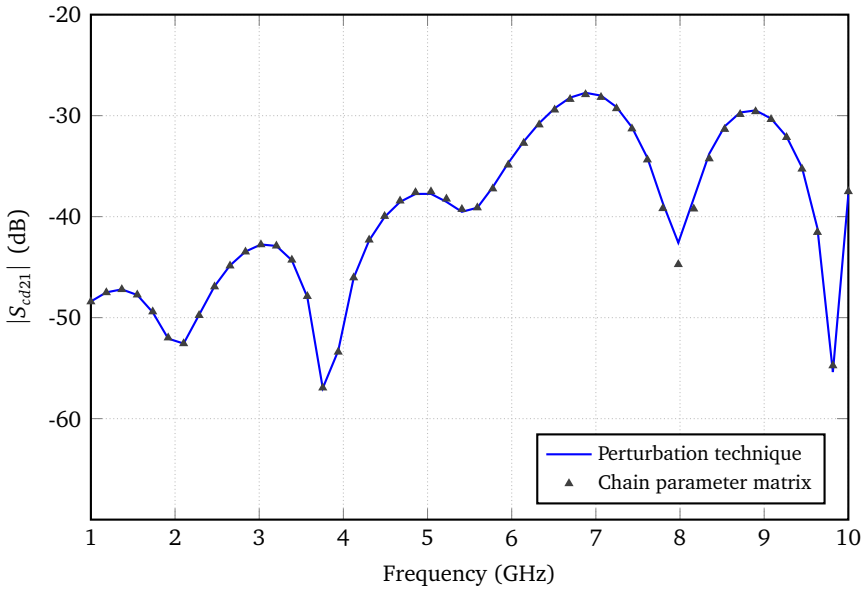

(b)

Figure 3.4: Modal S-parameters of the pair of coupled lines for the case when the maximum variation of p.u.l. capacitance and inductance is $\xi = 20\%$, using the *two-step* perturbation and the chain parameter matrix techniques. (a) Backward differential-to-common mode conversion. (b) Forward differential-to-common mode conversion.

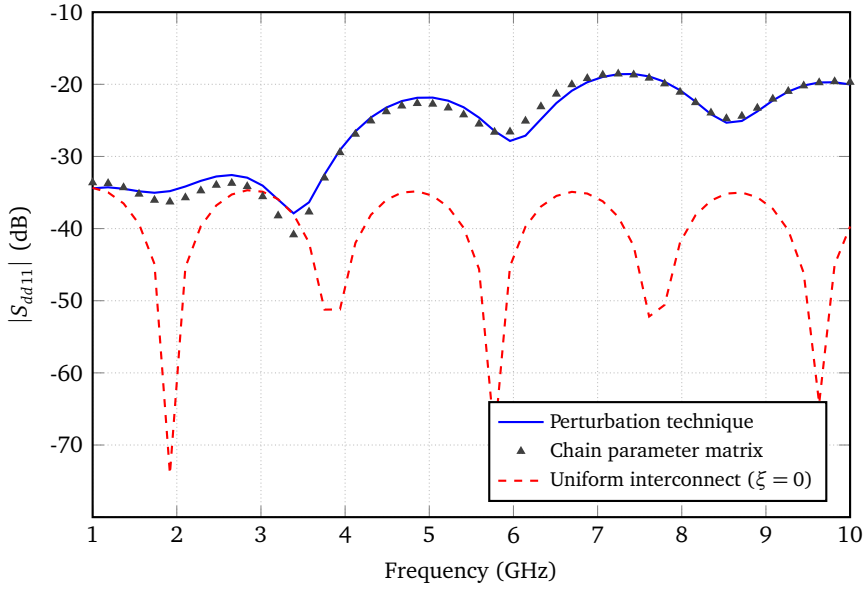

(a)

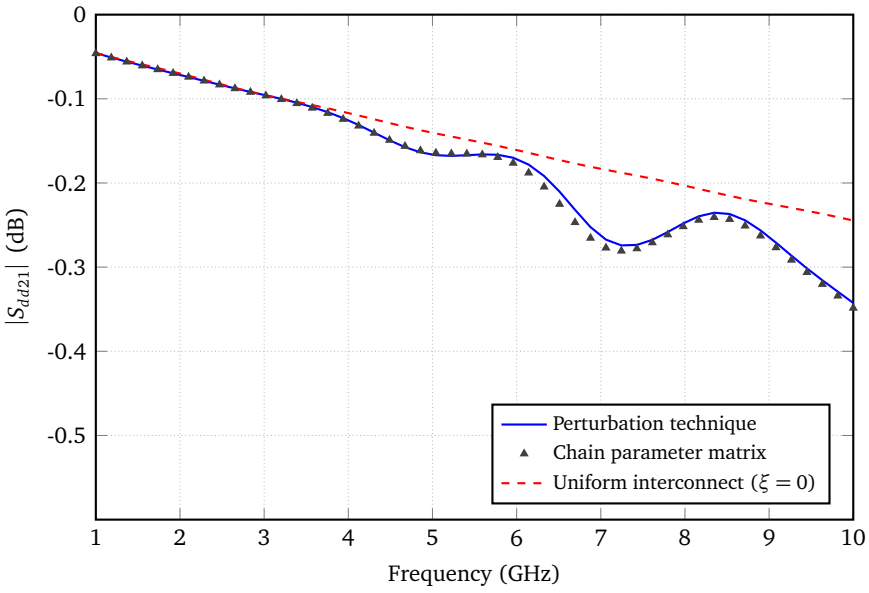

(b)

Figure 3.5: Modal S-parameters of the pair of coupled lines for the case when the maximum variation of p.u.l. capacitance and inductance is $\xi = 20\%$, using the *two-step* perturbation and the chain parameter matrix techniques. (a) Differential mode reflection coefficient. (b) Differential mode transmission coefficient. To indicate the influence of the perturbation, the S-parameters of the nominal, uniform line ($\xi = 0$) are also shown.

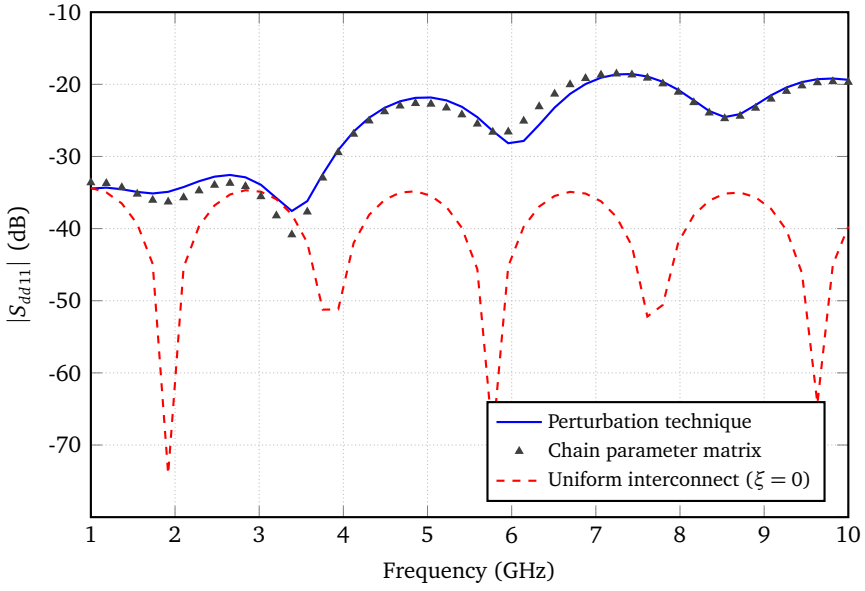

(a)

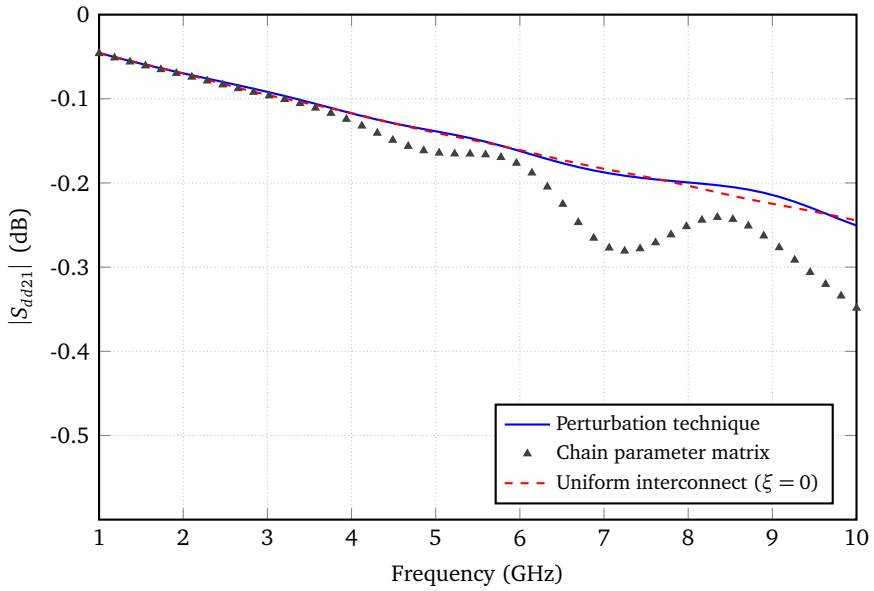

(b)

Figure 3.6: Differential mode reflection (a) and transmission (b) coefficients of the pair of coupled lines for the case when the maximum variation of p.u.l. capacitance and inductance is $\xi = 20\%$, using the *one-step* perturbation and the chain parameter matrix techniques.

At this point, it is instructive to demonstrate the importance of adopting a *two-step* perturbation. In Figs. 3.6, the results for $|S_{dd11}|$ and $|S_{dd21}|$ are shown when using a one-step perturbation. It is clearly observed that this might be sufficient for predicting the S-parameters at the near end (Fig. 3.6(a)). However, it clearly fails to capture the influence of the variation of the p.u.l. parameters along the line at the far end (Fig. 3.6(b)), leading to an $|S_{dd21}|$ that still closely resembles the results for the nominal line. The reader might wonder why the second perturbation step leads to considerable improvements for the transmission parameter, while the reflection result is only slightly affected and is already quite good after the first-order perturbation. An intuitive understanding (here given for a single line) can be obtained when considering a situation for which the nominal problem is already quite well adapted at its terminals, implying that the nominal solution is dominated by a voltage and a current wave travelling in the positive z-direction with phase dependence $e^{-jk_0 z}$. In the first-order perturbation, at a particular point z_0 along the line, this wave will give rise to a voltage source term proportional to $\frac{\Delta C}{C} e^{-jk_0 z_0}$ and a current source term proportional to $\frac{\Delta L}{L} e^{-jk_0 z_0}$. If the signal originating from these sources travels back to the near-end of the line, an extra phase factor $e^{-jk_0 z_0}$ is added. This effect is mathematically expressed through integrals of the type α (2.25) and β (2.26). If, however, the same signal travels to the far-end of the line, an extra phase factor $e^{-jk_0(l-z_0)}$ is added, leading to a total phase of $e^{-jk_0 l}$, independent of z_0. Hence, under the considered circumstances, all source contributions in the first-order perturbation are in-phase at the far-end of the line, as mathematically expressed by an integral of the type γ (2.27). When we select our nominal LC-values as the mean value over the line, i.e. $\gamma = 0$, it becomes clear that the first-order perturbation has little influence at the far-end. A second-order perturbation remedies the problem.

Adopting the *two-step* approach again, apart from the magnitude of the S-parameters, accurate results for the phase are obtained as well. This will be demonstrated now, and at the same time, the limitations of the method will be illustrated. Thereto, we calculate the relative error on the transmission coefficient S_{dd21}. The relative error is defined in a similar way as it was done for the LTML, accounting for both its magnitude and phase:

$$\Delta S_{dd21} = \left| \frac{S_{dd21}^{(ch)} - S_{dd21}^{(p)}}{S_{dd21}^{(ch)}} \right|, \tag{3.86}$$

where $S_{dd21}^{(ch)}$ and $S_{dd21}^{(p)}$ are obtained by means of the chain parameter matrix and perturbation technique respectively. The relative errors were calculated for the entire frequency range up to 10 GHz in order to determine the frequency for which the relative error is the highest. It was found that the highest relative error on S_{dd21} occurs at a frequency of 6.6 GHz. Table 3.1 shows that increasing the maximal values of $\Delta\mathcal{L}$ and $\Delta\mathcal{C}$, i.e. increasing ξ, makes the relative error larger. Nevertheless, as can be seen, the relative error remains limited to 1% if perturbations do not exceed 40% w.r.t. the nominal case.

Table 3.1: Influence of varying the maximal value of $\Delta\mathcal{L}$ and $\Delta\mathcal{C}$

Max. deviation (%)	ΔS_{dd21} @ 6.6 GHz (%)
10	0.05
15	0.1
20	0.17
25	0.29
30	0.41
35	0.58
40	0.79
45	1.04
50	1.34

Table 3.2: CPU time comparison

Number of sections	Perturbation technique	Reference solution	Speed-up factor
50	1.56 s	6.48 s	4.15
100	1.88 s	12.68 s	6.74
200	2.52 s	25.15 s	9.98
500	4.49 s	66.23 s	14.75

Finally, to demonstrate the efficiency of our novel technique, we consider the computation time of the code in Matlab R2009a. All calculations were performed on a computer with an Intel(R) Core(TM) Quad CPU Q9650 and 8 GB of installed memory (RAM). For the perturbation technique, the computational cost is attributed to the calculation of the integrals (3.56) and (3.76). For the reference technique, the computational complexity scales with the number of sections one uses, and hence, it is less efficient than the newly proposed method. This is demonstrated in Table 3.2, where the computation time is shown for 200 frequency samples (linearly spaced between 1 and 10 GHz) and for a varying number of sections. For example, in the case of 200 sections, we achieve a speed-up of about 10. This speed-up factor becomes even larger if we need to describe the variation of $\Delta\mathcal{L}$ and $\Delta\mathcal{C}$ along the line with more precision, i.e. when increasing the number of sections. Indeed, note that the chain parameter matrix approach always introduces a staircasing effect, this in contrast to the novel perturbation technique presented in this paper.

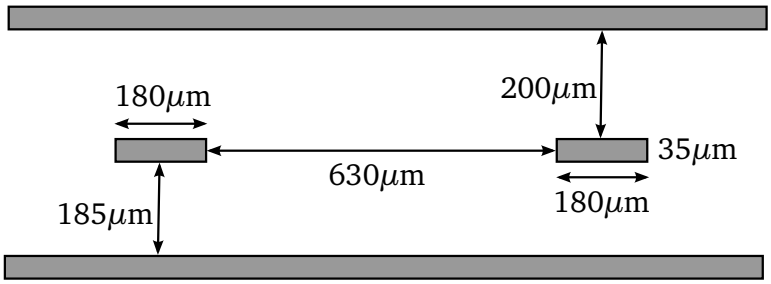

Figure 3.7: Geometry of the differential stripline pair.

3.3.2 Fiber weave application example

Description of the example

Consider the transmission of a differential signal over two copper ($\sigma = 5.8 \cdot 10^7$ S/m) stripline tracks embedded in a substrate. This substrate is nonhomogeneous due to the presence of fiber weave, as detailed below. The stripline pair is depicted in Fig. 3.7. The conductor thickness is 35 μm. The tracks are 180 μm wide with a distance of 630 μm separating them. The distance between top and bottom plate is 420 μm. These dimensions are such that at 10 GHz, a single line has an impedance of 50 Ω when a homogeneous background medium with $\varepsilon_r = 3.4$ is considered. However, here we consider a type 1080 fiber weave substrate, the top view of which is depicted in Fig. 3.8. To clearly illustrate the effect of fiber weave, we have opted to put the left line (line 1) on top of a glass bundle while the right line (line 2) mainly "sees" epoxy prepreg. Consequently, the tracks — which are running in the warp direction — are embedded in a periodically changing background medium. To model this background medium we consider two different cross-sections, indicated as cross-sections a and b in Fig. 3.8. These two cross-sections and all relevant dimensions are detailed in Figs. 3.9 and 3.10 respectively. The dielectric constant and the loss tangent of the glass and the epoxy prepreg are described by a Debye model. For the glass, Fig. 3.11 depicts the real part of the relative dielectric constant, i.e. ε_r', and the loss tangent, $\tan\delta$, as a function of frequency. At 1 GHz, $\varepsilon_r' = 6$ and $\tan\delta = 0.015$. For the epoxy a similar model is used with the same loss tangent but with $\varepsilon_r' = 3$ at 1 GHz. The RLGC-parameters in each cross-section are modeled using an integral equation for the equivalent polarization charges and for the equivalent differential surface currents [4].
In the propagation direction z, the stripline pair is now modeled as the concatenation of alternating sections a and b, i.e. $a-b-a-b-\ldots$ Section a has a length of 171 μm; section b has a length of 253 μm. We investigate such a line with a total length of 25.4 cm $= 10''$, i.e. sections a and b are alternately repeated 600 times.

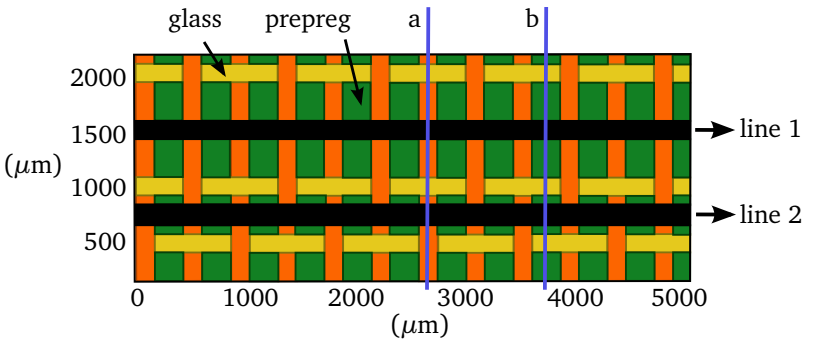

Figure 3.8: Top view of the positioning of the lines w.r.t. the fiber weave.

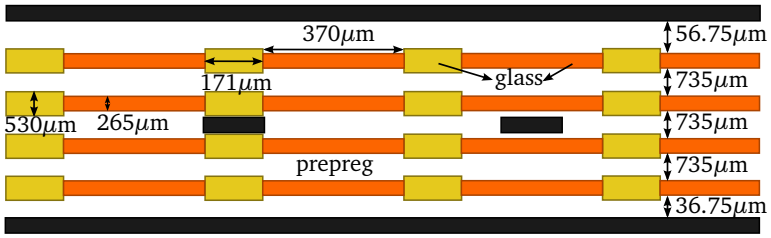

Figure 3.9: Detail of cross-section *a* as defined in Fig. 3.8.

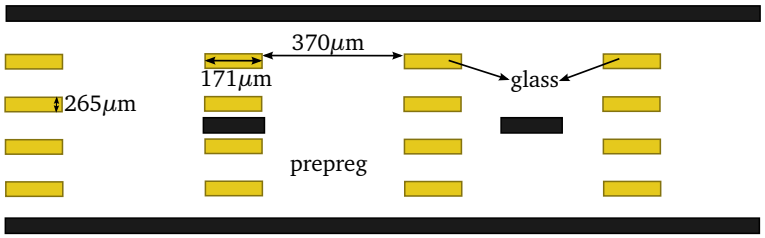

Figure 3.10: Detail of cross-section *b* as defined in Fig. 3.8.

Results

Such a model, where the p.u.l. parameters vary in a piecewise constant manner, allows using the chain matrix approach [7] as a reference technique. In this ap-

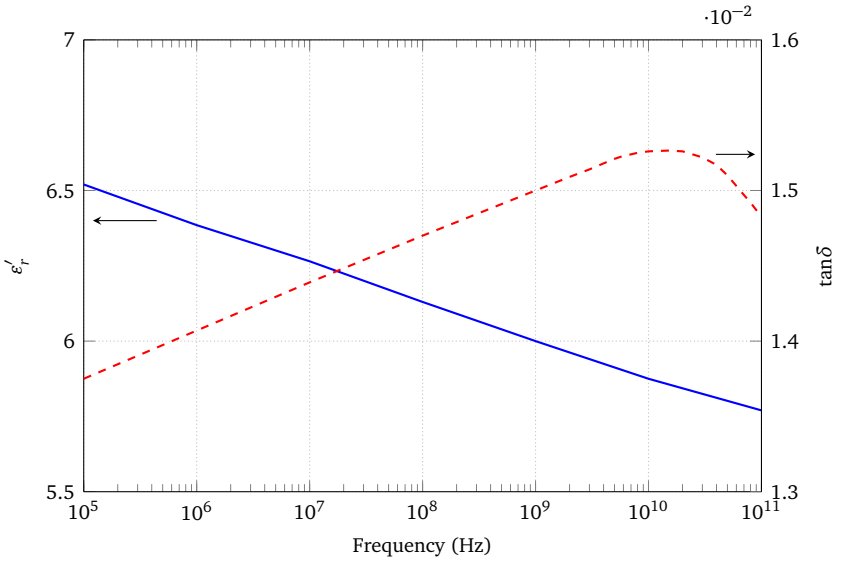

Figure 3.11: Variation of the real part of the relative dielectric permittivity (left) and the loss tangent (right) of the fiber weave glass as a function of frequency.

proach, the chain matrices of sections a and b are computed and the overall result is obtained by alternately concatenating the sections, i.e. by multiplication of the $2 \times 600 = 1200$ chain matrices. In contrast to the chain matrix approach, the proposed perturbation technique can also handle continuously varying p.u.l. parameters. Due care has to be taken, however, to ensure a high precision for electrically (very) long lines. Indeed, when the line becomes electrically long, say about five to ten wavelengths, phase errors start to accumulate. Unfortunately, the fiber weave effect as described in the introduction, is best visible for very long lines, such as the one we analyze here. (Indeed, assuming an average ϵ_r of 3.4, a line length of $10''$ corresponds to approximately 80 wavelengths at 50 GHz!) To improve the accuracy of the method at very high frequencies, we need to subdivide the long line into shorter sections, model these sections separately with the perturbation technique and concatenate the models. Nonetheless, the number of sections may remain limited, making the perturbation technique still much faster than the reference chain matrix technique, as shown below.

First, we focus on the accuracy of the perturbation technique by presenting mixed-mode S-parameters w.r.t. 50 Ω reference impedances [3]. In particular, we study the magnitude of the differential transmission coefficient S_{dd21} and the differential-to-common-mode conversion S_{cd21} in the frequency range from DC to 50 GHz, as shown in Figs. 3.12.

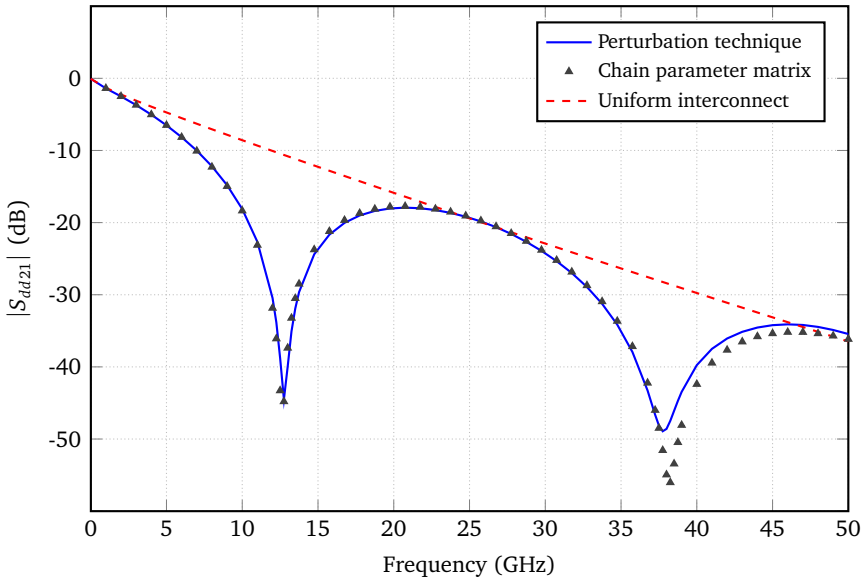

(a)

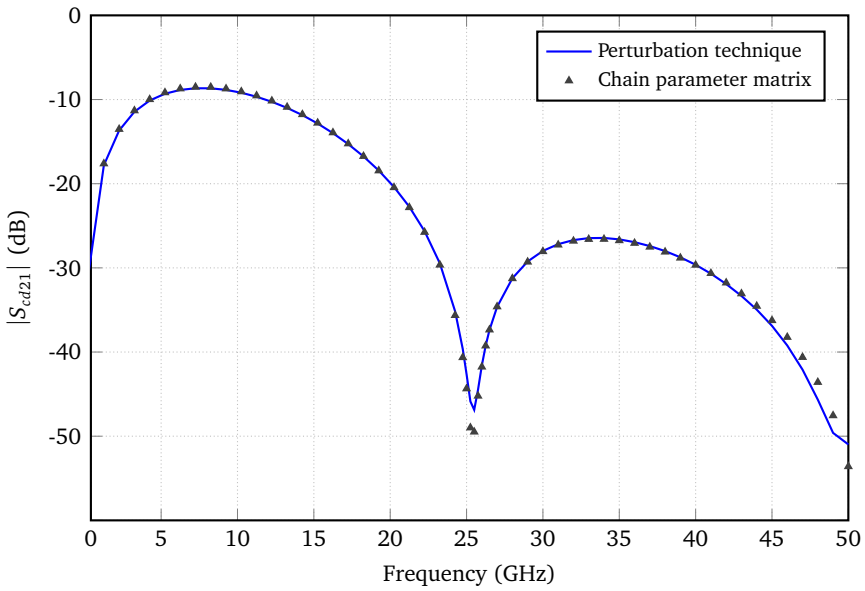

(b)

Figure 3.12: (a) Differential mode transmission coefficient and (b) forward differential-to-common mode conversion of the pair of coupled lines embedded in the fiber weave substrate. For the perturbation technique, the line was divided into 20 sections that were modeled separately and then concatenated. The chain matrix approach relies on a concatenation of all 1200 sections. To illustrate the fiber weave effect, the differential mode transmission coefficient for a uniform interconnect is also shown.

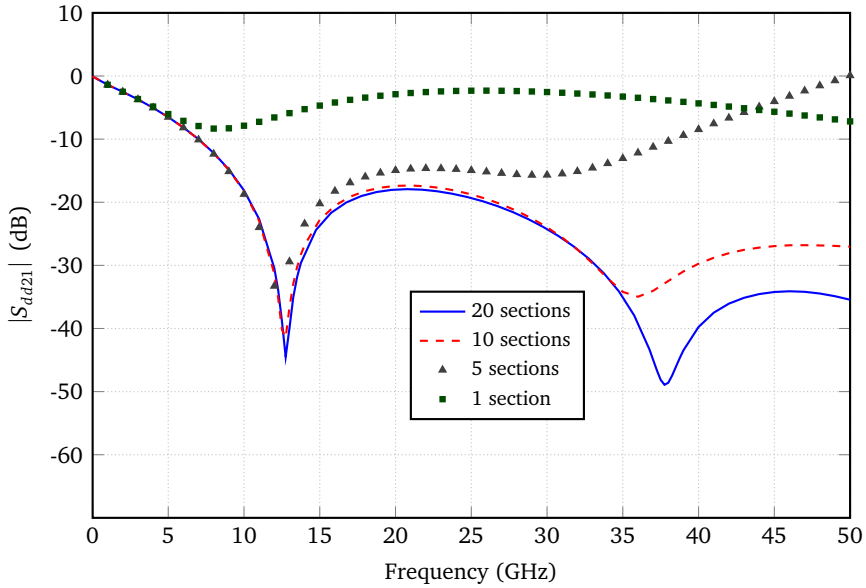

Figure 3.13: Differential mode transmission coefficient of the entire line obtained with the perturbation technique when subdividing the line into a varying number of sections.

To perform the perturbation analysis up to 50 GHz, the line was subdivided into 20 sections. As can be seen, the results of the perturbation approach are very accurate in comparison to the reference technique. To assess the influence of the fiber weave, the results for a *uniform* interconnect with constant (unperturbed) p.u.l. C- and L-matrices as specified in (3.4), are also shown. It is clear that, next to mode conversion, the presence of fiber weave leads to insertion loss suck-outs. Additionally, Fig. 3.13 is shown to demonstrate the evolution of the accuracy of the perturbation technique when we vary the number of concatenated sections. When modeling the entire line of $10''$ as one section, the perturbation technique captures the correct behavior accurately up to 5 GHz (ca. 8 wavelengths). Modeling five sections of $2''$ each, allows to improve the results up to the first insertion loss suck-out peak at ca. 13 GHz. A section of $1''$ can be accurately modeled up to 35 GHz and to obtain accurate results up to 50 GHz, 20 sections are needed, as was already presented in Fig. 3.12(a).

Second, to demonstrate the efficiency of our novel technique, we consider the computation time of the code in Matlab R2009a. All calculations were performed on a computer with an Intel(R) Core(TM) Quad CPU Q9650 and 8 GB of installed memory (RAM) for 201 frequency samples (linearly spaced between DC and 50 GHz). Table 3.3 shows the computation time of the perturbation method for a varying number of sections. The speed-up factor is calculated w.r.t. the CPU time of 156.3 s

Table 3.3: Efficiency of the perturbation technique.
The CPU time needed with the reference approach is 156.3 s.

Number of sections	CPU time	Speed-up factor
1	10.6 s	14.7
5	15.8 s	9.9
10	22.8 s	6.9
20	35.6 s	4.4

needed by the reference technique. As can be seen, even when subdividing the line into 20 sections, we still obtain a speed-up factor of 4.4.

3.4 Conclusion

A perturbation technique to model nonuniform differential transmission lines in the frequency domain was presented. The theory has been applied to a pair of coupled lines with random variation of the p.u.l. parameters along the line and to differential lines embedded in a substrate composed of woven glass fibers. The fiber weave effect causes a differential skew between the two traces, leading to insertion loss suck-outs and mode conversion. By subdividing electrically very long lines into a limited number of shorter sections of about 5 to 10 wavelengths, these fiber weave effects are precisely captured by the perturbation technique. Compared to a standard chain matrix approach, excellent accuracy and improved efficiency were obtained in both cases. The importance of employing a *two-step* perturbation to get sufficient accuracy for the transmission coefficients was highlighted. Additionally, it is worth mentioning that the reference chain matrix approach does not allow the modeling of NUTLs with continuously varying p.u.l. parameters.

References

[1] S. McMorrow and C. Heard, "The impact of PCB laminate weave on the electrical performance of differential signaling at multi-gigabit data", in *Proc. DesignCon*, 2005.

[2] E.-P. Li, X.-C. Wei, A. C. Cangellaris, E.-X. Liu, Y.-J. Zhang, M. D'Amore, J. Kim, and T. Sudo, "Progress review of electromagnetic compatibility analysis technologies for packages, printed circuit boards, and novel interconnects", *IEEE Trans. Electromagn. Compat.*, vol. 52, no. 2, pp. 248–265, May 2010.

[3] C. Gazda, D. Vande Ginste, H. Rogier, R.-B. Wu, and D. De Zutter, "A wideband common-mode suppression filter for bend discontinuities in differential signaling using tightly coupled microstrips", *IEEE Trans. Adv. Packag.*, vol. 33, no. 4, pp. 969–978, Nov. 2010.

[4] T. Demeester and D. De Zutter, "Quasi-TM transmission line parameters of coupled lossy lines based on the Dirichlet to Neumann boundary operator", *IEEE Trans. Microw. Theory Tech.*, vol. 56, no. 7, pp. 1649–1660, Jul. 2008.

[5] ——, "Construction of the Dirichlet to Neumann boundary operator for triangles and applications in the analysis of polygonal conductors", *IEEE Trans. Microw. Theory Tech.*, vol. 58, no. 1, pp. 116 –127, Jan. 2010.

[6] D. Vande Ginste, D. De Zutter, D. Deschrijver, T. Dhaene, P. Manfredi, and F. Canavero, "Stochastic modeling-based variability analysis of on-chip interconnects", *IEEE Trans. Compon., Packag., Manuf. Technol. A*, vol. 2, no. 7, pp. 1182–1192, Jul. 2012.

[7] C. R. Paul, *Analysis of Multiconductor Transmission Lines*. John Wiley & Sons, 1994.

[8] W. Fan, A. Lu, L. L. Wai, and B. K. Lok, "Mixed-mode S-parameter characterization of differential structures", in *5th Electronics Packaging Technology Conference, Singapore*, 2003, pp. 533 –537.

4

Extension of the Two-Step Perturbation Technique to Nonuniform Multiconductor Transmission Line Analysis

Based on:

Mykola Chernobryvko, Dries Vande Ginste and Daniël De Zutter, "Nonuniform Multiconductor Transmission Line Analysis by a Two-Step Perturbation Technique", accepted for publication in *IEEE Transactions on Components, Packaging and Manufacturing Technology*.

★ ★ ★

A two-step perturbation technique to model nonuniform multiconductor transmission lines in the frequency domain is presented. In this method nonuniformities are treated as perturbations with respect to the nominal uniform multiconductor line. Starting from the Telegrapher's equations and applying two consecutive perturbations steps, at each step, we obtain second-order ordinary differential equations with distributed source terms. Solving these equations together with the appropriate boundary conditions provides the sought-for voltages and currents along the interconnect structure. The method is validated by means of a frequency domain analysis of a ten conductor microstrip line with random uniformities, confirming its accuracy and efficiency. Additionally, the time domain accuracy and efficiency is demonstrated by means of a high-speed packaging nonuniform interconnect with six signal conductors.

4.1 Introduction

Nonuniform multiconductor transmission lines (NMTLs) have been widely used as interconnections in various microwave applications. Due to the increasing density, operation speed and complexity of modern integrated circuits, physical effects such as delay, ringing, distortion, and crosstalk cannot be neglected and must be captured properly as frequency increases. Moreover, skin, proximity, edge, and roughness effects can lead to signal integrity problems at high frequencies [1]. However, the analytical solution of differential equations describing the behavior of NMTLs with varying per-unit-length (p.u.l.) parameters along the line are not available for the general case. Recently, several methods for analyzing NMTLs have been proposed in both time and frequency domains. The straightforward way to perform the analysis is to approximate an NMTL as a cascade of discrete uniform transmission lines [2], [3]. However, many segments have to be used in order to get an accurate solution. One of the most commonly used tools to obtain a transient response is the inverse fast Fourier transform [4]. Nevertheless, it requires very many data points to avoid aliasing errors when very fast signals are studied. The method of characteristics [5]–[8], which discretizes both time and distance, can also be applied to obtain transients. Unfortunately, the technique becomes inefficient to account for frequency-dependent p.u.l. parameters. Another technique transforms the Telegrapher's equations into algebraic equations in frequency or in time domain using wavelet expansions [9]–[11]. The accuracy of the method depends on the number of components of the wavelet basis. Also, its complexity grows significantly with the number of signal conductors. Full-wave simulations of NMTLs based on the method of moments (MoM) [12], finite-difference time-domain (FDTD) technique [13]–[15], finite elements method (FEM) [16] or differential quadrature method (DQM) [17], [18] provide results with high accuracy, but the computational expenses of the full-wave techniques considerably exceed those of the quasi-TM approach.

In this chapter, we propose a two-step perturbation technique to analyze NMTLs in the frequency domain. Whereas only nonuniform single and differential lines could be treated using the theory described in the previous chapters, this chapter presents the general theory for the case with N signal conductors. The perturbation approach can be applied to NMTLs for which the cross-sectional properties vary in an arbitrary way. We perform the analysis using the well-known RLGC-matrix description for transmission lines in the quasi-TM regime [19]. The NMTL is represented as a uniform multiconductor transmission line with perturbations describing the nonuniformities. This uniform interconnect is considered to be the nominal structure in our approach. First, the nominal voltages and currents are found as a solution of the classical Telegrapher's equations. Next, in the first perturbation step, we obtain the first-order perturbation values of voltages and currents solving a similar set of Telegrapher's equations with additional distributed voltage and current sources. These source terms depend on the nominal voltages and currents and on the deviation of p.u.l. parameters from their nominal values

in each point along the line. As was already shown in Section 3.3.1, a second perturbation step is needed to significantly improve the accuracy of our technique. To demonstrate the accuracy and efficiency of the technique, two examples are worked out in detail. First, a nonuniform transmission line with ten signal conductors, for which the cross-sectional properties change randomly, is investigated in the frequency domain. The second example is a high-speed packaging interconnect example composed of six nonuniform lines. To perform the analysis of the second structure in the time domain, the results of the perturbation approach are imported into Agilent's ADS framework and compared to the full-wave solution of ADS.

The outline of this paper is as follows. Section 4.2 details the two-step perturbation technique for nonuniform transmission lines with N signal conductors. The details of the first-order perturbation solution are considered in Section 4.2.2 and of the second-order perturbation solution in Section 4.2.3. The theory is validated and illustrated in Section 4.3. Section 4.4 summarizes our work and conclusions.

4.2 Formalism for a general nonuniform multiconductor line case

We analyse NMTLs within the framework of the quasi-TM approach and in the frequency domain (with the $e^{j\omega t}$ dependency suppressed). Consider voltage and current $N \times 1$ column vectors $\mathcal{V}$ and $\mathcal{I}$, holding the N voltages and N currents along the lines where N is the number of signal conductors and with the voltages defined with respect to a common reference conductor (conductor $N+1$). To simplify the notation, we work with $N \times N$ complex p.u.l. inductance $\mathcal{L}$ and capacitance $\mathcal{C}$ matrices, i.e. the p.u.l. resistance $\mathcal{R}$ and conductance $\mathcal{G}$ are understood to be part of $\mathcal{L}$ and $\mathcal{C}$ ($\mathcal{L} = \mathcal{L}_{lossless} + \frac{\mathcal{R}}{j\omega}$ and $\mathcal{C} = \mathcal{C}_{lossless} + \frac{\mathcal{G}}{j\omega}$). The Telegrapher's equations and expansions of $\mathcal{V}$, $\mathcal{I}$, $\mathcal{C}$ and $\mathcal{L}$ are identical to those used for the differential line case in Chapter ndl. However, we reiterate them to avoid confusion. The Telegrapher's equations are:

$$\frac{d\mathcal{V}(z)}{dz} = -j\omega\mathcal{L}(z)\mathcal{I}(z), \tag{4.1}$$

$$\frac{d\mathcal{I}(z)}{dz} = -j\omega\mathcal{C}(z)\mathcal{V}(z), \tag{4.2}$$

with z being the signal propagation direction. Voltages, currents, capacitances and inductances are introduced as:

$$\begin{aligned}
\mathcal{V}(z) &= \tilde{\mathcal{V}}(z) + \Delta\mathcal{V}_1(z) + \Delta\mathcal{V}_2(z) + ..., \\
\mathcal{I}(z) &= \tilde{\mathcal{I}}(z) + \Delta\mathcal{I}_1(z) + \Delta\mathcal{I}_2(z) + ..., \\
\mathcal{C}(z) &= \tilde{\mathcal{C}} + \Delta\mathcal{C}(z), \\
\mathcal{L}(z) &= \tilde{\mathcal{L}} + \Delta\mathcal{L}(z).
\end{aligned} \tag{4.3}$$

To simplify notations, the z-dependence between the brackets will be dropped in the sequel. Substituting (4.3) into (4.1) and (4.2) and collecting terms of the same order, for the unperturbed quantities we have:

$$\frac{d\tilde{\mathcal{V}}}{dz} = -j\omega\tilde{\mathcal{L}}\tilde{\mathcal{I}}, \tag{4.4}$$

$$\frac{d\tilde{\mathcal{I}}}{dz} = -j\omega\tilde{\mathcal{C}}\tilde{\mathcal{V}}, \tag{4.5}$$

while the perturbations of order one and two satisfy

$$\frac{d\Delta\mathcal{V}_1}{dz} = -j\omega\tilde{\mathcal{L}}\Delta\mathcal{I}_1 - j\omega\Delta\mathcal{L}\tilde{\mathcal{I}}, \tag{4.6}$$

$$\frac{d\Delta\mathcal{I}_1}{dz} = -j\omega\tilde{\mathcal{C}}\Delta\mathcal{V}_1 - j\omega\Delta\mathcal{C}\tilde{\mathcal{V}}, \tag{4.7}$$

$$\frac{d\Delta\mathcal{V}_2}{dz} = -j\omega\tilde{\mathcal{L}}\Delta\mathcal{I}_2 - j\omega\Delta\mathcal{L}\Delta\mathcal{I}_1, \tag{4.8}$$

$$\frac{d\Delta\mathcal{I}_2}{dz} = -j\omega\tilde{\mathcal{C}}\Delta\mathcal{V}_2 - j\omega\Delta\mathcal{C}\Delta\mathcal{V}_1. \tag{4.9}$$

4.2.1 The unperturbed problem

Let us now summarize what is relevant to the solution of the unperturbed problem. Both $\tilde{\mathcal{V}}$ and $\tilde{\mathcal{I}}$ satisfy a wave equation:

$$\frac{d^2\tilde{\mathcal{V}}}{dz^2} + \omega^2(\tilde{\mathcal{L}}\tilde{\mathcal{C}})\tilde{\mathcal{V}} = 0, \tag{4.10}$$

$$\frac{d^2\tilde{\mathcal{I}}}{dz^2} + \omega^2(\tilde{\mathcal{C}}\tilde{\mathcal{L}})\tilde{\mathcal{I}} = 0. \tag{4.11}$$

To solve (4.10) and (4.11), the voltages are expanded in terms of the eigenvectors V_i of $\tilde{\mathcal{L}}\tilde{\mathcal{C}}$ and the currents in terms of the eigenvectors I_i of $\tilde{\mathcal{C}}\tilde{\mathcal{L}}$:

$$\tilde{\mathcal{V}} = \sum_{i=1}^{N} \alpha_i V_i, \tag{4.12}$$

$$\tilde{\mathcal{I}} = \sum_{i=1}^{N} \tilde{\alpha}_i I_i. \tag{4.13}$$

From now on we will systematically introduce vector and matrix notations to avoid working with individual eigenvectors. Let us store the coefficients α_i in the $N \times 1$ column vector $\mathbf{a}$ and likewise, the coefficients $\tilde{\alpha}_i$ in the column vector $\tilde{\mathbf{a}}$. The eigenvectors V_i are collected in a $N \times N$ matrix $\mathbf{v}$, column i of which is V_i and the I_i's are similarly collected in $\mathbf{i}$. Hence, (4.12) and (4.13) can be concisely written

as

$$\tilde{\mathcal{V}} = \mathbf{v}\mathbf{a} \tag{4.14}$$

$$\tilde{\mathcal{I}} = \mathbf{i}\tilde{\mathbf{a}}. \tag{4.15}$$

As proven in Appendix A (and is well-known), the eigenvectors of voltages and currents are orthogonal and hence, with proper normalization, we can assert that $\mathbf{v}^T\mathbf{i} = \mathbf{i}^T\mathbf{v} = \mathcal{I}_N$, where $\mathcal{I}_N$ is the $N \times N$ unit matrix. The critical reader will remark that this orthonormalization does not uniquely determine the eigenvectors as a particular voltage eigenvector can be multiplied by a constant, provided the corresponding current eigenvector is divided by that same factor. We will not pursue this issue here but remark that in the end, the actual voltages and currents as given by (4.12) and (4.13) remain unchanged. Furthermore (also proven in Appendix A), the eigenvalues λ_i of voltage and current eigenvectors are *identical*. For further use, we will need a diagonal $N \times N$ matrix Λ, with diagonal elements λ_i. With this eigenvalue matrix, the eigenvector matrices $\mathbf{v}$ and $\mathbf{i}$ satisfy

$$\begin{aligned}(\tilde{\mathcal{L}}\tilde{\mathcal{C}})\mathbf{v} &= \mathbf{v}\Lambda,\\ (\tilde{\mathcal{C}}\tilde{\mathcal{L}})\mathbf{i} &= \mathbf{i}\Lambda.\end{aligned} \tag{4.16}$$

Using the above and substituting (4.14) into (4.1) and (4.15) into (4.2) shows that:

$$\frac{d^2\mathbf{a}}{dz^2} + \omega^2\Lambda\mathbf{a} = 0, \tag{4.17}$$

$$\frac{d^2\tilde{\mathbf{a}}}{dz^2} + \omega^2\Lambda\tilde{\mathbf{a}} = 0. \tag{4.18}$$

Let us go back to (4.4), insert the eigenvector expansions (4.14) and (4.15) and project both sides of the equation on the current eigenvectors. This yields

$$\frac{d\mathbf{a}}{dz} = -j\omega\mathbf{L}\tilde{\mathbf{a}}, \tag{4.19}$$

with the matrix $\mathbf{L}$ given by

$$\mathbf{L} = \mathbf{i}^T\tilde{\mathcal{L}}\mathbf{i}. \tag{4.20}$$

As proven in Appendix A, the current eigenvectors satisfy the orthogonality property $(I_i)^T\tilde{\mathcal{L}}I_j = 0$ for $i \neq j$, hence, $\mathbf{L}$ is a diagonal matrix. Similarly, starting from (4.5) we arrive at

$$\frac{d\tilde{\mathbf{a}}}{dz} = -j\omega\mathbf{C}\mathbf{a}, \tag{4.21}$$

$$\mathbf{C} = \mathbf{v}^T\tilde{\mathcal{C}}\mathbf{v}, \tag{4.22}$$

with $\mathbf{C}$ a diagonal matrix as a consequence of the orthogonality property $(V_i)^T\tilde{\mathcal{C}}V_j = 0$ for $i \neq j$ (see Appendix A). Futhermore, we have

$$\mathbf{L}\mathbf{C} = \mathbf{C}\mathbf{L} = \Lambda. \tag{4.23}$$

Let us now proceed by first solving (4.17) yielding

$$\mathbf{a} = e^{-j\mathbf{K}z}\mathbf{A} + e^{+j\mathbf{K}z}\mathbf{B}, \tag{4.24}$$

with $\mathbf{K} = \omega\sqrt{\Lambda}$ and with $\mathbf{A}$ and $\mathbf{B}$ complex amplitude $N \times 1$ vectors. The matrix exponential and square root are well-defined as Λ is a diagonal matrix. From (4.24), (4.17) and (4.23) it is found that

$$\tilde{\mathbf{a}} = \mathbf{Z}_m^{-1}(e^{-j\mathbf{K}z}\mathbf{A} - e^{+j\mathbf{K}z}\mathbf{B}), \tag{4.25}$$

with the (diagonal) modal impedance matrix $\mathbf{Z}_m$ given by

$$\mathbf{Z}_m = \sqrt{\mathbf{L}\mathbf{C}^{-1}} = \sqrt{\mathbf{C}^{-1}\mathbf{L}}. \tag{4.26}$$

In order to determine the actual values of $\mathbf{A}$ and $\mathbf{B}$ we have to impose the boundary conditions. For an NTML of length l at $z = 0$ and $z = l$, we impose that

$$\tilde{\mathcal{V}}(z = 0) + \mathcal{Z}_s\tilde{\mathcal{I}}(z = 0) = \mathcal{V}_s, \tag{4.27}$$

$$\tilde{\mathcal{V}}(z = l) - \mathcal{Z}_L\tilde{\mathcal{I}}(z = l) = 0, \tag{4.28}$$

where the currents are directed in the positive z-direction at both the source and load side and with $\mathcal{Z}_s$ and $\mathcal{Z}_L$ the $N \times N$ source side and load side impedance matrices resp. and with $\mathcal{V}_s$ the $N \times 1$ source column vector. At the source, (4.14), (4.15), (4.24), (4.25) and (4.27) show that

$$\mathbf{v}(\mathbf{A} + \mathbf{B}) + \mathcal{Z}_s\mathbf{i}\mathbf{Z}_m^{-1}(\mathbf{A} - \mathbf{B}) = \mathcal{V}_s. \tag{4.29}$$

Left multiplication with $\mathbf{i}^T$ yields

$$(\mathbf{A} + \mathbf{B}) + \mathbf{Z}_s\mathbf{Z}_m^{-1}(\mathbf{A} - \mathbf{B}) = \mathbf{V}_{so}, \tag{4.30}$$

where we have introduced the following quantities

$$\mathbf{Z}_s = \mathbf{i}^T\mathcal{Z}_s\mathbf{i}, \tag{4.31}$$

$$\mathbf{V}_{so} = \mathbf{i}^T\mathcal{V}_s. \tag{4.32}$$

Note the similarity between (4.31) and (4.20). The $N \times 1$ voltage vector $\mathbf{V}_{so}$ is the original voltage vector $\mathcal{V}_s$ projected on the current eigenvectors. At the load, (4.14), (4.15), (4.24), (4.25) and (4.27) now show that

$$\mathbf{v}(e^{-j\mathbf{K}l}\mathbf{A} + e^{+j\mathbf{K}l}\mathbf{B}) - \mathcal{Z}_L\mathbf{i}\mathbf{Z}_m^{-1}(e^{-j\mathbf{K}l}\mathbf{A} - e^{+j\mathbf{K}l}\mathbf{B}) = 0. \tag{4.33}$$

Left multiplication with $\mathbf{i}^T$ gives

$$(e^{-j\mathbf{K}l}\mathbf{A} + e^{+j\mathbf{K}l}\mathbf{B}) - \mathbf{Z}_L\mathbf{Z}_m^{-1}(e^{-j\mathbf{K}l}\mathbf{A} - e^{+j\mathbf{K}l}\mathbf{B}) = 0, \tag{4.34}$$

with

$$\mathbf{Z}_L = \mathbf{i}^T\mathcal{Z}_L\mathbf{i}. \tag{4.35}$$

Finally, (4.30) and (4.34) yield the following set of equations for the unknown complex wave amplitudes:

$$\begin{pmatrix} \mathcal{I}_N + \mathbf{Z}_s\mathbf{Z}_m^{-1} & \mathcal{I}_N - \mathbf{Z}_s\mathbf{Z}_m^{-1} \\ (e^{-j\mathbf{K}l} - \mathbf{Z}_L\mathbf{Z}_m^{-1}e^{-j\mathbf{K}l}) & (e^{+j\mathbf{K}l} + \mathbf{Z}_L\mathbf{Z}_m^{-1}e^{+j\mathbf{K}l}) \end{pmatrix} \begin{pmatrix} \mathbf{A} \\ \mathbf{B} \end{pmatrix} = \begin{pmatrix} \mathbf{V}_{so} \\ 0 \end{pmatrix}. \tag{4.36}$$

To emphasize the analogy with the single line problem, the above result is rewritten as

$$\begin{pmatrix} \mathbf{S}_s & \mathbf{V}_s \\ \mathbf{V}_L e^{-j\mathbf{K}l} & \mathbf{S}_L e^{+j\mathbf{K}l} \end{pmatrix} \begin{pmatrix} \mathbf{A} \\ \mathbf{B} \end{pmatrix} = \begin{pmatrix} \mathbf{V}_{so} \\ 0 \end{pmatrix}, \tag{4.37}$$

with

$$\begin{aligned} \mathbf{S} &= \mathcal{I}_N + \mathbf{Z}\mathbf{Z}_m^{-1}, \\ \mathbf{V} &= \mathcal{I}_N - \mathbf{Z}\mathbf{Z}_m^{-1}, \end{aligned} \tag{4.38}$$

and where the subindex “s" or “L" is added to distinguish between the source and load impedance matrices resp. The product $\mathbf{S}^{-1}\mathbf{V}$ represents a generalized reflection coefficient.
To conclude this subsection, we would like to draw the attention to the fact that the modal impedance matrix $\mathbf{Z}_m$ is not uniquely defined. Indeed, the eigenvectors in the eigenvector matrix $\mathbf{v}$ are only defined up to a multiplicative constant, implying that $\mathbf{C}$ and $\mathbf{L}$ are also not uniquely defined. This does not influence the eigenvalues: they remain fixed. Going back to the original voltages $\tilde{\mathcal{V}}$ and currents $\tilde{\mathcal{I}}$, using (4.14), (4.15), (4.24) and (4.25), we readily deduce that $\tilde{\mathcal{V}} = \mathbf{Z}_{in}\tilde{\mathcal{I}}$, with the input impedance matrix of the infinite multiconductor line given by

$$\mathbf{Z}_{in} = \mathbf{v}\mathbf{Z}_m\mathbf{v}^T. \tag{4.39}$$

Using (4.20), (4.22) and the fact that $\mathbf{v}^T\mathbf{i} = \mathbf{i}^T\mathbf{v} = \mathcal{I}_N$, one can prove that $\mathbf{Z}_{in}$ is indeed unique, as it should be.

4.2.2 First-order perturbation for a nonuniform multiconductor line

Let us now turn to the perturbations. Taking the z-derivative of (4.6) and using (3.8), we find that

$$\frac{d^2\Delta\mathcal{V}_1}{dz^2} + \omega^2(\tilde{\mathcal{L}}\tilde{\mathcal{C}})\Delta\mathcal{V}_1 = -\omega^2(\tilde{\mathcal{L}}\Delta\mathcal{C})\tilde{\mathcal{V}} - j\omega\frac{d}{dz}(\Delta\mathcal{L}\tilde{\mathcal{I}}). \tag{4.40}$$

Voltage and current perturbations of order one are also expanded in the corresponding eigenvectors as,

$$\Delta\mathcal{V}_1 = \sum_{i=1}^{N} \beta_i V_i = \mathbf{vb}, \tag{4.41}$$

$$\Delta\mathcal{I}_1 = \sum_{i=1}^{N} \tilde{\beta}_i I_i = \mathbf{i}\tilde{\mathbf{b}}. \tag{4.42}$$

The β_i and $\tilde{\beta}_i$ coefficients have been collected in the vectors $\mathbf{b}$ and $\tilde{\mathbf{b}}$ resp. Inserting these expansions into (4.40) and taking the proper orthogonality into account, shows that

$$\frac{d^2\mathbf{b}}{dz^2} + \omega^2 \Lambda \mathbf{b} = -\omega^2(\mathbf{i}^T \tilde{\mathcal{L}} \Delta\mathcal{C}\mathbf{v})\mathbf{a} - j\omega \frac{d}{dz}[(\mathbf{i}^T \Delta\mathcal{L}\mathbf{i})\tilde{\mathbf{a}}] \tag{4.43}$$

Once differential equation (4.43) is solved for $\mathbf{b}$, (4.6) shows that $\tilde{\mathbf{b}}$ can be solved from

$$\frac{d\mathbf{b}}{dz} = -j\omega[\mathbf{L}\tilde{\mathbf{b}} + (\mathbf{i}^T \Delta\mathcal{L}\mathbf{i})\tilde{\mathbf{a}}]. \tag{4.44}$$

To simplify further calculations and analogous to (4.20) and (4.22), we introduce

$$\begin{aligned} \Delta\mathbf{L} &= \mathbf{i}^T \Delta\mathcal{L}\mathbf{i}, \\ \Delta\mathbf{C} &= \mathbf{v}^T \Delta\mathcal{C}\mathbf{v}. \end{aligned} \tag{4.45}$$

Contrary to $\mathbf{L}$ and $\mathbf{C}$, these matrices are not diagonal. With this notation, (4.43) and (4.44) become

$$\frac{d^2\mathbf{b}}{dz^2} + \omega^2 \Lambda \mathbf{b} = -\omega^2 \mathbf{L}\Delta\mathbf{C}\mathbf{a} - j\omega \frac{d}{dz}(\Delta\mathbf{L}\tilde{\mathbf{a}}), \tag{4.46}$$

$$\frac{d\mathbf{b}}{dz} = -j\omega(\mathbf{L}\tilde{\mathbf{b}} + \Delta\mathbf{L}\tilde{\mathbf{a}}). \tag{4.47}$$

A particular solution to (4.46) can be found by applying the general theory for second-order differential equations with an arbitrary source term (see e.g. [20] or Appendix A of [21]), i.e.

$$\begin{aligned} &-\frac{1}{2j}\mathbf{K}^{-1} e^{-j\mathbf{K}z} \int_0^z e^{+j\mathbf{K}z'}[-\omega^2 \mathbf{L}\Delta\mathbf{C}\mathbf{a} - j\omega \frac{d}{dz'}(\Delta\mathbf{L}\tilde{\mathbf{a}})]dz' \\ &+\frac{1}{2j}\mathbf{K}^{-1} e^{+j\mathbf{K}z} \int_0^z e^{-j\mathbf{K}z'}[-\omega^2 \mathbf{L}\Delta\mathbf{C}\mathbf{a} - j\omega \frac{d}{dz'}(\Delta\mathbf{L}\tilde{\mathbf{a}})]dz'. \end{aligned} \tag{4.48}$$

The above expression can now be simplified by applying partial integration to the terms with the derivative d/dz'. Careful calculations show that the resulting contributions of the upper limit of the integration interval (i.e. $z' = z$) drop out, while

the contributions of the lower limit of the integration interval (i.e. $z' = 0$) are of the form $\mathbf{C}e^{\pm j\mathbf{K}z}$ with $\mathbf{C}$ a constant vector. Hence, it turns out that these contributions are solutions to the homogeneous equation, i.e. (4.46) without source. Consequently, we still have a valid particular solution if these contributions are dropped. The final result for $\mathbf{b}$, including an arbitrary solution to the homogeneous equation, then becomes

$$\begin{aligned}\mathbf{b} = e^{-j\mathbf{K}z}\mathbf{P} + e^{+j\mathbf{K}z}\mathbf{Q}\\ -\frac{j\omega}{2}e^{-j\mathbf{K}z}\int_0^z e^{+j\mathbf{K}z'}(\mathbf{Z}_m\Delta\mathbf{C}\mathbf{a} + \Delta\mathbf{L}\tilde{\mathbf{a}})dz'\\ +\frac{j\omega}{2}e^{+j\mathbf{K}z}\int_0^z e^{-j\mathbf{K}z'}(\mathbf{Z}_m\Delta\mathbf{C}\mathbf{a} - \Delta\mathbf{L}\tilde{\mathbf{a}})dz',\end{aligned} \tag{4.49}$$

with $\mathbf{P}$ and $\mathbf{Q}$ as yet undetermined and where we have used the identity $\mathbf{K}^{-1}\mathbf{L} = \mathbf{Z}_m/\omega$. We can now turn to the calculation of $\tilde{\mathbf{b}}$ by substituting $\mathbf{b}$ into (4.47). This yields

$$\begin{aligned}\tilde{\mathbf{b}} = \mathbf{Z}_m^{-1}(e^{-j\mathbf{K}z}\mathbf{P} - e^{+j\mathbf{K}z}\mathbf{Q})\\ -\frac{j\omega}{2}\mathbf{Z}_m^{-1}e^{-j\mathbf{K}z}\int_0^z e^{+j\mathbf{K}z'}(\mathbf{Z}_m\Delta\mathbf{C}\mathbf{a} + \Delta\mathbf{L}\tilde{\mathbf{a}})dz'\\ -\frac{j\omega}{2}\mathbf{Z}_m^{-1}e^{+j\mathbf{K}z}\int_0^z e^{-j\mathbf{K}z'}(\mathbf{Z}_m\Delta\mathbf{C}\mathbf{a} - \Delta\mathbf{L}\tilde{\mathbf{a}})dz'.\end{aligned} \tag{4.50}$$

To determine the values of $\mathbf{P}$ and $\mathbf{Q}$ we again have to impose the boundary conditions at $z = 0$ and $z = l$

$$\Delta\mathcal{V}_1(z=0) + \mathcal{Z}_s\Delta\mathcal{I}_1(z=0) = 0, \tag{4.51}$$

$$\Delta\mathcal{V}_1(z=l) - \mathcal{Z}_L\Delta\mathcal{I}_1(z=l) = 0. \tag{4.52}$$

At $z = 0$, the result is similar to (4.30), but with $\mathbf{A}$ and $\mathbf{B}$ replaced by $\mathbf{P}$ and $\mathbf{Q}$ and without source term:

$$(\mathbf{P} + \mathbf{Q}) + \mathbf{Z}_s\mathbf{Z}_m^{-1}(\mathbf{P} - \mathbf{Q}) = 0. \tag{4.53}$$

To apply (4.52), we first need $\mathbf{b}$ and $\tilde{\mathbf{b}}$ at $z = l$:

$$\begin{aligned}\mathbf{b}(z=l) = e^{-j\mathbf{K}l}\mathbf{P} + e^{+j\mathbf{K}l}\mathbf{Q}\\ -\frac{j\omega}{2}e^{-j\mathbf{K}l}[(\mathbf{Z}_m\mathbf{F}_{+,-} + \mathbf{G}_{+,-}\mathbf{Z}_m^{-1})\mathbf{A}\\ +(\mathbf{Z}_m\mathbf{F}_{+,+} - \mathbf{G}_{+,+}\mathbf{Z}_m^{-1})\mathbf{B}]\\ +\frac{j\omega}{2}e^{+j\mathbf{K}l}[(\mathbf{Z}_m\mathbf{F}_{-,-} - \mathbf{G}_{-,-}\mathbf{Z}_m^{-1})\mathbf{A}\\ +(\mathbf{Z}_m\mathbf{F}_{-,+} + \mathbf{G}_{-,+}\mathbf{Z}_m^{-1})\mathbf{B}]\end{aligned} \tag{4.54}$$

and

$$\begin{aligned}\tilde{\mathbf{b}}(z=l) &= \mathbf{Z}_m^{-1}(e^{-j\mathbf{K}l}\mathbf{P} - e^{+j\mathbf{K}l}\mathbf{Q}) \\ &-\frac{j\omega}{2}\mathbf{Z}_m^{-1}e^{-j\mathbf{K}l}[(\mathbf{Z}_m\mathbf{F}_{+,-} + \mathbf{G}_{+,-}\mathbf{Z}_m^{-1})\mathbf{A} \\ &\quad +(\mathbf{Z}_m\mathbf{F}_{+,+} - \mathbf{G}_{+,+}\mathbf{Z}_m^{-1})\mathbf{B}] \\ &-\frac{j\omega}{2}\mathbf{Z}_m^{-1}e^{+j\mathbf{K}l}[(\mathbf{Z}_m\mathbf{F}_{-,-} - \mathbf{G}_{-,-}\mathbf{Z}_m^{-1})\mathbf{A} \\ &\quad +(\mathbf{Z}_m\mathbf{F}_{-,+} + \mathbf{G}_{-,+}\mathbf{Z}_m^{-1})\mathbf{B}]. \end{aligned} \tag{4.55}$$

Symbols $\mathbf{F}_{+,-}$ and $\mathbf{G}_{+,-}$ are defined as

$$\begin{aligned}\mathbf{F}_{+,-} &= \int_0^l e^{+j\mathbf{K}z'}\Delta\mathbf{C}e^{-j\mathbf{K}z'}dz', \\ \mathbf{G}_{+,-} &= \int_0^l e^{+j\mathbf{K}z'}\Delta\mathbf{L}e^{-j\mathbf{K}z'}dz', \end{aligned} \tag{4.56}$$

where the subindex notation $+,-$ points to the fact that the first exponential under the integral sign has a plus-sign while the second one has a minus-sign. All the other **F** and **G** symbols are defined in an analogous way. In an easy to understand notation we rewrite (4.54) and (4.55) as

$$\mathbf{b}(z=l) = e^{-j\mathbf{K}l}\mathbf{P} + e^{+j\mathbf{K}l}\mathbf{Q} - e^{-j\mathbf{K}l}(\mathbf{T}_1\mathbf{A} + \mathbf{U}_1\mathbf{B}) + e^{+j\mathbf{K}l}(\mathbf{T}_2\mathbf{A} + \mathbf{U}_2\mathbf{B}) \tag{4.57}$$

and

$$\tilde{\mathbf{b}}(z=l) = \mathbf{Z}_m^{-1}[e^{-j\mathbf{K}l}\mathbf{P} - e^{+j\mathbf{K}l}\mathbf{Q} - e^{-j\mathbf{K}l}(\mathbf{T}_1\mathbf{A} + \mathbf{U}_1\mathbf{B}) - e^{+j\mathbf{K}l}(\mathbf{T}_2\mathbf{A} + \mathbf{U}_2\mathbf{B})]. \tag{4.58}$$

Applying (4.52) yields

$$\mathbf{b}(z=l) - \mathbf{Z}_L\mathbf{Z}_m^{-1}[\mathbf{Z}_m\tilde{\mathbf{b}}(z=l)] = 0. \tag{4.59}$$

Finally, (4.53) and (4.59) can be combined to determine **P** and **Q**:

$$\begin{pmatrix} \mathbf{S}_s & \mathbf{V}_s \\ \mathbf{V}_L e^{-j\mathbf{K}l} & \mathbf{S}_L e^{+j\mathbf{K}l} \end{pmatrix}\begin{pmatrix} \mathbf{P} \\ \mathbf{Q} \end{pmatrix} = \begin{pmatrix} 0 & 0 \\ \mathbf{S}_A & \mathbf{S}_B \end{pmatrix}\begin{pmatrix} \mathbf{A} \\ \mathbf{B} \end{pmatrix}, \tag{4.60}$$

with

$$\begin{aligned}\mathbf{S}_A &= e^{-j\mathbf{K}l}\mathbf{T}_1 - e^{+j\mathbf{K}l}\mathbf{T}_2 - \mathbf{Z}_L\mathbf{Z}_m^{-1}(e^{-j\mathbf{K}l}\mathbf{T}_1 + e^{+j\mathbf{K}l}\mathbf{T}_2) \\ &= \mathbf{V}_L e^{-j\mathbf{K}l}\mathbf{T}_1 - \mathbf{S}_L e^{+j\mathbf{K}l}\mathbf{T}_2, \end{aligned} \tag{4.61}$$

$$\begin{aligned}\mathbf{S}_B &= e^{-j\mathbf{K}l}\mathbf{U}_1 - e^{+j\mathbf{K}l}\mathbf{U}_2 - \mathbf{Z}_L\mathbf{Z}_m^{-1}(e^{-j\mathbf{K}l}\mathbf{U}_1 + e^{+j\mathbf{K}l}\mathbf{U}_2) \\ &= \mathbf{V}_L e^{-j\mathbf{K}l}\mathbf{U}_1 - \mathbf{S}_L e^{+j\mathbf{K}l}\mathbf{U}_2. \end{aligned} \tag{4.62}$$

4.2.3 Second-order perturbation for a nonuniform multiconductor line

The second-order perturbed voltage $\mathcal{V}_2$ satisfies the following wave equation, obtained by taking z-derivative of (4.8) accounting (4.9)

$$\frac{d^2\Delta\mathcal{V}_2}{dz^2}+\omega^2(\tilde{\mathcal{L}}\tilde{\mathcal{C}})\Delta\mathcal{V}_2=-\omega^2(\tilde{\mathcal{L}}\Delta\mathcal{C})\mathcal{V}_1-j\omega\frac{d}{dz}(\Delta\mathcal{L}I_1). \tag{4.63}$$

To solve (4.63), we again expand the voltage and current perturbations of the second order in the eigenvectors used in the unperturbed case

$$\Delta\mathcal{V}_2=\sum_{i=1}^{N}\gamma_i V_i=\mathbf{vc}, \tag{4.64}$$

$$\Delta\mathcal{I}_2=\sum_{i=1}^{N}\tilde{\gamma}_i I_i=\mathbf{i}\tilde{\mathbf{c}}. \tag{4.65}$$

The γ_i and $\tilde{\gamma}_i$ coefficients have been collected in the vectors $\mathbf{c}$ and $\tilde{\mathbf{c}}$ respectively. Substituting these expansions in (4.63) and taking the proper orthogonality into account, give us

$$\frac{d^2\mathbf{c}}{dz^2}+\omega^2\Lambda\mathbf{c}=-\omega^2(\mathbf{i}^T\tilde{\mathcal{L}}\Delta\mathcal{C}\mathbf{v})\mathbf{b}-j\omega\frac{d}{dz}[(\mathbf{i}^T\Delta\mathcal{L}\mathbf{i})\tilde{\mathbf{b}}]. \tag{4.66}$$

Knowing the solution for differential equation (4.66) and using (4.8), the vector $\tilde{\mathbf{c}}$ can be found from the following equation

$$\frac{d\mathbf{c}}{dz}=-j\omega[\mathbf{L}\tilde{\mathbf{c}}+(\mathbf{i}^T\Delta\mathcal{L}\mathbf{i})\tilde{\mathbf{b}}]. \tag{4.67}$$

Using the same notations of $\Delta\mathbf{L}$ and $\Delta\mathbf{C}$ as for the first perturbation step, (4.66) and (4.67) can be rewritten as

$$\frac{d^2\mathbf{c}}{dz^2}+\omega^2\Lambda\mathbf{c}=-\omega^2\mathbf{L}\Delta\mathbf{C}\mathbf{b}-j\omega\frac{d}{dz}(\Delta\mathbf{L}\tilde{\mathbf{b}}), \tag{4.68}$$

$$\frac{d\mathbf{c}}{dz}=-j\omega(\mathbf{L}\tilde{\mathbf{c}}+\Delta\mathbf{L}\tilde{\mathbf{b}}). \tag{4.69}$$

Analogous to the first-order perturbation, a particular solution to the differential equation (4.68) takes the following form

$$\begin{aligned}&-\frac{1}{2j}\mathbf{K}^{-1}e^{-j\mathbf{K}z}\int_0^z e^{+j\mathbf{K}z'}[-\omega^2\mathbf{L}\Delta\mathbf{C}\mathbf{b}-j\omega\frac{d}{dz'}(\Delta\mathbf{L}\tilde{\mathbf{b}})]dz'\\&+\frac{1}{2j}\mathbf{K}^{-1}e^{+j\mathbf{K}z}\int_0^z e^{-j\mathbf{K}z'}[-\omega^2\mathbf{L}\Delta\mathbf{C}\mathbf{b}-j\omega\frac{d}{dz'}(\Delta\mathbf{L}\tilde{\mathbf{b}})]dz'.\end{aligned} \tag{4.70}$$

As we see, the above expression is similar to (4.48) with only $\mathbf{c}$ and $\tilde{\mathbf{c}}$ instead of $\mathbf{b}$ and $\tilde{\mathbf{b}}$ respectively. Therefore, we simplify (4.70) following the same procedure from the first perturbation step. Also, the contributions corresponding to the upper limit of the integration interval, being solutions to the homogeneous equation, have been dropped. Thus, after aforementioned simplifications, $\mathbf{c}$ is found to be

$$\begin{aligned}\mathbf{c} = e^{-j\mathbf{K}z}\mathbf{M} + e^{+j\mathbf{K}z}\mathbf{N}\\ -\frac{j\omega}{2}e^{-j\mathbf{K}z}\int_0^z e^{+j\mathbf{K}z'}(\mathbf{Z}_m\Delta\mathbf{C}\mathbf{b} + \Delta\mathbf{L}\tilde{\mathbf{b}})dz'\\ +\frac{j\omega}{2}e^{+j\mathbf{K}z}\int_0^z e^{-j\mathbf{K}z'}(\mathbf{Z}_m\Delta\mathbf{C}\mathbf{b} - \Delta\mathbf{L}\tilde{\mathbf{b}})dz',\end{aligned} \tag{4.71}$$

with $\mathbf{M}$ and $\mathbf{N}$ as yet undetermined. Substitution of $\tilde{\mathbf{c}}$ into (4.69) yields

$$\begin{aligned}\tilde{\mathbf{c}} = \mathbf{Z}_m^{-1}(e^{-j\mathbf{K}z}\mathbf{M} - e^{+j\mathbf{K}z}\mathbf{N})\\ -\frac{j\omega}{2}\mathbf{Z}_m^{-1}e^{-j\mathbf{K}z}\int_0^z e^{+j\mathbf{K}z'}(\mathbf{Z}_m\Delta\mathbf{C}\mathbf{b} + \Delta\mathbf{L}\tilde{\mathbf{b}})dz'\\ -\frac{j\omega}{2}\mathbf{Z}_m^{-1}e^{+j\mathbf{K}z}\int_0^z e^{-j\mathbf{K}z'}(\mathbf{Z}_m\Delta\mathbf{C}\mathbf{b} - \Delta\mathbf{L}\tilde{\mathbf{b}})dz'.\end{aligned} \tag{4.72}$$

To obtain the values of $\mathbf{M}$ and $\mathbf{N}$ as well for the second perturbation step we need to account, for the following boundary conditions at $z = 0$ and $z = l$

$$\Delta\mathcal{V}_2(z=0) + \mathcal{Z}_s\Delta\mathcal{I}_2(z=0) = 0, \tag{4.73}$$

$$\Delta\mathcal{V}_2(z=l) - \mathcal{Z}_L\Delta\mathcal{I}_2(z=l) = 0. \tag{4.74}$$

At $z = 0$ the result is similar to (4.53), but with $\mathbf{P}$ and $\mathbf{Q}$ replaced by $\mathbf{M}$ and $\mathbf{N}$

$$(\mathbf{M}+\mathbf{N}) + \mathbf{Z}_s\mathbf{Z}_m^{-1}(\mathbf{M}-\mathbf{N}) = 0. \tag{4.75}$$

The vectors $\mathbf{c}$ and $\tilde{\mathbf{c}}$ at $z = l$ are represented in the following form

$$\begin{aligned}\mathbf{c}(z=l) = e^{-j\mathbf{K}l}\mathbf{M} + e^{+j\mathbf{K}l}\mathbf{N} - \frac{j\omega}{2}e^{-j\mathbf{K}l}[(\mathbf{Z}_m\mathbf{F}_{+,-}\\ +\mathbf{G}_{+,-}\mathbf{Z}_m^{-1})\mathbf{P} + (\mathbf{Z}_m\mathbf{F}_{+,+} - \mathbf{G}_{+,+}\mathbf{Z}_m^{-1})\mathbf{Q}]\\ -\frac{j\omega}{2}(\mathbf{Z}_m\mathbf{F}^{\Delta C\Delta C}_{+,-,+} + \mathbf{Z}_m\mathbf{F}^{\Delta C\Delta L}_{+,-,+} - \mathbf{Z}_m\mathbf{F}^{\Delta C\Delta C}_{+,+,-}\\ +\mathbf{Z}_m\mathbf{F}^{\Delta C\Delta L}_{+,+,-} + \mathbf{G}^{\Delta L\Delta C}_{+,-,+} + \mathbf{G}^{\Delta L\Delta L}_{+,-,+} + \mathbf{G}^{\Delta L\Delta C}_{+,+,-} - \mathbf{G}^{\Delta L\Delta L}_{+,+,-})]\\ +\frac{j\omega}{2}e^{+j\mathbf{K}l}[(\mathbf{Z}_m\mathbf{F}_{-,-} - \mathbf{G}_{-,-}\mathbf{Z}_m^{-1})\mathbf{P}\\ +(\mathbf{Z}_m\mathbf{F}_{-,+} + \mathbf{G}_{-,+}\mathbf{Z}_m^{-1})\mathbf{Q}]\\ -\frac{j\omega}{2}(\mathbf{Z}_m\mathbf{F}^{\Delta C\Delta C}_{-,-,+} + \mathbf{Z}_m\mathbf{F}^{\Delta C\Delta L}_{-,-,+} - \mathbf{Z}_m\mathbf{F}^{\Delta C\Delta C}_{-,+,-}\\ +\mathbf{Z}_m\mathbf{F}^{\Delta C\Delta L}_{-,+,-} - \mathbf{G}^{\Delta L\Delta C}_{-,-,+} - \mathbf{G}^{\Delta L\Delta L}_{-,-,+} - \mathbf{G}^{\Delta L\Delta C}_{-,+,-} + \mathbf{G}^{\Delta L\Delta L}_{-,+,-})]\end{aligned} \tag{4.76}$$

and

$$\begin{aligned}\tilde{\mathbf{c}}(z=l) &= \mathbf{Z}_m^{-1}(e^{-j\mathbf{K}l}\mathbf{M} - e^{+j\mathbf{K}l}\mathbf{N}) \\ &-\frac{j\omega}{2}\mathbf{Z}_m^{-1}e^{-j\mathbf{K}l}[(\mathbf{Z}_m\mathbf{F}_{+,-} + \mathbf{G}_{+,-}\mathbf{Z}_m^{-1})\mathbf{P} \\ &+(\mathbf{Z}_m\mathbf{F}_{+,+} - \mathbf{G}_{+,+}\mathbf{Z}_m^{-1})\mathbf{Q}] \\ &-\frac{j\omega}{2}(\mathbf{Z}_m\mathbf{F}_{+,-,+}^{\Delta C\Delta C} + \mathbf{Z}_m\mathbf{F}_{+,-,+}^{\Delta C\Delta L} - \mathbf{Z}_m\mathbf{F}_{+,+,-}^{\Delta C\Delta C} \\ &+\mathbf{Z}_m\mathbf{F}_{+,+,-}^{\Delta C\Delta L} + \mathbf{G}_{+,-,+}^{\Delta L\Delta C} + \mathbf{G}_{+,-,+}^{\Delta L\Delta L} + \mathbf{G}_{+,+,-}^{\Delta L\Delta C} - \mathbf{G}_{+,+,-}^{\Delta L\Delta L})] \\ &-\frac{j\omega}{2}\mathbf{Z}_m^{-1}e^{+j\mathbf{K}l}[(\mathbf{Z}_m\mathbf{F}_{-,-} - \mathbf{G}_{-,-}\mathbf{Z}_m^{-1})\mathbf{P} \\ &+(\mathbf{Z}_m\mathbf{F}_{-,+} + \mathbf{G}_{-,+}\mathbf{Z}_m^{-1})\mathbf{Q}] \\ &-\frac{j\omega}{2}(\mathbf{Z}_m\mathbf{F}_{-,-,+}^{\Delta C\Delta C} + \mathbf{Z}_m\mathbf{F}_{-,-,+}^{\Delta C\Delta L} - \mathbf{Z}_m\mathbf{F}_{-,+,-}^{\Delta C\Delta C} \\ &+\mathbf{Z}_m\mathbf{F}_{-,+,-}^{\Delta C\Delta L} - \mathbf{G}_{-,-,+}^{\Delta L\Delta C} - \mathbf{G}_{-,-,+}^{\Delta L\Delta L} - \mathbf{G}_{-,+,-}^{\Delta L\Delta C} + \mathbf{G}_{-,+,-}^{\Delta L\Delta L})].\end{aligned} \tag{4.77}$$

Symbols $\mathbf{F}_{+,-,+}$ and $\mathbf{G}_{+,-,+}$ are defined as

$$\begin{aligned}\mathbf{F}_{+,-,+}^{\Delta C\Delta C} &= \int_0^l [e^{+j\mathbf{K}z}\Delta\mathbf{C}e^{-j\mathbf{K}z}\mathbf{Z}_m(\int_0^z e^{+j\mathbf{K}z'}\Delta\mathbf{C}\mathbf{a}dz')]dz, \\ \mathbf{F}_{+,-,+}^{\Delta C\Delta L} &= \int_0^l [e^{+j\mathbf{K}z}\Delta\mathbf{C}e^{-j\mathbf{K}z}(\int_0^z e^{+j\mathbf{K}z'}\Delta\mathbf{L}\tilde{\mathbf{a}}dz')]dz, \\ \mathbf{G}_{+,-,+}^{\Delta L\Delta C} &= \int_0^l [e^{+j\mathbf{K}z}\Delta\mathbf{L}e^{-j\mathbf{K}z}(\int_0^z e^{+j\mathbf{K}z'}\Delta\mathbf{C}\mathbf{a}dz')]dz, \\ \mathbf{G}_{+,-,+}^{\Delta L\Delta L} &= \int_0^l [e^{+j\mathbf{K}z}\Delta\mathbf{L}e^{-j\mathbf{K}z}\mathbf{Z}_m^{-1}(\int_0^z e^{+j\mathbf{K}z'}\Delta\mathbf{L}\tilde{\mathbf{a}}dz')]dz,\end{aligned} \tag{4.78}$$

where the subscript notation $+,-,+$ denotes the first and second sign of the exponential under the outer integral, while the third sign represents the sign of the exponential under the inner integral. The superscript notation $\Delta C\Delta L$ indicates that we have ΔC under the outer integral sign and ΔL under the inner integral sign. All the other $\mathbf{F}$ and $\mathbf{G}$ symbols are defined in an analogous way. In an easy to understand way, (4.76) and (4.77) are written as

$$\begin{aligned}\mathbf{c}(z=l) &= e^{-j\mathbf{K}l}\mathbf{M} + e^{+j\mathbf{K}l}\mathbf{N} \\ -e^{-j\mathbf{K}l}(\mathbf{T}_1\mathbf{P} + \mathbf{U}_1\mathbf{Q} + \mathbf{X}_1) &+ e^{+j\mathbf{K}l}(\mathbf{T}_2\mathbf{P} + \mathbf{U}_2\mathbf{Q} + \mathbf{X}_2)\end{aligned} \tag{4.79}$$

and

$$\begin{aligned}\tilde{\mathbf{c}}(z=l) &= \mathbf{Z}_m^{-1}[e^{-j\mathbf{K}l}\mathbf{M} - e^{+j\mathbf{K}l}\mathbf{N} \\ -e^{-j\mathbf{K}l}(\mathbf{T}_1\mathbf{P} + \mathbf{U}_1\mathbf{Q} + \mathbf{X}_1) &- e^{+j\mathbf{K}l}(\mathbf{T}_2\mathbf{P} + \mathbf{U}_2\mathbf{Q} + \mathbf{X}_2)].\end{aligned} \tag{4.80}$$

Figure 4.1: The nominal uniform microstrip line interconnection with ten signal conductors.

Enforcing (4.74), we get

$$\mathbf{c}(z=l)-\mathbf{Z}_L\mathbf{Z}_m^{-1}[\mathbf{Z}_m\tilde{\mathbf{c}}(z=l)]=0. \tag{4.81}$$

Finally, to determine $\mathbf{M}$ and $\mathbf{N}$ we use (4.75) together with (4.81), which leads to

$$\begin{pmatrix} \mathbf{S}_s & \mathbf{V}_s \\ \mathbf{V}_L e^{-j\mathbf{K}l} & \mathbf{S}_L e^{+j\mathbf{K}l} \end{pmatrix}\begin{pmatrix} \mathbf{M} \\ \mathbf{N} \end{pmatrix}=\begin{pmatrix} 0 & 0 \\ \mathbf{S}_A & \mathbf{S}_B \end{pmatrix}\begin{pmatrix} \mathbf{P} \\ \mathbf{Q} \end{pmatrix}+\begin{pmatrix} 0 \\ \mathbf{S}_X \end{pmatrix} \tag{4.82}$$

with

$$\mathbf{S}_X=\mathbf{V}_L e^{-j\mathbf{K}l}\mathbf{X}_1-\mathbf{S}_L e^{+j\mathbf{K}l}\mathbf{X}_2. \tag{4.83}$$

4.3 Validation examples

4.3.1 Frequency domain results

The theory proposed above for NMTLs is validated by applying it to a ten conductor microstrip line interconnection with random nonuniformities. The nominal structure is shown in Fig. 4.1. The track width of every line is $w = 1.8$ mm and the spacing between any two neighboring lines is $s = 700$ μm. The microstrips and ground plane have a thickness $t = 35$ μm and a conductivity $\sigma = 5.8{\cdot}10^7$ S/m. The microstrip lines reside on a Roger's RO4350B substrate with a thickness $h = 1.524$ mm, a relative permittivity $\varepsilon_r = 3.66$, and a loss tangent $\tan\delta = 0.003$. The total length of the multiconductor microstrip line is $l = 40$ mm.

The nominal frequency dependent $\tilde{\mathcal{L}}$- and $\tilde{\mathcal{C}}$-matrices are obtained with the technique of [19] and [22]. This 2-D electromagnetic numerical technique solves

Table 4.1: Influence of varying the maximal value of $\Delta\mathcal{L}$ and $\Delta\mathcal{C}$

Max. deviation (%)	$\Delta S_{12\text{-}2}$ @ 20 GHz (%)
10	0.17
15	0.30
20	0.46
25	0.67
30	0.96
35	1.39
40	2.07

the pertinent complex capacitance and complex inductance problem assuming the quasi-TM behavior of the fields. To model the presence of random nonuniformities, the nominal structure is divided in 100 equal sections. Each element of the $\tilde{\mathcal{L}}$ and $\tilde{\mathcal{C}}$ 10×10 matrices for any single section is then multiplied with the same random variable (RV) that is uniformly distributed within the interval [1 - ξ, 1 + ξ]. In such a way, we retain perturbed p.u.l. $\mathcal{L}$ and $\mathcal{C}$ matrices that are positive-definite as required for any passive $2D$ structure. However, for different sections, different RVs are used. The number ξ determines the maximum deviation from the nominal case. We employ the chain parameter matrix approach [2] as a reference solution. In this method the voltages and currents at the input for each individual section are related to the voltages and currents at the output by means of 20×20 chain parameter matrix. Finally, S-parameters can be easily derived from the overall chain parameter matrix obtained as a product of the 100 chain parameter matrices of the individual sections.

We compute the S-parameters with respect to 50 Ω reference impedances at all ports of the investigated structure. As a sample result, the transmission from port 2 to port 12 is chosen in order to have the transmission through a line which has strong coupling with two neighboring lines. Figs. 4.2 and 4.3 show the magnitude of the reflection coefficient $S_{2\text{-}2}$, the backward crosstalk $S_{1\text{-}2}$, the transmission coefficient $S_{12\text{-}2}$ and the forward crosstalk $S_{11\text{-}2}$, when the maximum deviation $\xi = 25\%$ with respect to the nominal $\tilde{\mathcal{L}}$ and $\tilde{\mathcal{C}}$ values. As can be seen, the results obtained by applying the perturbation technique are in a very good agreement with the reference method. The phase of the S-parameters is also modeled with a very high accuracy. The S-parameters for the nominal uniform interconnect are also shown to indicate the influence of random nonuniformities.

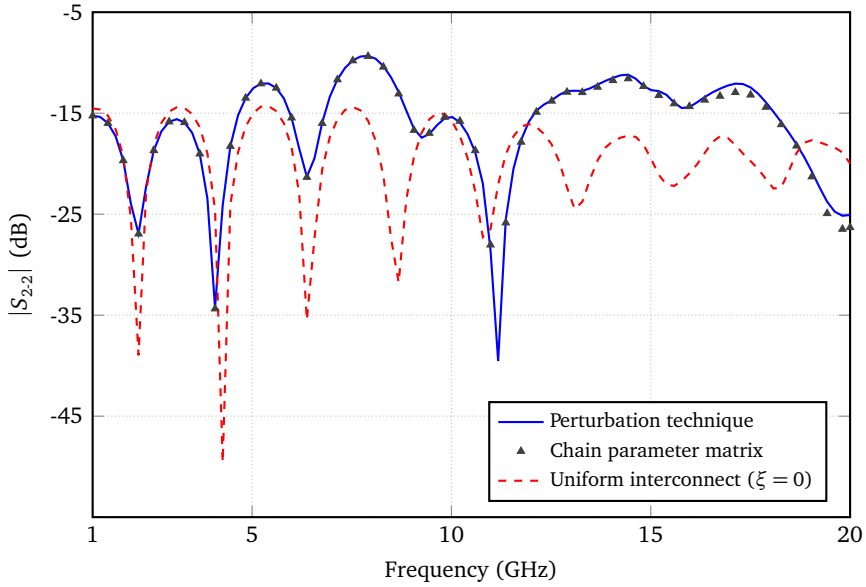

(a)

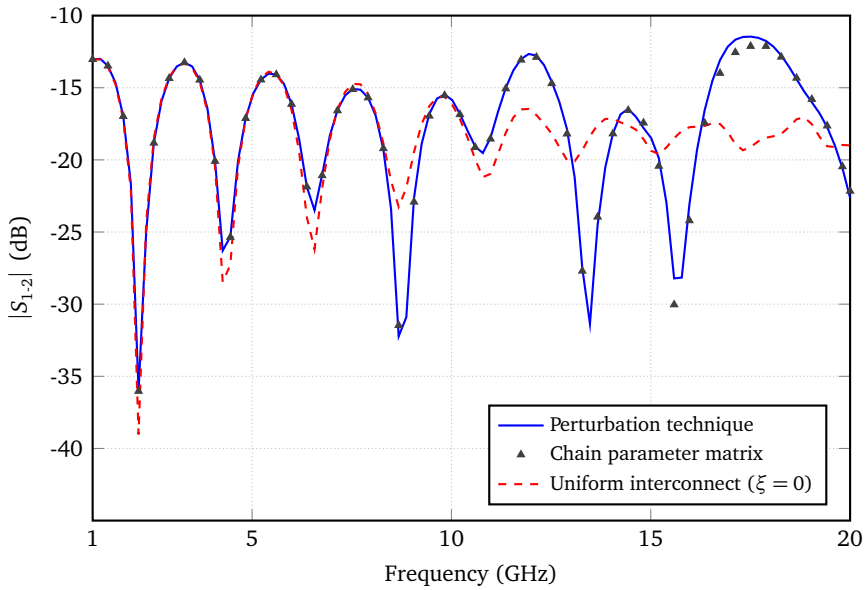

(b)

Figure 4.2: S-parameters of the ten conductor microstrip line for the case when the maximum variation of the p.u.l. capacitance and inductance is $\xi = 25\%$ using the two-step perturbation and chain parameter matrix techniques. (a) Reflection coefficient $S_{2\text{-}2}$. (b) Backward crosstalk $S_{1\text{-}2}$. To indicate the influence of the perturbation, the S-parameters of the nominal uniform line ($\xi = 0$) are also shown.

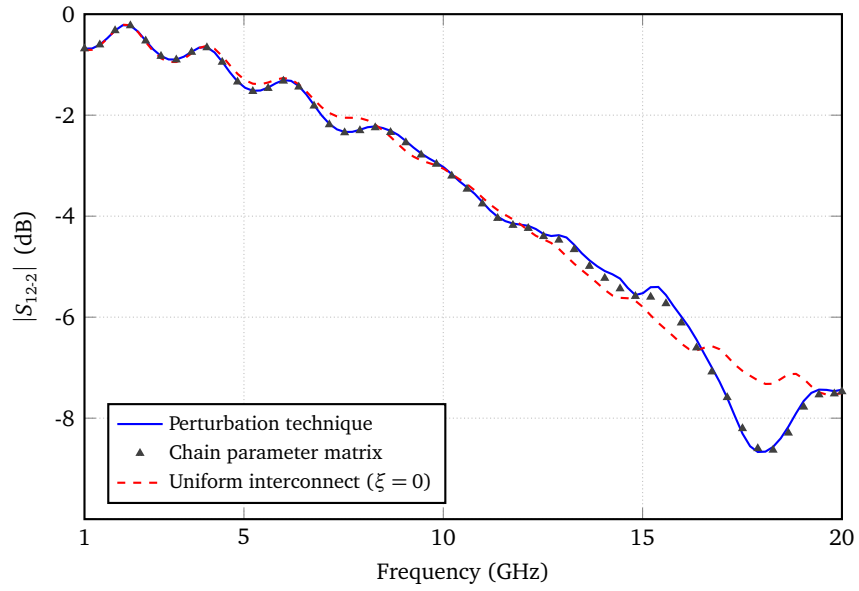

(a)

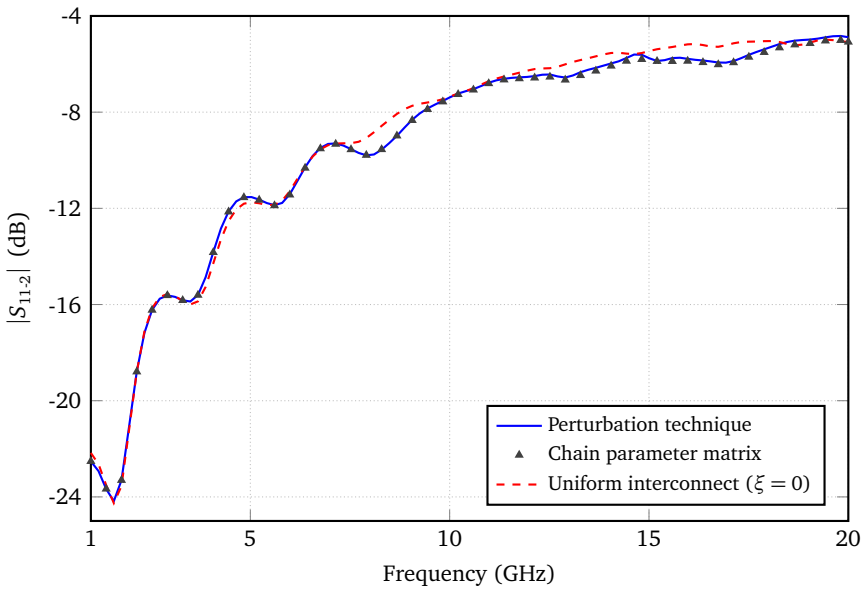

(b)

Figure 4.3: S-parameters of the ten conductor microstrip line for the case when the maximum variation of the p.u.l. capacitance and inductance is $\xi = 25\%$ using the two-step perturbation and chain parameter matrix techniques. (a) Transmission coefficient $S_{12\text{-}2}$. (b) Forward crosstalk $S_{11\text{-}2}$. To indicate the influence of the perturbation, the S-parameters of the nominal uniform line ($\xi = 0$) are also shown.

Table 4.2: CPU time comparison

Number of sections	Perturbation technique	Reference solution	Speed-up factor
50	7.16 s	33.41 s	4.67
100	10.83 s	62.67 s	5.79
200	19.05 s	120.08 s	6.30
500	41.01 s	288.13 s	7.03

To further demonstrate the accuracy and limitations of the perturbation approach, a study of the relative error on the transmission coefficient $S_{12\text{-}2}$ at the highest frequency of 20 GHz is performed. For different values of the maximum deviation ξ, we define the relative error on $S_{12\text{-}2}$ taking both magnitude and phase into account as

$$\Delta S_{12\text{-}2} = \left| \frac{S_{12\text{-}2}^{(ch)} - S_{12\text{-}2}^{(p)}}{S_{12\text{-}2}^{(ch)}} \right|, \tag{4.84}$$

where $S_{12\text{-}2}^{ch}$ and $S_{12\text{-}2}^{p}$ are obtained by means of the chain parameter matrix and perturbation techniques, respectively. Table 4.1 shows the growing relative error when increasing the maximal values of $\Delta\mathcal{L}$ and $\Delta\mathcal{C}$. However, this error remains limited to 1% if the perturbations do not exceed 30% with respect to the nominal case.

Finally, we study the execution time of the code in Matlab 2009a to illustrate the efficiency of the two-step perturbation technique. All calculations were performed on a computer with an Intel Core i7 3630QM Processor and 16 GB of installed memory (RAM). The calculations of the integrals occuring in (4.49), (4.50), (4.71) and (4.72) determine the computational costs for the perturbation approach. The computational complexity of the reference method is proportional to the number of sections used in concatenation. Table 4.2 shows the CPU time for both techniques for 100 frequency samples linearly spaced between 1 and 20 GHz and for a varying number of sections. For example, in the case of 200 sections, the speed-up factor is about 6.3.

4.3.2 Time domain results

The transient analysis is performed on the high-speed packaging interconnect investigated in [23], which is depicted in Fig. 4.4. The structure contains six conductors providing an electrical connection between different components on a PCB. The conductors and ground plane are 20 μm thick with conductivity $\sigma = 5.8{\cdot}10^7$ S/m. The structure is symmetrical with respect to the dashed straight line depicted in Fig. 4.4 with a total nominal length AB of 7 mm measured along the

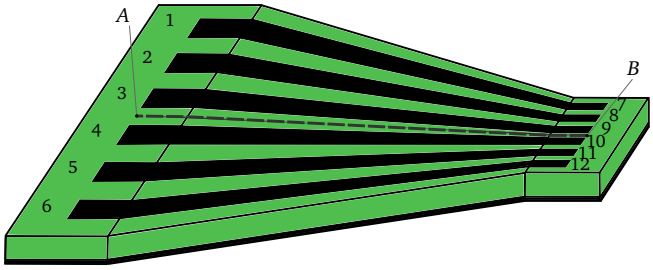

Figure 4.4: A high-speed packaging interconnect taper [23].

dashed central line. The widths and distances between two neighboring conductors are equal to 1 mm at the left terminations and to 0.125 mm at the right termination.

At both sides, the interconnection structure has 1 mm long uniform multiconductor line. The interconnect pattern resides on a substrate with a thickness $h = 400$ μm, a relative permittivity $\varepsilon_r = 4.5$, and a loss tangent $\tan\delta = 0.001$. Before employing the perturbation technique, the p.u.l. parameters are obtained for nine cross sections orthogonal to the line of symmetry with the method described in [19]. Then, interpolation provides the p.u.l. parameters for the entire structure. Afterwards, we calculate the S-parameters applying the two-step perturbation technique to the resulting structure. The numbering of the ports is specified in Fig. 4.4. The resulting 12×12 S-parameters are imported into Agilent's Schematic ADS 2013.06 tool in S12P format for analysis in the time domain. In addition, we perform a full-wave simulation of the investigated structure using Momentum of ADS 2013.06. Then, the results of the full-wave modeling are also used in Schematic to serve as a reference solution. A ramped step signal, going from 0 V to 1 V with a rise time of $t_r = 50$ ps, is applied to the input port 1. All ports are matched to 50 Ω. Figs. 4.5 and 4.6 show the voltages at the input ports 1 and 2 together with the transient response at the output ports 7 and 8. As can be seen, the results of the perturbation technique represented in time domain are in a very good agreement with the reference full-wave solution. However, the CPU time needed for the transient analysis using the perturbation approach is significantly less than the CPU time needed for the full-wave modeling. In both cases, S-parameters were calculated for 100 frequency samples logarithmically spaced in the frequency range from DC to 60 GHz. The perturbation technique including calculations of p.u.l. parameters by means of the method described in [19] takes 9 minutes on a computer with Intel(R) Core(TM) Quad CPU Q9650 and 8 GB of installed memory (RAM). In contrast, the full-wave analysis requires about 16 hours to perform the same calculations. This clearly defines our perturbation technique as a very efficient one.

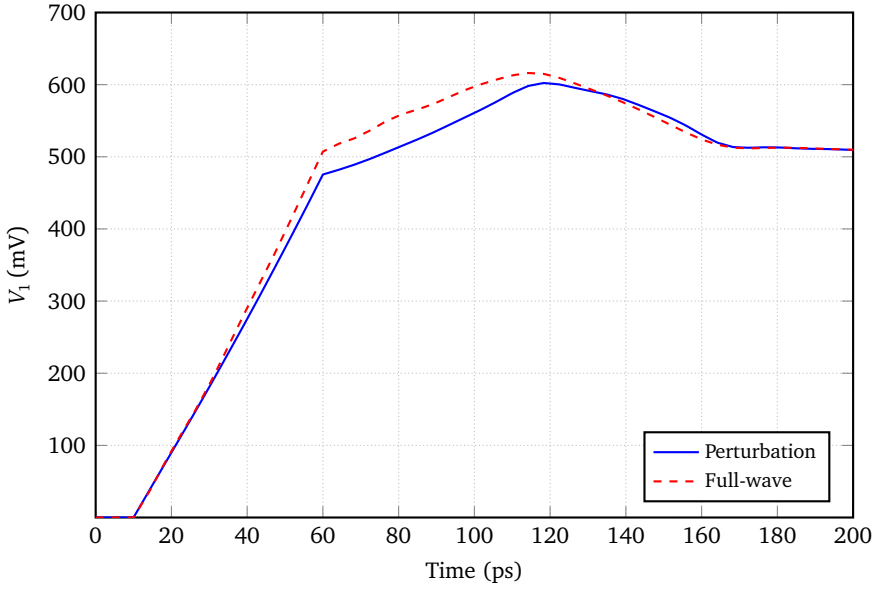

(a)

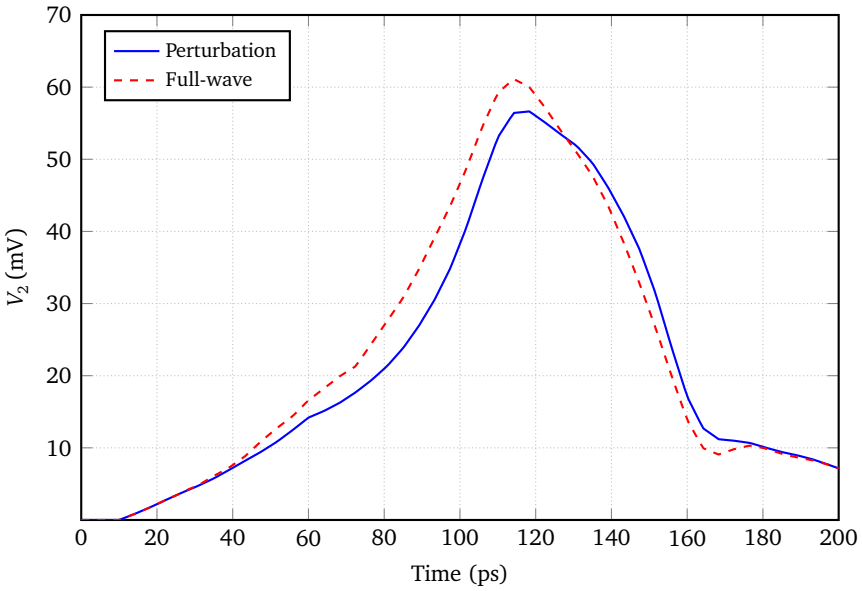

(b)

Figure 4.5: Time domain analysis of the high-speed packaging nonuniform interconnect with six signal conductors of Fig. 4.4. (a) Transient waveform at port 1. (b) Transient response at port 2.

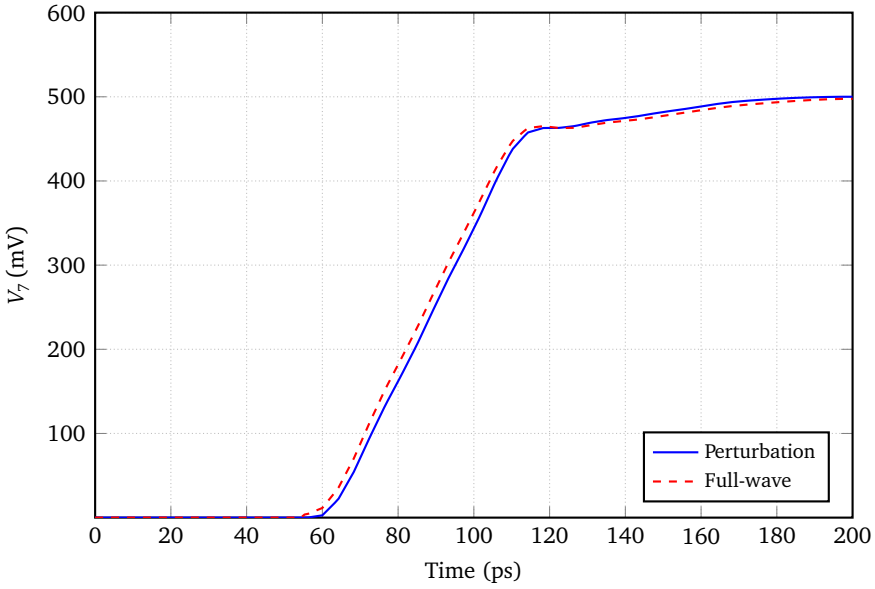

(a)

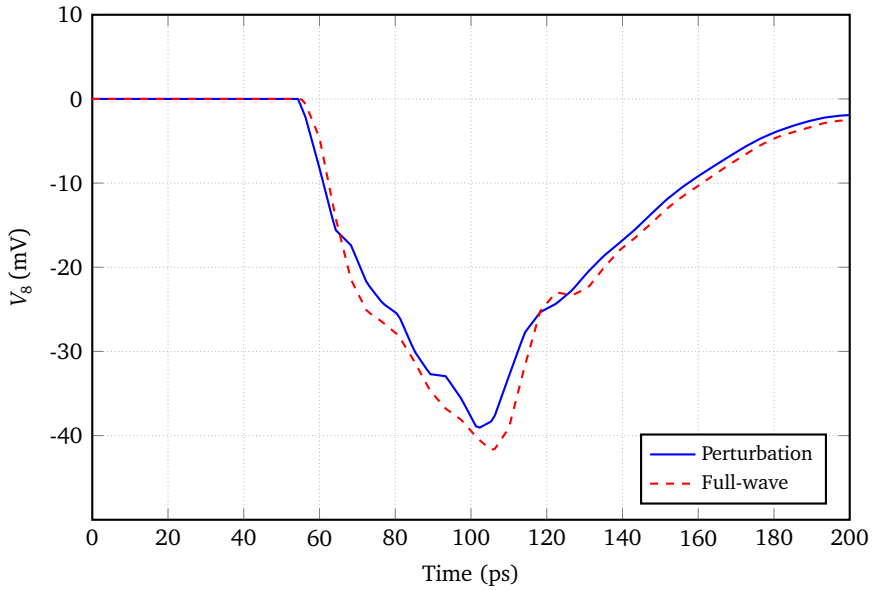

(b)

Figure 4.6: Time domain analysis of the high-speed packaging nonuniform interconnect with six signal conductors of Fig. 4.4. (a) Transient response at port 7. (b) Transient response at port 8.

4.4 Conclusion

In this chapter, a two-step perturbation technique has been presented to analyze NMTLs. Nonuniformities were represented as perturbations with respect to a nominal configuration, allowing an interconnect designer to easily see what the effect of (unwanted) perturbations might be. Relying on the Telegrapher's equations, the perturbation approach derives voltages and currents along the multiconductor interconnection from second-order differential equations for the nominal configuration with source terms accounting for the perturbations.

The presented methodology was validated by modeling a ten conductor microstrip line with random uniformities in frequency domain. Compared to a chain parameter matrix approach, excellent accuracy and improved efficiency was achieved. Moreover, a transient analysis performed on a high-speed packaging nonuniform interconnect confirms the validity and very good efficiency of the perturbation method with respect to full-wave modeling.

References

[1] B. Curran, I. Ndip, S. Guttowski, and H. Reichl, "A methodology for combined modeling of skin, proximity, edge, and surface roughness effects", *IEEE Trans. Microw. Theory Tech.*, vol. 58, no. 9, pp. 2448–2455, Sep. 2010.

[2] C. R. Paul, *Analysis of Multiconductor Transmission Lines*. John Wiley & Sons, 1994.

[3] J. F. Mao and Z. F. Li, "Analysis of the time response of nonuniform multiconductor transmission lines with a method of equivalent cascaded network chain", *IEEE Trans. Microw. Theory Tech.*, vol. 40, no. 5, pp. 948–954, May 1992.

[4] A. R. Djordjevic and T. Sakar, "Analysis of time response of lossy multiconductor transmission line networks", *IEEE Trans. Microw. Theory Tech.*, vol. 35, no. 10, pp. 898–908, Oct. 1987.

[5] N. Orhanovic, P. Wang, and V. K. Tripathi, "Time-domain simulation of uniform and nonuniform multiconductor lossy lines by the method of characteristics", *IEEE Trans. Comput.-Aided Design Integr. Circuits Syst.*, vol. 12, no. 6, pp. 900–904, Jun. 1993.

[6] D. Kuznetsov, "Efficient circuit simulation of nonuniform transmission lines", *IEEE Trans. Microw. Theory Tech.*, vol. 46, no. 5, pp. 546 –550, May 1998.

[7] S. Grivet-Talocia, H. M. Huang, A. E. Ruehli, F. Canavero, and I. M. Elfadel, "Transient analysis of lossy transmission lines: an efficient approach based on the method of characteristics", *IEEE Trans. Adv. Packag.*, vol. 27, no. 1, pp. 45–56, Feb. 2004.

[8] Q. Xu, Z. F. Li, J. Wang, and J. F. Mao, "Transient analysis of lossy interconnects by modified method of characteristics", *IEEE Trans. Circuits Syst. I*, vol. 47, no. 3, pp. 363–375, Mar. 2000.

[9] F.-Y. Chang, "Transient simulation of nonuniform coupled lossy transmission lines characterized with frequency-dependent parameters. I. Waveform relaxation analysis", *IEEE Trans. Circuits Syst. I*, vol. 39, no. 8, pp. 585 –603, Aug. 1992.

[10] S. Grivet-Talocia and F. Canavero, "Wavelet-based adaptive solution for the nonuniform multiconductor transmission lines", *IEEE Microw. Guided Wave Lett.*, vol. 8, no. 8, pp. 287–289, Aug. 1998.

[11] S. Barmada and M. Raugi, "Transient numerical solutions of nonuniform MTL equations with nonlinear loads by wavelet expansion in time or space domain", *IEEE Trans. Circuits Syst. I*, vol. 47, no. 8, pp. 1178 –1190, Aug. 2000.

[12] M. Tong, G. Pan, and G. Lei, "Full-wave analysis of coupled lossy transmission lines using multiwavelet-based method of moments", *IEEE Trans. Microw. Theory Tech.*, vol. 53, no. 7, pp. 2362 –2370, Jul. 2005.

[13] A. Orlandi and P. C. R., "FDTD analysis of lossy, multiconductor lines terminated in arbitrary loads", *IEEE Trans. Electromagn. Compat.*, vol. 38, no. 3, pp. 388–399, Aug. 1996.

[14] J. Roden, C. R. Paul, W. Smith, and S. Gedney, "Finite-difference, time-domain analysis of lossy transmission lines", *IEEE Trans. Electromagn. Compat.*, vol. 38, no. 1, pp. 15 –24, Feb. 1996.

[15] K. Afrooz and A. Abdipour, "Efficient method for time-domain analysis of lossy nonuniform multiconductor transmission line driven by a modulated signal using FDTD technique", *IEEE Trans. Electromagn. Compat.*, vol. 54, no. 2, pp. 482 –494, Apr. 2012.

[16] H.-H. Chen, "Finite-element method coupled with method of lines for the analysis of planar or quasi-planar transmission lines", *IEEE Trans. Microw. Theory Tech.*, vol. 51, no. 3, pp. 848 –855, Mar. 2003.

[17] Q. Xu and P. Mazumder, "Accurate modeling of lossy nonuniform transmission lines by using differential quadrature methods", *IEEE Trans. Microw. Theory Tech.*, vol. 50, no. 10, pp. 2233–2246, Oct. 2002.

[18] M. Tang and J. Mao, "A differential quadrature method for the transient analysis of multiconductor transmission lines", in *International Conference on Microwave and Millimeter Wave Technology, Nanjing, P. R. China*, 2008, pp. 1423 –1426.

[19] T. Demeester and D. De Zutter, "Quasi-TM transmission line parameters of coupled lossy lines based on the Dirichlet to Neumann boundary operator", *IEEE Trans. Microw. Theory Tech.*, vol. 56, no. 7, pp. 1649–1660, Jul. 2008.

[20] L. A. Hayden and V. K. Tripathi, "Nonuniformly coupled microstrip transversal filters for analog signal-processing", *IEEE Trans. Microw. Theory Tech.*, vol. 39, no. 1, pp. 47–53, Jan. 1991.

[21] M. Khalaj-Amirhosseini, "Analysis of nonuniform transmission lines using the equivalent sources", *Progress In Electromagnetics Research*, vol. 71, pp. 95–107, 2007.

[22] T. Demeester and D. De Zutter, "Construction of the Dirichlet to Neumann boundary operator for triangles and applications in the analysis of polygonal conductors", *IEEE Trans. Microw. Theory Tech.*, vol. 58, no. 1, pp. 116 –127, Jan. 2010.

[23] S. Grivet-Talocia and F. Canavero, "A class of space-expansion methods for the transient simulation of the nonuniform multiconductor transmission lines", in *International Symposium on Signals, Systems, and Electronics, Pisa, Italy*, 1998, pp. 219–222.

5
Conclusions and future work

5.1 Conclusions

An efficient semi-analytical perturbation technique has been developed for general nonuniform multiconductor transmission lines. In contrast to what is typically done when using a perturbation approach, a two-step procedure has been put forward. It has been clearly shown that adding a second perturbation step has a very significant influence on the accuracy. The formalism of the perturbation approach is such that the modeling of nonuniform MTLs with continuously varying p.u.l. parameters can readily be achieved.

Special attention has been devoted to the influence of fiber weave on high-speed signaling. The fiber weave effects have been precisely captured by the perturbation technique. Additionally, the methodology explaining how to deal with electrically long transmission lines has been also considered. Such a methodology is necessary to avoid accumulation of phase errors.

Excellent accuracy and efficiency have been demonstrated by a number of examples both in time and frequency domain. The examples comprise the application of the perturbation approach to a linearly tapered microstrip line, differential and ten conductor microstrip transmission lines with random nonuniformities and a high-speed packaging nonuniform interconnect with six signal conductors.

5.2 Future work

Future research could be dedicated to the investigation of the accuracy of the two-step perturbation technique. It would therefore be interesting to develop a theory

being able to predict the accuracy of the perturbation technique. Another challenge is to investigate if further perturbation steps could lead to an even higher accuracy. An attempt to develop such a theory has been tried but turned out to be as yet unsuccessful.

An alternative way to exploit the theory highlighted in this dissertation is to cast the wave equations in a form such that all perturbations appear in the right-hand side as yet unknown sources and to transform these wave equations into integral equations with voltages and currents as unknowns. As a matter of fact, the approach followed in this thesis can be considered to be the iterative solution of these integral equations. It might turn out, however, that solving integral equations is too time consuming.

As to the applications, other examples of interest could be examined such as twisted pair interconnects or interconnects in high-speed connectors. In addition to the information concerning to the range of applicability of the perturbation technique, it could also provide empirical data about the limitations of the method.

In many applications, the nonuniformities are caused by the manufacturing process. Therefore, these nonuniformities are not always known in deterministic way, but can best be described as stochastic processes. A combination of the methodology described in this work with advanced stochastic solution techniques, leveraging for example the Polynominal Chaos framework, is also potentially very interesting.

Appendix

A

Eigenvectors of voltages and currents

The capacitance and inductance matrices $\tilde{\mathcal{C}}$ and $\tilde{\mathcal{L}}$ are symmetric square $N \times N$ matrices. The eigenvalues λ of $\tilde{\mathcal{L}}\tilde{\mathcal{C}}$ are the solutions of $det(\tilde{\mathcal{L}}\tilde{\mathcal{C}} - \lambda\mathcal{I}) = 0$ with $\mathcal{I}$ the $N \times N$ unit matrix. The determinant of the transpose of a matrix is identical to the determinant of the matrix itself. As $(\tilde{\mathcal{L}}\tilde{\mathcal{C}})^T = \tilde{\mathcal{C}}^T\tilde{\mathcal{L}}^T = \tilde{\mathcal{C}}\tilde{\mathcal{L}}$, we immediately see that $det[(\tilde{\mathcal{L}}\tilde{\mathcal{C}} - \lambda\mathcal{I})^T] = det(\tilde{\mathcal{C}}\tilde{\mathcal{L}} - \lambda\mathcal{I}) = 0$ and hence we remark that $\tilde{\mathcal{L}}\tilde{\mathcal{C}}$ and $\tilde{\mathcal{C}}\tilde{\mathcal{L}}$ have the same eigenvalues.
Now suppose that V_i is an eigenvector of $\tilde{\mathcal{L}}\tilde{\mathcal{C}}$ with eigenvalue λ_i and I_j is an eigenvector of $\tilde{\mathcal{C}}\tilde{\mathcal{L}}$ with eigenvalue λ_j. Consequently,

$$\begin{aligned} (V_i)^T\lambda_j I_j &= (V_i)^T\tilde{\mathcal{C}}\tilde{\mathcal{L}}I_j = (\tilde{\mathcal{L}}^T\tilde{\mathcal{C}}^T V_i)^T I_j \\ &= (\tilde{\mathcal{L}}\tilde{\mathcal{C}}V_i)^T I_j = (V_i)^T\lambda_i I_j. \end{aligned} \tag{A.1}$$

For distinct eigenvalues this implies that $(V_i)^T I_j = 0$.
Next, we will show that the following orthogonality property holds for two distinct eigenvectors V_i and V_j:

$$(V_j)^T\tilde{\mathcal{C}}V_i = 0. \tag{A.2}$$

The proof runs along the same lines as above. We know that

$$\tilde{\mathcal{L}}\tilde{\mathcal{C}}V_i = \lambda_i V_i. \tag{A.3}$$

Hence,

$$\begin{aligned} \lambda_i(V_j)^T\tilde{\mathcal{C}}V_i &= (V_j)^T\tilde{\mathcal{C}}\tilde{\mathcal{L}}\tilde{\mathcal{C}}V_i \\ &= (\tilde{\mathcal{L}}^T\tilde{\mathcal{C}}^T V_j)^T\tilde{\mathcal{C}}V_i \\ &= (\tilde{\mathcal{L}}\tilde{\mathcal{C}}V_j)^T\tilde{\mathcal{C}}V_i \\ &= \lambda_j(V_j)^T\tilde{\mathcal{C}}V_i, \end{aligned} \tag{A.4}$$

which implies (A.2) for distinct eigenvalues. Similarly, we have that

$$(I_j)^T \tilde{\mathcal{L}} I_i = 0. \tag{A.5}$$

We next prove that $\mathbf{LC} = \mathbf{CL} = \Lambda$. It suffices to prove that $\mathbf{LC} = \Lambda$ as taken the transpose immediately yields the remaining identity. From (4.20) and (4.22) we have that

$$\begin{aligned} \mathbf{LC} &= \mathbf{i}^T \tilde{\mathcal{L}} \mathbf{i} \mathbf{v}^T \tilde{\mathcal{C}} \mathbf{v} \\ &= \mathbf{i}^T \mathbf{v} \mathbf{v}^{-1} \tilde{\mathcal{L}} \mathbf{i} \mathbf{v}^T \mathbf{i} \mathbf{i}^{-1} \tilde{\mathcal{C}} \mathbf{v}. \end{aligned} \tag{A.6}$$

Using the orthogonality properties $\mathbf{v}^T \mathbf{i} = \mathbf{i}^T \mathbf{v} = \mathcal{I}_N$, (A.6) becomes

$$\begin{aligned} \mathbf{LC} &= \mathbf{v}^{-1} \tilde{\mathcal{L}} \mathbf{i} \mathbf{i}^{-1} \tilde{\mathcal{C}} \mathbf{v} \\ &= \mathbf{v}^{-1} \tilde{\mathcal{L}} \tilde{\mathcal{C}} \mathbf{v} = \mathbf{v}^{-1} \mathbf{v} \Lambda = \Lambda, \end{aligned} \tag{A.7}$$

where we have used (4.15).